Mathematical Modeling of Silica Alcogel Drying With Supercritical Carbon Dioxide

by

Yaprak Özbakır

A Thesis Submitted to the
Graduate School of Engineering
in Partial Fulfillment of the Requirements for
the Degree of

Master of Science
in
Chemical and Biological Engineering

Koç University

September 2013

Koç University

Graduate School of Sciences and Engineering

This is to certify that I have examined this copy of a master's thesis by

Yaprak Özbakır

and have found that it is complete and satisfactory in all respects,
and that any and all revisions required by the final
examining committee have been made.

Committee Members:

_____

Can Erkey, Ph. D. (Advisor)

_____

Seda Kızılel, Ph. D.

_____

Murat Sözer, Ph. D.

Date: 09.09.2013

ABSTRACT

Supercritical extraction is an important and the most time consuming step in aerogel production. An understanding of the drying process is crucial to provide information about scale-up and optimization of the process. As a result, drying times of the wet gels can be shortened and thus, more economically feasible aerogel production can be achieved. In this study, mathematical models for supercritical drying have been developed to predict drying times of alcogels. The models based on Fick's Law with a concentration-dependent diffusion coefficient were used to simulate the supercritical drying of the wet gels using a parallel pore model in which all pores of various dimensions are positioned in parallel. The model equations were developed for two types of supercritical drying: batch supercritical drying and continuous supercritical drying. In the first part, extraction of solvent fully occupying the pores of spherical, cylindrical and rectangular alcogels into supercritical CO_2 (sc-CO_2) in the batch system was studied. The model equations were one-dimensional and unsteady state.

In the second part, model equations for supercritical extraction of the cylindrical gel, with length much longer than its thickness (1.19 cm in diameterx15.92cm in length), in continuous sc-CO_2 flow were developed. Two dimensional and unsteady state model equation governing the mass transfer inside of the pores of the wet gel was developed. Additionally, a model equation for variation of ethanol concentration in the bulk flow as a function of time and position was also derived. The coupled partial differential equations that govern the drying of the wet gel in continuous supercritical drying were solved using numerical techniques.

In this study, supercritical extraction of the gel (1.19 cm in diameter x15.92cm in length) was also performed. Mass of ethanol collected during the supercritical extraction of

the wet gel prepared in the laboratory was compared to model results. It was found that the present model proposed for the continuous supercritical dying of the wet gels with sc-CO_2 for replacement of ethanol from the porous structure of the gel fits sufficiently well with the experimental data. Furthermore, the mass transfer coefficient regressed from experimental data was compared with the correlations proposed in the literature for supercritical extraction for the operation conditions (1.5 L sc-CO_2/min volumetric flow rate and 313.15 K and 100 bar) at which supercritical extraction was executed. The predicted and calculated values were found to be close each other.

The governing model equations for supercritical drying with carbon dioxide were solved using the finite difference method and MATLAB program. The effect of operation variables, including temperature, mass transfer coefficient, gel porosity and tortuosity, as well as thickness of the gels on drying time in the batch system were investigated using simulations. It was found that mass transfer coefficient and gel dimensions are the most predominant parameters which affect the extraction time. Time for the diffusion of sc-CO_2 notably decreased with increasing mass transfer coefficient and increased with increasing thickness.

ÖZET

Süper kritik karbondioksit (sc-CO_2) ortamında alkojel kurutma işlemi silika aerojel üretiminin önemli ve en çok zaman alan aşamasıdır. Jel kurutma işleminin anlaşılması üretim sürecinin optimizasyonu hakkında önemli bilgi sağlar. Sonuç olarak, ıslak jellerin kurutma süreleri kısaltılarak, üretim maliyeti düşük aerojel üretimi gerçekleştirilir. Bu çalışmada aerojellerin kurutma sürelerini tahmin edebilmek amacıyla matematiksel modeller geliştirilmiştir. Farklı iki kurutma türü olan kesikli kurutma ve sürekli kurutma için model denklemler çıkarılmıştır. İlk bölümde, küre, silindir ve dikdörtgen şeklindeki ıslak jellerin tüm gözeneklerini dolduran çözücünün kesikli sistemde süper kritik fazdaki karbon dioksite ekstraksiyonu çalışılmıştır. Tek yönlü ve zamana bağlı kütle transfer model denklemleri, difüzyon katsayısının sistem kompozisyonuna bağlı korelasyonu kullanılarak, Fick Kanununa dayandırılarak geliştirilmiştir. Model denklemlerde, jel içinde bulunan değişik boyutlardaki tüm gözeneklerin paralel olarak sıralandığı paralel gözenek modeli kullanılmıştır.

İkinci bölümde, 1.19 cm çapında 15.92 cm uzunluğunda üretilmiş olan silindir şeklindeki ıslak jelin sürekli süper kritik karbon dioksit ortamında ekstraksiyonu için model denklemler geliştirilmiştir. Islak jelin porları içindeki kütle transferi için geçerli olan model denklemler oluşturulmuştur. Ayrıca, CO_2' in yüksek basınçlı kurutma kabı içerisindeki sürekli akışı içerisindeki etanol derişimini zamana ve pozisyona bağlı inceleyen model denklem elde edilmiştir. Islak jelin kurumasında geçerli olan birleştirilmiş kısmi diferansiyel denklemler nümerik yöntemler kullanılarak çözülmüştür.

Bu çalışmada, model çalışmalarına ilaveten süper kritik jel ektraksiyonunun deneysel çalışması da yapılmıştır. Laboratuarda hazırlanmış olan silindir şeklindeki ıslak jelin (1.19 cm çapında x 15.92 cm uzunluğunda) kurutulması sırasında toplanan etanol

miktarı model sonucu ile karşılaştırılmıştır. Gözenekler içerisindeki etanolun sürekli süper kritik CO_2 ortamında akış ile uzaklaştırılması için öngörülen bu modelin deneysel çalışma ile elde edilen sonuçlar ile iyi bir şekilde uygunluk sağladığı bulunmuştur. Buna ilaveten bu çalışmada, deneysel veriler kullanılarak, kütle transfer katsayı değeri tayin edilmiştir ve bu değer literatürde var olan, süper kritik kurutma için elde edilmiş korelâsyonlar ile karşılaştırılmıştır. Tahmin edilen ve hesaplanan değerlerin birbirine yakın olduğu bulunmuştur.

Karbon dioksit ile süper kritik kurutma için geçerli olan model denklemler sonlu farklar yöntemi ile kullanılarak MATLAB programı yardımı ile çözülmüştür. Sıcaklık ve kütle transfer katsayısı gibi işlem parametreleri ile gözenekli, dolambaçlı yapısı ve jel kalınlığı gibi jel özelliklerinin kesikli kurutma sisteminde kurutma süresine etkisi simülasyonlar kullanılarak araştırılmıştır. Kütle transfer katsayısı ve jel boyutlarının ekstraksiyon süresini en çok etkileyen parametreler olduğu sonucuna varılmıştır. Artan kütle transfer katsayısı ile süper kritik CO_2 'in difüzyonu için geçen sürenin önemli oranda azaldığı ve artan jel kalınlığı ile bu sürenin arttığı sonucuna varılmıştır.

ACKNOWLEDGEMENTS

First and foremost, I would like to express my special appreciation and thanks to my advisor Prof. Dr. Can Erkey for giving me the opportunity to pursue a master study in his group, his guidance and understanding during my master thesis study at Koç University.

I acknowledge the financial support of European Union (EU) Program for the funding of Nanoinsulate Project EC.00015.02.

I would also like to gratefully and sincerely thank to my thesis committee members Asst. Prof. Dr. Seda Kızılel and Assoc. Prof. Dr. Murat Sözer for their careful reading and comments for my thesis. Additionally, I would also like to express my special thanks to Asst. Prof. Dr. Rıza Kızılel for his invaluable suggestions and comments for my study.

I would like to sincerely thank to my current colleagues Zeynep Ülker, Deniz Şanlı, Metin Karayılan, İbrahim Şahin and Amir Hossein Habibi. I am very grateful to all of you.

My sincere thanks also goes to my friends Ayşe Dilan Çelebi, Ayşe Uğurcan Atmaca, Volkan Balcı, Hasan Şıldır, Caner Nazlı and Fatih Rahim for all encouragement and supports during writing period of this thesis. I am truly happy for your sincere friendship.

I would like to especially thank my family for their love, patience and continuous support they have given me throughout my entire life; I could not have done it without you. Finally, I would like to thank to my little and lovely nephew Efe Rüzgar Özdemir for his presence and endless effort to make me happier.

TABLE OF CONTENTS

LIST OF TABLES

LIST OF FIGURES

NOMENCLATURE

1:	CO_2
2:	Ethanol
C_a	Concentration of ethanol in pores (kmol/ m^3)
C_e	Concentration of CO_2 in pores (kmol/ m^3)
C_i	Initial concentration of ethanol in the pores (kmol/m^3)
Ca_s	Concentration of ethanol at the surface of gel (kmol/m^3)
C_v	Concentration of ethanol in bulk flow of sc-CO_2 in vessel (kmol/m^3)
V_{pore}	Pore volume of the gel network,
V_{total}	Total volume of the gel structure
A_{pore}	Surface area of pore
Na	Molar flux of ethanol (kmol/m^2s)
Ne	Molar flux of sc-CO_2
$C_{e,s}$	Concentration of sc-CO_2 on the surface of the aerogel
$C_{surface}$	Concentration of ethanol on cylindrical rod gel surface
v_z	Velocity of sc-CO_2 flow through high pressure vessel
Q	Volumetric flow rate of sc-CO_2 flow in high pressure vessel
$\dot{m}$	Mass flow rate of the sc-CO_2 in high pressure vessel
ε	Porosity of gel structure
D	Diameter of wet gel (cm)
R	Raius of high pressure vessel (cm)
l	Length of cylindrical wet gel (cm)
T	Time (s)
ρ	Density (kg/m^3)
μ	Viscosity (Pa·s)
D_e	Effective Diffusion Coefficient (m^2/s)

D^{g}_{21}	Diffusion coefficient of CO_2 in ethanol (m^2/s)
D^{l}_{12}	Diffusion coefficient of ethanol in CO_2 (m^2/s)
r	Radius of wet gel (cm)
σ	Liquid-vapor interfacial surface tension,
θ	Contact angle at which the liquid-vapor interface meets the solid surface
Θ	Rate of contraction of the pores
$\dot{e}_s$	Syneresis strain rate
K_G	Bulk viscosity of the gel network
D	Permeability of the gel
η_L	Liquid viscosity
Π	Permeability factor
$\dot{x}_2$	Solvent association parameter
M_2	Molecular weight of solvent

Chapter 1

INTRODUCTION

Silica aerogels are nanoporous materials noted for having the lowest density of any solid. Their nano-scale structure gives silica aerogels several unique properties. They have large internal surface area, large pore volume, interconnected pore structure, high porosity, low apparent density, high thermal insulation value and low dielectric constant [1, 2]. These properties based upon the open texture of these materials make them outstanding for a wide variety of applications. Silica aerogels are produced by a set of chemical reactions resulting first in a sol and subsequently in a gel and the liquid solvent is then eliminated from the wet gel formed, which is drying of the gel. Evacuation of the liquid solvent in the pores of the wet gel in such a way to avoid pore collapse preserving original intact, porous texture of the wet gel material is the most complex step in aerogel production. Solvent removal from the porous gel structure of the wet gel without shrinkage and any physical damages on the porous gel structure can be achieved by supercritical drying technique [2].

However, the supercritical drying is a complex and the most time consuming step in crack-free aerogel production. Therefore, drying time of the wet gel has a direct and substantial impact on the production cost.

Therefore, an understanding of the drying process is crucial to provide information about scale-up and optimization of the process. As a consequence, drying times of the wet gels can be shortened and thus, less expensive aerogel production can be achieved. Despite the dependence of aerogel production on supercritical drying, there has been hardly any study on transport phenomena of drying with supercritical CO_2 in the literature. In this study, the goal is to understand of the drying process to obtain information about scale-up

and optimization of the process by formulating and solving mass transfer model equations governing the supercritical drying process in batch and continuous supercritical drying. As a result of this objective, drying times of the wet gels can be accelerated and thus, more economically feasible aerogel production can be achieved.

Chapter 2, Chapter 2 provides necessary literature review and background on silica aerogels, supercritical fluids and supercritical extraction, respectively. Properties of silica aerogels and their production methods are firstly explained. Subsequently, a general overview about the supercritical extraction and supercritical fluids for a better understanding of the following sections are given. Then, the previous studies into the supercritical extraction and previous models for prediction of alcogel drying time in the literature are reviewed.

Experimental method to synthesis silica wet gel rod and supercritical drying of it drying are described in Chapter 3. Thereafter, proposed mechanism underlying batch and continuous supercritical drying and mass transfer modeling including derivation of governing model equations are presented. The following chapter includes all results of mathematical modeling and experimental data of supercritical drying of silica wet gel rod. It includes the simulation results investigating effect of operation variables, including temperature, mass transfer coefficient, gel porosity and tortuosity, as well as thickness of the gels on drying time in the batch supercritical drying as well as the entire simulation results of continuous supercritical drying of the cylindrical wet gel consisting of concentration profiles in the gel and in the bulk flow of supercritical CO_2 in the vessel as a function of time and position.

The thesis is concluded with a short summary of the total work performed and any discussion which was made using the results presented in the previous Chapter.

Chapter 2

LITERATURE REVIEW

2.1 Silica Aerogels

Silica aerogels, continuous network of microscopic beads or connected strand chains, are nanoporous solid materials with several unique properties [1]. These materials have interconnected open pore structure, large internal surface area, large pore volume, high porosity, low density, low thermal conductivity and low dielectric constant [1, 2]. The properties of silica aerogels are also summarized in Table 2.1.1.

These versatile nanoporous materials are synthesized from a wide range of molecular precursors using traditional sol-gel chemistry followed by removal of solvent from the gel network using special drying techniques to produce so-called xerogels, aerogels and cryogels [2, 3]. The resulting materials maintain the very unusual porous texture which they had in the wet stage. These nonporous materials are metastable and they often go through a structural evolution by chemical transformation during aging step in a liquid medium and/or heat treatment [4].

Aerogels may combine the properties of being highly divided solids with their metastable character, resulting in their development as very attractive physical and chemical properties not achievable by other means of low temperature soft chemical synthesis [2, 4]. The particularly remarkable properties of aerogels result from the unusual

flexibility of the sol-gel processing, coupled with original drying techniques. As a result, they form a new class of solids to be used in a wide range of applications [1-4].

In the past few years, aerogels have drawn increasingly more attention in numerous scientific and technological fields due to their outstanding properties based upon the open texture of these materials. They have been found to be ideal candidates for broad range of advanced applications [4, 5]. Monolithic silica aerogels are used as Cherenkov detectors due to their good optical properties such as transparency and low refractive index [5]. As these materials have very low thermal conductivity, their use as transparent, thermal, optical and acoustic insulators, in space vehicles or in constructions have been becoming more and more common and important [5,6]. Silica aerogels are also suitable for use as catalytic supports, adsorbents and sensors because of their high porosity and low density characteristics [7]. These materaials can also be used as inter-metal dielectric materials because of their favorable electrical properties [7, 8].

Table 2.1.1: Typical Properties of Silica Aerogels

Property	Value	Comment
Density	0.003-0.1 g/cm^3	Lowest density solid [2]
Porosity	80-99.8%	High porosity [4]
Surface Area	500-1200 m^2/g	Determined by Nitrogen Adsorption/Desorption (BET) [2,5]
Mean Pore Diameter	20-150 nm	Mostly in mesoporous range [2]
Thermal Conductivity	0.013-0.040 W/m.K	High thermal insulation property[2, 7]
Thermal Tolerance	Up to 500 ^{o}C	Shrinkage starts at 500^{o}C and increases with temperature. Melting point is 1200 ^{o}C [7]
Dielectric Constant	1.0-2.0	Low for a solid material [2]
Sound Velocity	100 m/s	One of the lowest velocities for a solids[2]
Poisson's Ratio	0.2	Independent of density, similar to the dense silica [7]
Young's Modulus	0.002-100 MPa	Very small compared to dense silica (10^4MPa) [8]

The gel porous network is the key feature for their use in these various applications. Thus, it is important to remove the solvent, residues and the unreacted chemicals in the pores of the gel from the network in a way that the internal textural properties of the gel are preserved. As solvent evaporates from the gel network, the curvature of vapor-liquid

interface changes and the curvature of the meniscus decrease with time, which is shown in Figure 2.1. As a consequence, capillary force occurs [9, 10].

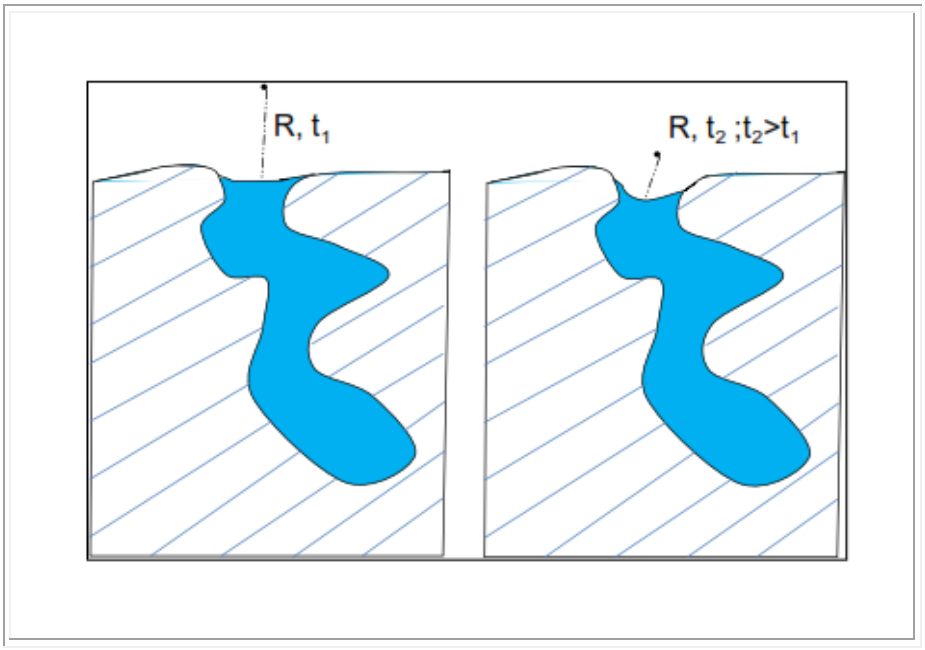

Figure 2.1.1: Change in liquid-vapor meniscus radius as a function of drying time at the pore surface

The pressure difference between the liquid and vapor phase can be given by Laplace's equation.

$$\Delta P = -\frac{\sigma \cos\theta}{R} \qquad \text{(Eq. 2.1)}$$

where σ is the liquid-vapor interfacial surface tension, R is the meniscus radius and θ is the contact angle at which the liquid-vapor interface meets the solid surface. The presence of this interface results in compression stresses. Due to the high capillary pressure induced

upon solvent evaporation and the fragility of the gel structure, cracks and shrinkages are formed on the gel structure. This pressure induced during drying is directly related to surface tension value. It can be reduced by using a solvent which has a low interfacial surface tension value. Table 2.1.2 shows the interfacial surface tension of some fluids which can be used as a solvent for the gel [9]. However, since the capillary force depends also on the radius of the capillary, pore radius, which is in the nano-scale, the capillary forces induced by the lowest possible interfacial surface tension will be large enough to damage the textural structure of the gel. Figure 2.1.2 shows the capillary forces created by different solvents as a function of the pore radius, assuming θ is zero. As can be seen in this figure, the capillary forces are decreased using solvents with lower surface tension, however, the capillary forces can be extremely large as much as several thousands of bars [10]. Moreover, a gradient of the capillary forces is formed because of the pore size distribution, leading to inhomogeneous distribution of the forces acting on the fragile porous gel structure, which certainly causes the destruction of the network.

Table 2.1.2: Interfacial surface tension of some fluids

Solvent	**σ (mN/m)**	**T(°C)**
Water	72.8	20
Acetone	25.20	20
Acetonitrile	29.10	20
Methanol	22.61	20
n-Hexane	18.43	20
Carbon dioxide	1.16	20
Nitrogen	6.6	-183

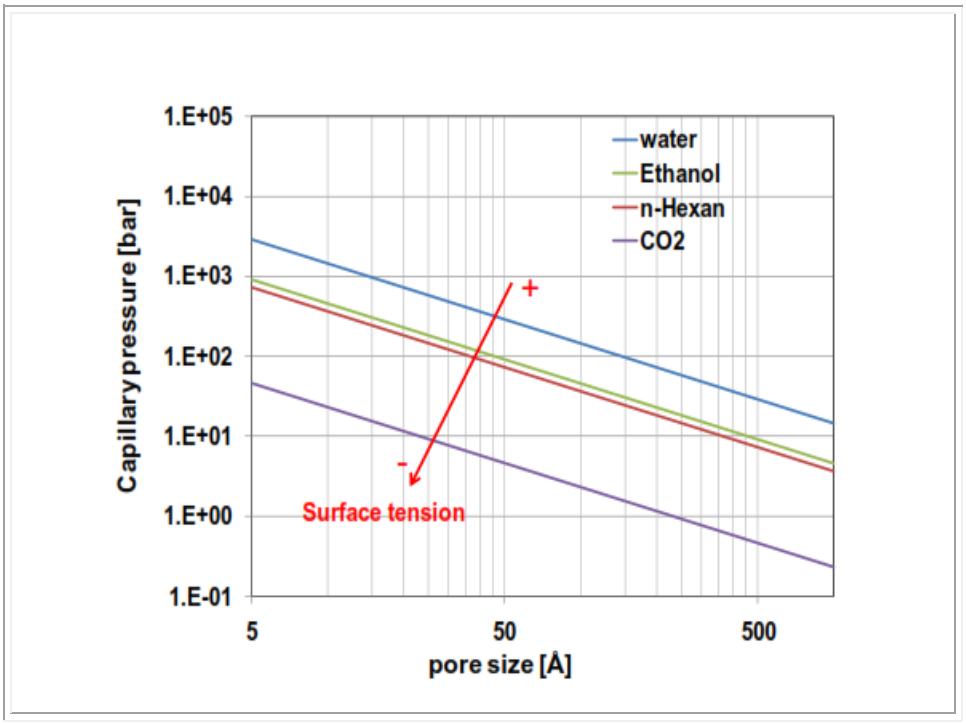

Figure 2.1.2: Capillary pressure of different solvents at different pore sizes

2.1.1 Aerogel Production

Aerogel materials are produced using sol-gel technology. A typical two step sol-gel process is also summarized in Figure 2.1.1.1 It can be seen that three main steps are followed to produce aerogel: 1) mixing the precursors and the formation of the sol 2) gelation of the sol solution and aging of the gel 3) extraction of the solvent from the gel. [11, 12].

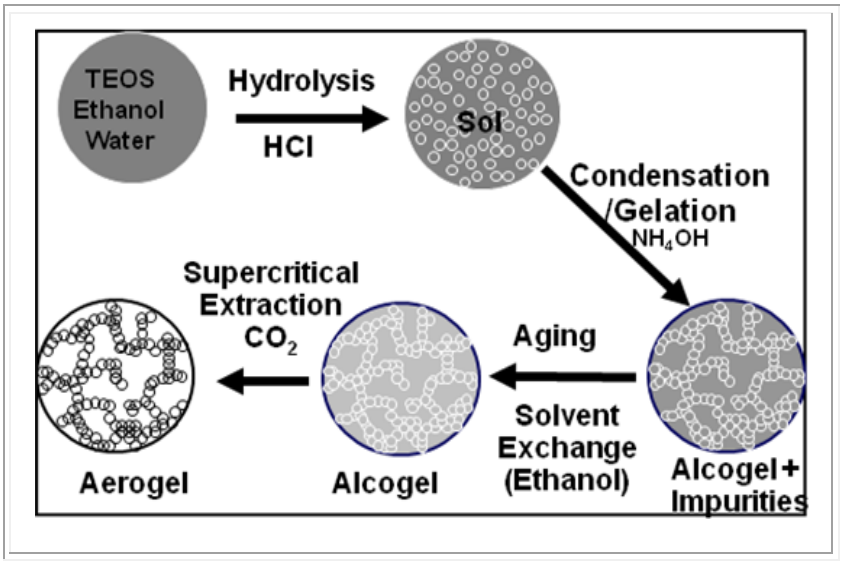

Figure 2.1.1.1: Main steps in two step sol-gel process

2.1.1.1.1 Sol

As a result of the set of chemical reactions, a colloidal particles, dispersed within the solution and having partial internally crosslinked structures are formed. This colloidal suspension is known as the "sol" (Figure 2.1.1.1.1 (a)). A sol is an independent colloidal suspension of tiny particles or polymers with a size range of ~1-1000 nm suspended in a liquid. These particles have partial internally crosslinked structures. Understanding of the mechanisms behind the sol formation gives the tool to master and control the gel properties and eventually, the aerogels properties.

As a result of mixing silica precursors with a hydrolysis agent and a solvent, the sol of silica particles is obtained [13, 14].

2.1.1.1.2 Gel

Further reactions after sol formation result in connecting these particles. Subsequently, the sol converts to a structure, interconnected rigid network consisting of submicrometer sized pores filled with liquid phase and chains whose average length is greater than a micrometer, is formed [12]. This structure is called as "gel". This gel is composed of three dimensional silicon oxide arrangement entirely filled with a liquid [12, 13]. If the pore liquid is an alcohol used in the process, the final material is named as alcogel (Figure 2.1.1.1.1 (b)). The subsequent step is aging in which the wet gel is strengthened [14].

2.1.1.3 Precursors

Silicon alkoxides are the most commonly used precursors for the sol gel process. They react readily with water. Tetramethyl orthosilicate (TMOS) and tetraethyl orthosilicate (TEOS) are the most popular among them. These organic precursors have partial positive charges that make them less susceptible to nucleophilic attack [12-14]. TMOS undergo fast hydrolysis and condensation reactionsresulting in the fast formation of a stable gel. However, it is toxic and expensive. TEOS is less toxic and is a cheaper precursor than TMOS. In addition, the hydrolysis of Tetramethylorthosilicate (TMOS) is faster than that of Tetraethylorthosilicate (TEOS). The reason is that TEOS has bulkier ethoxide groups (compared to methoxide groups of TMOS) that slow the process of hydrolysis [4, 14, 15]. Bulkier alkoxide groups exert more effect on the rate of the hydrolysis since larger groups create more steric hindrance and they overcrowd the transition state leading to a slower reaction.

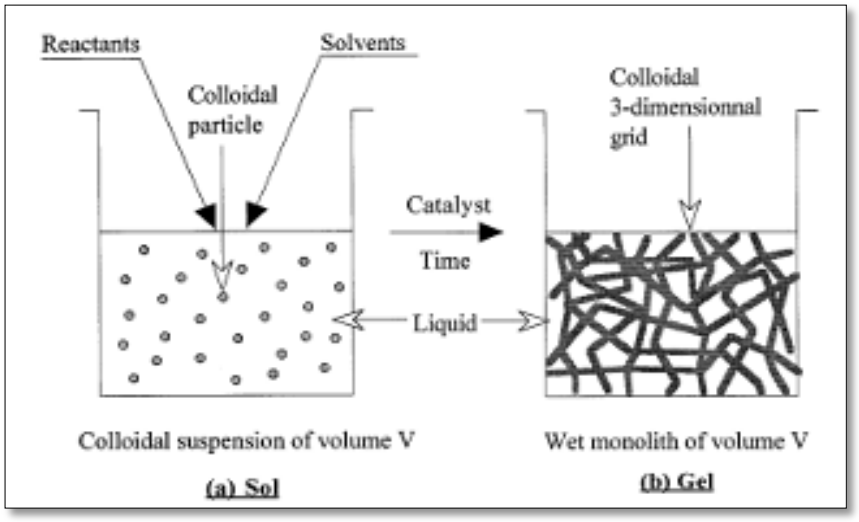

Figure 2.1.1.1.1: The sol-gel process: (a) Sol; (b) Gel [4].

2.1.1.2 Reaction Mechanism of the Sol Formation

2.1.1.2.1 Hydrolysis

Hydrolysis is the primary step of the sol-gel process. Alkoxide groups (OR) of the organic precursor -$Si(OR)_4$- are replaced by hydroxyl groups (OH) one by one with the help of a acid catalyst forming the silanol groups (Si-OH).

As a result a hydroxyl group is attached to the metal (silicon) as shown in the following reaction:

$$Si(OR)_4 + 4H_2O \rightleftharpoons Si(OH)_4 + 4ROH \qquad \text{(Eq. 2.1.1.2.1)}$$

where R represents the alkoxide group. The reverse process is called esterification. Depending on the presence of water molecules and the catalyst in the media, the reaction

can go towards complete hydrolysis, or stop resulting in a partially hydrolyzed alkoxide. Rate and extent of the hydrolysis depend upon the strength and the concentration of the catalyst as well as the temperature and the choice of the solvent. [13, 14].

The replaced alkoxide group of the precursor appears in the alcohol corresponding to it. Since water is immiscible with alkoxysilanes due to the hydrophobicity of the alkoxide groups, alcohols, such as ethanol and methanol are also added into the sol to achieve the miscibility between the constituents. Ternary phase diagram of ethanol/water/alkoxide combination given in Figure 2.1.1.2.1 can be used to determine minimum amount of alcohol required to achieve miscibility along the required stoichiometry between the organic precursor and water (for a homogeneous mixture) [16, 17].

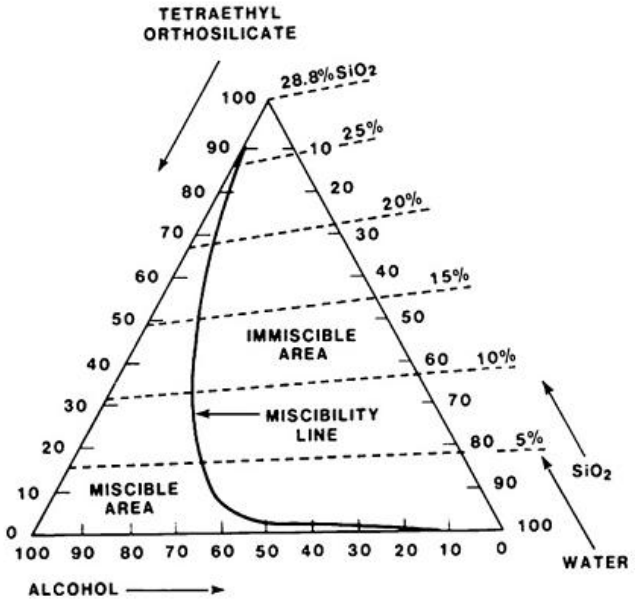

Figure 2.1.1.2.1: Ternary Phase Diagram of TEOS-Ethanol-Water system at 25^{o}C [2].

2.1.1.2.2 Condensation

Upon the reaction silanol groups (Si-OH) is formed in hydrolysis reactions, these silanol groups (Si-OH) connect to each other leading to formation of a siloxane bridge (Si-O-Si) [17]. Each Si molecule can make up to 4 siloxane bridges, allowing many small molecules to join together forming a giant molecules with thousands of Si-O bridges. These molecules assemble to form the silica nanoparticles. The polymerization reactions leading to the formation of siloxane bonds is condensation reactions [17, 18].

Condensation reactions occur simultaneously with hydrolysis reactions as soon as hydrolyzed species appear in the solution. Two partially hydrolyzed molecules may combine by condensation reaction forming water or alcohols. These reactions are classified in two different types such as water condensation (Eq 2.1.1.2.2.1) and alcohol condensation (Eq 2.1.1.2.2.2), given below. The reverse reactions are hydrolysis and alcoholysis, respectively [18].

$$HO\text{-}Si\text{-}(OR)_3 + HO\text{-}Si(OR)_3 \longleftrightarrow (OR)_3Si\text{-}O\text{-}Si(OR)_3 + HOH \quad \text{(Eq 2.1.1.2.2.1)}$$

or

$$HO\text{-}Si\text{-}(OR)_3 + HO\text{-}Si(OR)_3 \longleftrightarrow (OR)_3Si\text{-}O\text{-}Si(OR)_3 + ROH \quad \text{(Eq 2.1.1.2.2.2)}$$

Several thousand of the reactions of 2 and 3 can take place leading to formation of a giant molecule with a size of few nanometers by the so-called polymerization reaction:

$$n[Si\text{-}(OR)_4 + Si\text{-}(OR)_4] \longleftrightarrow n[(OH)_3Si\text{-}Si(OH)_3] + 2nH_2O \quad \text{(Eq 2.1.1.2.2.3)}$$

2.1.1.2.2.1 Gel Formation

Gel formation is the last step of the condensation reactions [18]. The gel forms when the sol loses its fluidity and takes on the appearance of an elastic solid accompanied by a great increase in its viscosity. This process can be simply explained in a way that upon hydrolysis and condensation siloxane bridges between silicon molecules is built [17-19]. As a consequence, large number of silicon molecule interconnects forming the primary nanoparticles that form the sol. The size of these primary particles eventually finish to grow instead they agglomerate with another primary particle nearby, forming clusters of the particles. It can be envisaged that these clusters swim in the solvent. As a result of collision with another cluster, it is possible to form bridges connecting these clusters together. The gel point is a statistical event indicating the first appearance of a cluster that covers the vessel holding the sol [18-20].

2.1.1.2.3 Aging of the Gel

After gel is formed when the last span cluster bonds to three dimensional network, the formation of new siloxane bonds (Si-O- Si) still continues because of the flexible hydroxyl free groups (Si–OH), on the surface of the gels. Condensation processes continue within the network if the silanols are close enough to react with each other. This process increases the connectivity of the network and its fractal dimension. When the gel is kept in its pore liquid for a period of time, which is called aging, its structure, the composition, properties of the gel continue to change with time even after its gelation point [18-20]. Aging is characterized by increasing the stiffness of the gel. This can be understood by knowing the three main processes involved in the aging step: (1) polymerization; (2) syneresis; (3) ripening [21].

As condensation reactions proceed, the increase in bridging bonds results in contraction of the gel network. Syneresis is the shrinkage of the gel and the resulting expulsion of the solvent (alcohol, water) from the pores in alcoholic gel structure. Consequently, the bridging bonds within the network increases and it causes shrinkage of the gel pores [20]. Furthermore, these new bonds may occur between two flexible chains while coming in contact, resulting in increasing the stiffness of the gel as well as extensive shrinkages. Effect of syneresis on the shrinkage of the gel is illustrated in Figure 2.1.1.2.3 [22].

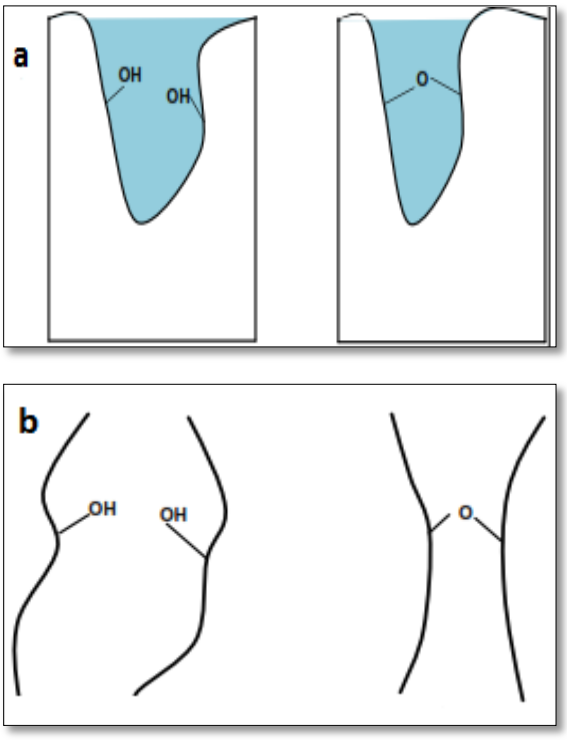

Figure 2.1.1.2.3: Syneresis scenarios: a) bonds between two neighboring molecules resulting in shrinkage upon relaxation of the new bond, b) two flexible chains may connect resulting in restriction the extent of flexibility and extensive shrinkage.

When necks between particles grow and small pores may be filled in, the average pore size of the gel increases and the specific surface area decreases. As a result of this decrease of the surface area, coarsening occurs [22].

Aging processes, during which wet gels are placed into suitable solutions, are applied after the gelation step. The gelation time is accepted as the moment when the last bond is formed in the chains constituting the spanning cluster. After gelation occurs, condensation reactions do not stop but continue because of the flexible hydroxyl groups on the surface of the gels [20, 21].

Aging of the wet gel is essential to give the gel stability and mechanical strength to withstand the following drying step to obtain aerogel. As a result of aging process, stiffer and stronger networks by forming new bridging bonds are created [23].

2.2 Supercritical Fluid Drying

Supercritical fluid drying is basically removing liquids from materials with assistance of supercritical fluids [24]. In this process, the liquid in the subastance is replaced with a gas isolate the solid component from the substance without destroying the material's fragile nanaostructured pore network. This because supercritical drying is performed in the absence of surface tension and capillary pressure. Therefore, supercritical drying is commmonly applicable to porous material with delicate structures such as the dendrites in aged silica gel to produce aerogel, tiny machinery of microelectromechanical devices and cell walls. Supercritical drying is also called supercritical extraction.

2.2.1 Supercritical Fluids

Under atmospheric conditions, materials can be found in three different states: solid, liquid and gaseous. A fourth state, called supercritical, can be achieved by tuning temperature and pressure above critical point. A critical point, also known as a critical state, occurs under conditions, such as specific values of temperature, pressure, or composition at which no phase boundaries exist [24, 25].

Every substance has a critical temperature (Tc) and pressure (Pc) above which no applied pressure can force the substance into its liquid phase, as shown in Figure 2.2.1. A supercritical fluid is a fluid at a temperature and pressure higher than or equal to its critical temperature and pressure. Supercritical fluid is described loosely as a solvent above their critical temperatures because under those conditions the solvent exists as a single phase regardless of pressure.

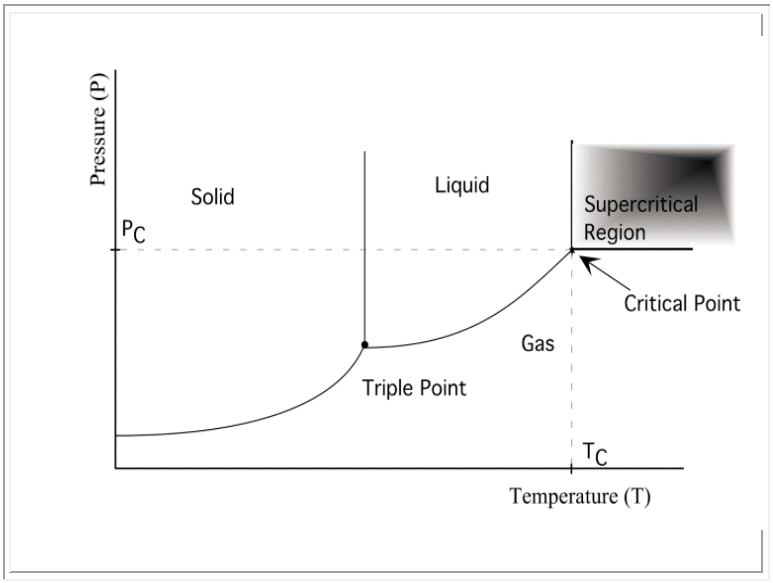

Figure 2.2.1: Schematic Pressure-temperature diagram for a pure component [26].

The fluid can be defined as neither a gas nor a liquid. These fluids show gas-like transport properties and liquid-like density under normal working pressures since at the critical point, there is no distinction between the phases; the density of the gas and liquid phases is the same. They can spread out along a surface more easily than a true liquid because they have lower surface tensions than liquids [27]. The transition from a gas-liquid state to a supercritical state can be visualized by the disappearance of the meniscus between two phases, as it becomes one phase. Figure 2.2.2.6 shows evolution of CO_2 to supercritical conditions in a liquid-vapor equilibrium high-pressure cell, as it can be observed that two phases are initially obviously distinct and then, the meniscus disappears and as temperature increases [28, 34].

As can be seen form Table 2.2.1, in which characteristic values for the gaseous, supercritical fluid and liquid state are listed, in the supercritical state, liquid-like densities are approached while viscosity is near that of normal gases and diffusivity is about two orders of magnitude higher than in typical.

Supercritical fluids maintain the property of a liquid to dissolve substances, which a gas cannot do. The solvating power of the fluids can be modified by changing the pressure or temperature, or by adding co-solvents [28, 29]. Since the properties of the supercritical fluid can be changed by adjusting the temperature and pressure in the vicinity of the critical point, they become equivalent of a series of different solvents, hence providing selective extraction properties. Moreover, separation of compounds from a mixture by using either vapour pressure or polarity differences between the compounds can be achieved by many supercritical fluids since the solubility of a solute in supercritical fluids can also be adjusted significantly by adding one or more extra solute and/or solvent, leading to substantial enhancement of polarity of the SCFs without affecting the supercritical condition [28, 33].

The solubility behavior of many compounds in SCFs is rather general. At high pressure an increase in temperature enhances the solubility, while at lower pressures the

opposite effect occurs. The changes in density of a pure substance near its critical point can be seen in Figure 2.2.4 (relative critical pressure) [25]. The density of a pure supercritical fluid is easily modified by relatively tiny changes in pressure or temperature near the critical point, hence, the solubility power of the supercritical fluid changes.

Brogle (1982) discovered that the solvating power of the supercritical fluid is highly dependent on temperature and pressure. At low pressure, the solvent power of CO_2 surprisingly decreases with rising temperature whereas at high pressure it which is illustrated in Figure 2.2.2 [24].

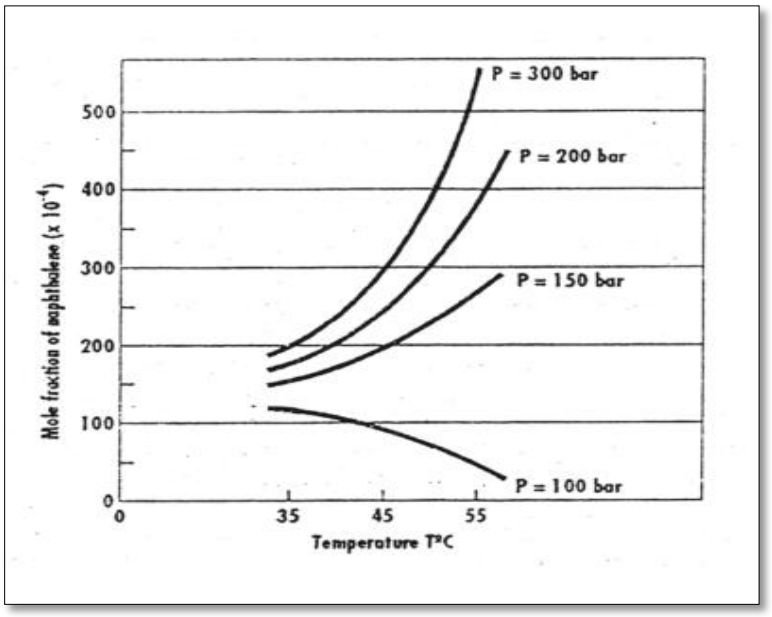

Figure 2.2.2: Solubility (mole fraction) of Naphthalene in CO_2 as a function of temperature at various pressures [24].

Furthermore, relationship between density and pressure can be explained as follows. At a reduced temperature ($T_R=T/T_C$), from 0.9 to 1.2, small increase in reduced pressure ($P_R=P/P_C$) will result in a dramatic increase in solvent reduced density ($\rho_R=\rho/\rho_c$) from 0.1 which is close to gas density to 2.5 which is near liquid density. This is shown in Figure 2.2.3. Since solvent reduced density becomes near liquid density, supercritical fluid acts as a liquid solvent. Thus, supercritical fluid properties can be altered from gas which has low solvent power to liquid which is higher solvent power by changing temperature and pressure values [25, 26]

Table 2.2.1: Generalized Physical Properties for Gas, Liquid and Supercritical Fluids [25]

State of Fluid	**Density (ρ,g/cm^3)**	**Diffusivity (D_{AB},cm^2/s)**	**Viscosity (μ,gs/cm)**
Gas P=1 atm; T= 21 °C	10^{-3}	10^{-1}	10^{-4}
Liquid P=1 atm; T= 15-30 °C	1	$<10^{-5}$	10^{-2}
Supercritical $P=P_c$; $T=T_c$	0.3-0.8	10^{-3}-10^{-4}	10^{-4}-10^{-3}

The most frequently used supercritical fluids and their properties are given in Table 2.2.2.

Table 2.2.2: Critical Properties of Various Solvents [25]

Substance	T_c (K)	P_c (MPa)	Critical Density (g/cm^3)
Methane	190.6	4.60	0.162
Ethylene	282.4	5.03	0.218
Chlorotrifluromethane	302.0	3.92	0.579
Carbon dioxide	304.2	7.38	0.468
Ethane	305.4	4.88	0.203
Propylene	365.0	4.62	0.233
Propane	369.8	4.24	0.217
Ammonia	405.6	11.30	0.235
Diethyl ether	467.7	3.64	0.265
n-Pentane	469.6	3.37	0.237
Acetone	508.1	4.70	0.278
Methanol	512.6	8.09	0.272
Benzene	562.1	4.89	0.302
Toluene	591.7	4.11	0.292
Pyridine	620.0	5.63	0.312
Water	647.3	22.0	0.322
Xenon	289.7	5.84	1.113

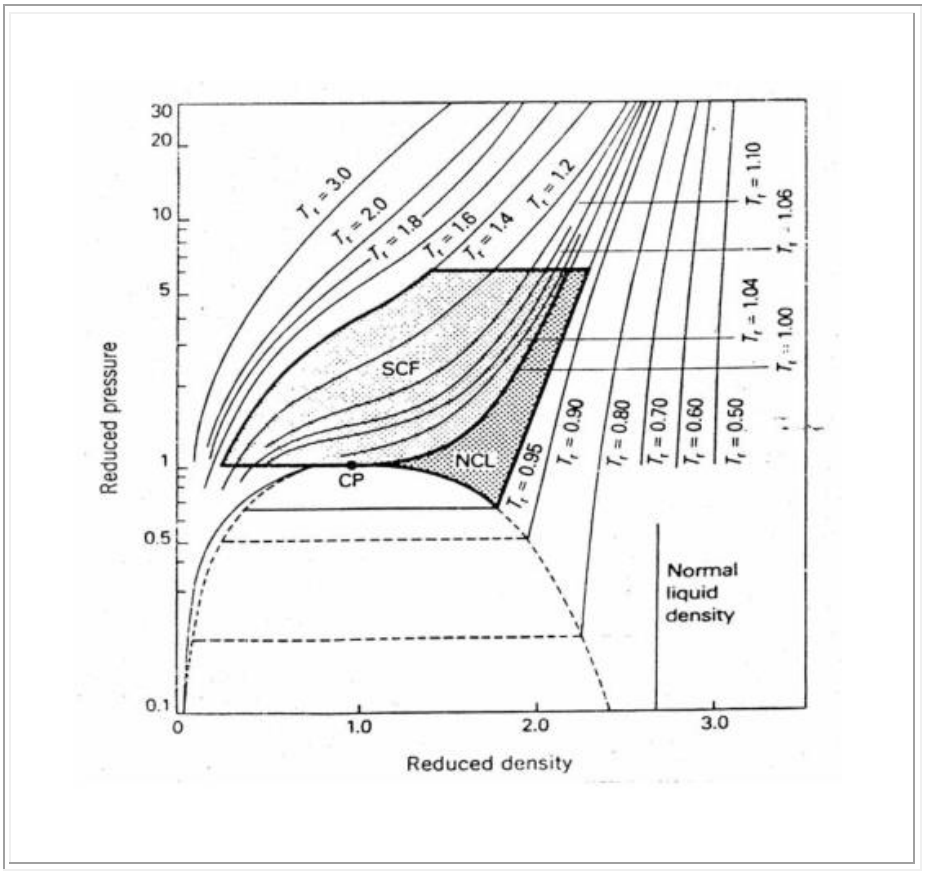

Figure 2.2.3: Variation of the reduced pressure (P_R) with density (ρ_R) of a pure component at various temperatures (T_R) [26].

ρ_R= Relative critical density

T_R= Relative critical temperature

P_C= Critical pressure

T_C= Critical temperature

ρ_C= Critical density

The viscosity behavior of the supercritical fluids comparing gas and liquid viscosity characteristics is explained as follows.

The viscosity of gases at low density is independent of pressure and is a function of temperature. In this case, the viscosity is proportional to the square root of the absolute temperature, T, and dilute gases become more viscous at higher temperatures. This behavior of the gases can be explained trough simple kinetic theory. In this theory, the gaseous viscosity of spherically symmetric monatomic molecules at low pressure is described by the following equation [25-27]:

$$\mu = \frac{\rho v l}{3} \qquad \text{(Eq 2.2.)}$$

where ρ is density of the gas, v is average velocity of monatomic molecule and l is the mean free path. Average velocity of a monatomic molecule is proportional to $T^{1/2}$; therefore, the viscosity of the gas is also proportional to $T^{1/2}$.

Viscosity of liquids decreases exponentially with increasing temperature due to the formation of a hole or increase of the free volume.

Supercritical fluid isothermal viscosity usually increases with increasing pressure. However, it decreases with increase of temperature at a constant pressure up to a minimum as in the case of liquid, then increases with temperature as in the case of a gas at high reduced temperatures. The viscosity of CO_2 as a function of pressure at different temperatures is illustrated in Figure 2.2.4. It can be said that viscosity rises rapidly around the critical state, then increases gradually with increasing temperature and at 380 K viscosity starts to increase smoothly beyond the critical pressure, while at 900 K, pressure variation does not considerably affect. At constant pressure, around critical pressure, viscosity firstly reduces then increases with rising temperature. However, above Pc, viscosity decreases with rising temperature [28-30].

Basically, viscosity changes rapidly in the critical region, even at the high pressure values of 300-400 bar it is only about 0.09 centipoises (cps), an order of magnitude below typical viscosities of liquid organic solvents [30, 32].

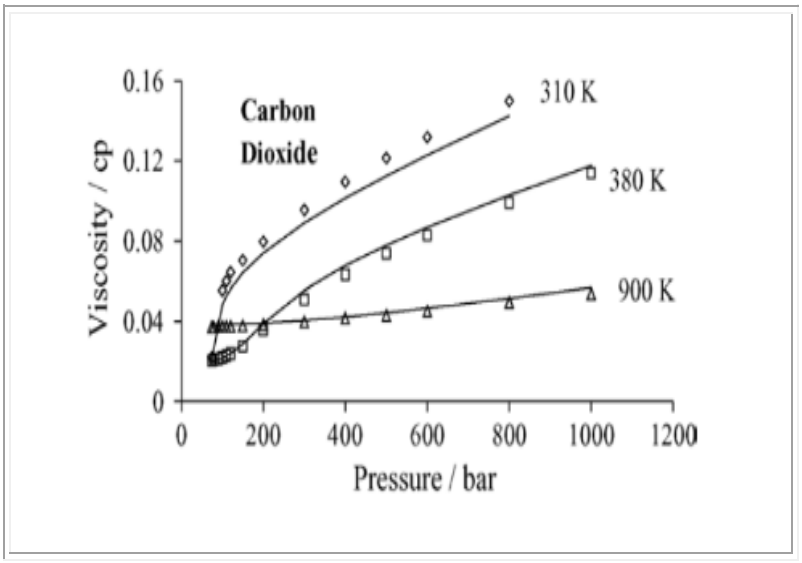

Figure 2.2.4: Viscosity behavior of carbon dioxide as a function of pressure at different temperatures [30]

As for diffusion coefficients in supercritical fluids, it can be said to be intermediate of those in gases and liquids. Figure 2.2.5 illustrates the self-diffusivity of carbon dioxide (CO_2) over a broad pressure-temperature range. Similar to viscosity behavior shown in Figure 2.2.4, diffusivity changes rapidly in the critical region. As the case for density, viscosity and diffusivity values are dependent on temperature and pressure. The viscosity and diffusivity on the supercritical fluid approach those of a liquid as pressure is increased, whereas an increase in temperature brings about an increase in viscosity of a gas, the opposite is valid in the case of supercritical fluids. However, diffusivity will increase in

temperature. As shown in Figure 2.2.4, changes in diffusivity are most pronounced in the region about the critical point. At high pressures, such as 300-400 atm, diffusivity of supercritical fluids differs by 1-2 orders of magnitude from normal liquids [25, 28].

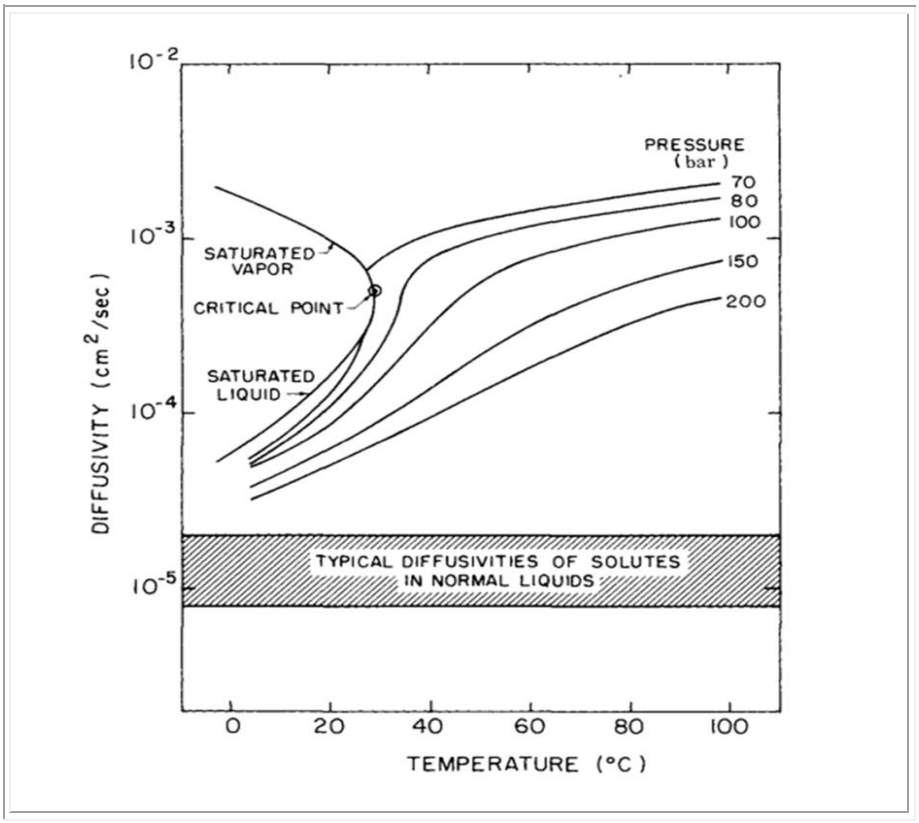

Figure 2.2.4: Diffusivity behavior of carbon dioxide [25].

Non-dimensional numbers such as Reynolds number (flow effect), Prandlt number (for heat transfer), Schmidt number (for mass transfer) and including all of them Nusselt number are usually used to evaluate transfer processes in various media such as mass, energy and momentum transfer. Figure 2.2.5 indicates the general behavior of liquids, gases and supercritical fluids regarding Pr and Sc numbers. As can be seen in Figure 2.2.5,

supercritical fluids are far better than gases in heat and mass transfer. Moreover, Table 2.1.1 demonstrates that a supercritical fluid has the ability to have a higher mass transfer rate than a liquid solvent [32].

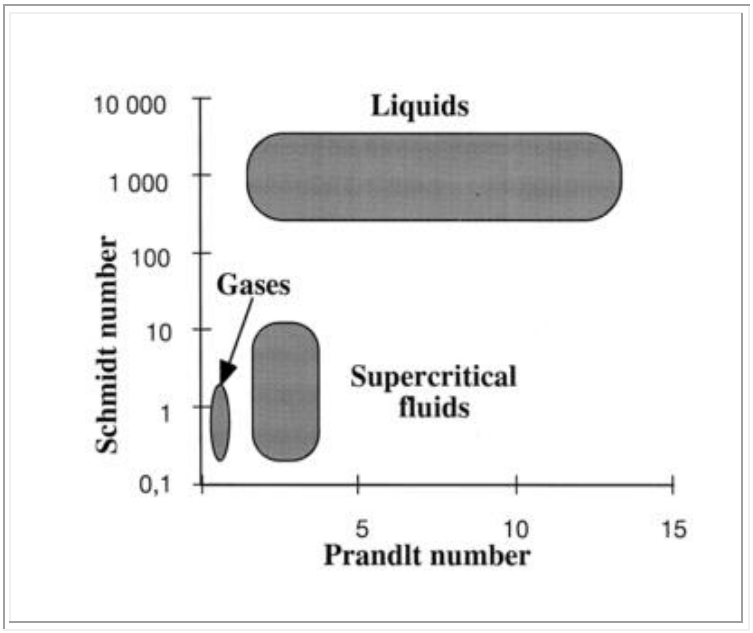

Figure 2.2.5: Transport properties of supercritical fluids [32]

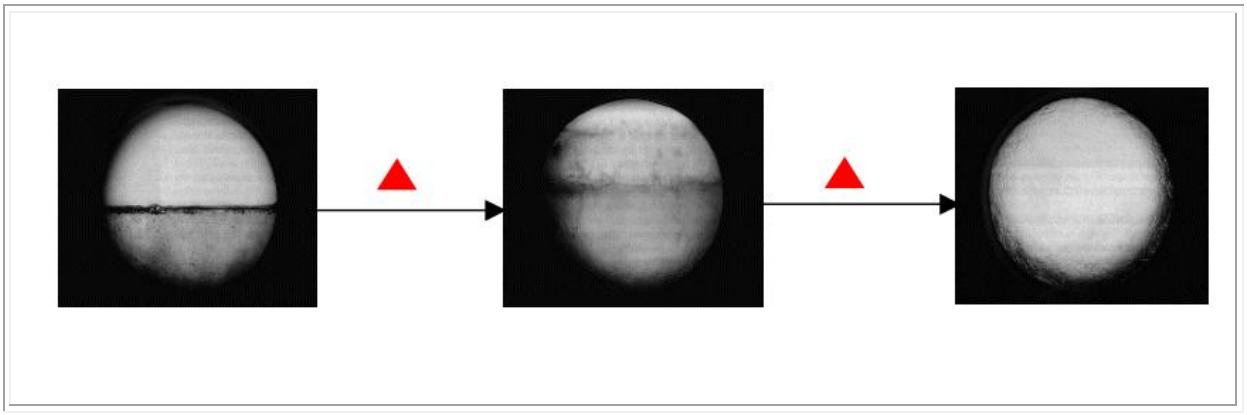

Figure 2.2.6: Liquid-Vapor (L-V) Equilibrium High-Pressure Cell [34].

2.3 Drying of the Wet Gel

2.3.1 Phenomenology

Drying of the wet gel is liquid removal from the pores of the gel. It is particularly important step in sol-gel processing since gels tend to warp and crack. The stages of drying are shown schematically in Figure 2.3.1.1. The initial condition of the gel is illustrated in Figure 2.3.1.1 (a). This is before evaporation begins and meniscus is flat. Figure 2.3.1.1 (b) shows the following steps in drying. The gel consists of a continuous solid network incorporating a continuous liquid phase; the liquid tends to extend over it since the solid-vapor interface has a higher energy ($^{\gamma}_{SV}$) than the solid-liquid interface ($^{\gamma}_{SL}$). As the liquid stretches to cover the solid, tensile stress is created in the liquid and compressive stress is imposed on the solid network. The gel network is so compliant that it collapses into the liquid so that the gel structure shrinks as fast as liquid evaporates, and the liquid-vapor meniscus stays at the exterior surface of the gel. In this stage of drying, the volume of the body reduces by one unit volume for every unit volume of liquid, therefore, the liquid-vapor interface remains at the surface of the body. The force causing the shrinkage of the solid network is the capillary pressure. When evaporation of the liquid from the pores is exposed to the solid phase, a solid-liquid interface is replaced by a more energetic solid-vapor interface. In order to prevent such an increase in the energy of the system, the liquid tends to extend from the inside of the body to cover that interface [35]. Due to the reduction of the liquid volume through evaporation, the meniscus must become curved as illustrated in Figure 2.3.1.2.

The final step in drying is illustrated in Figure 2.3.1.1 (c). As the gel shrinks, stiffness of it increases since the solid network is becoming more densely packed. As the gel stiffens, the pressure in the liquid at exterior (P_e), shown in Eq 2.3.1.1 (b), rises until the

meniscus achieves its maximum curvature. Maximum capillary tension (P_R) in the liquid occurs with the radius of the meniscus which is small enough to fit into the pore [35].

a) Initial condition

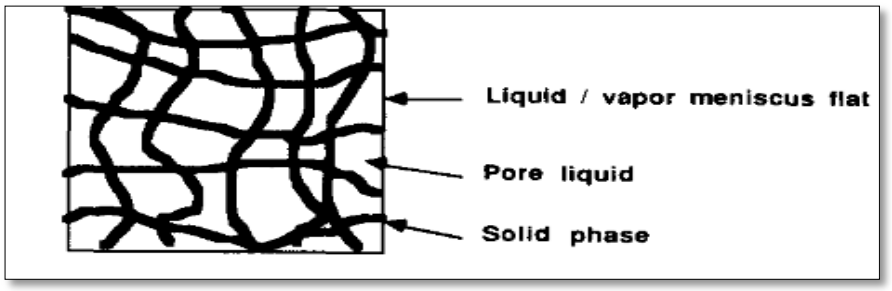

b) Evaporation from surface

Evaporation forms meniscus with a radius r

Pressure in liquid at exterior: $Pe = \frac{2(\gamma_{SV} - \gamma_{SL})}{r}$ (Eq. 2.3.2.1 (b))

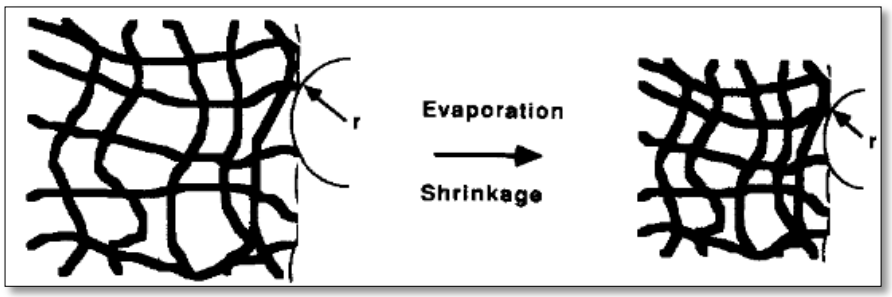

c) Dry region forms

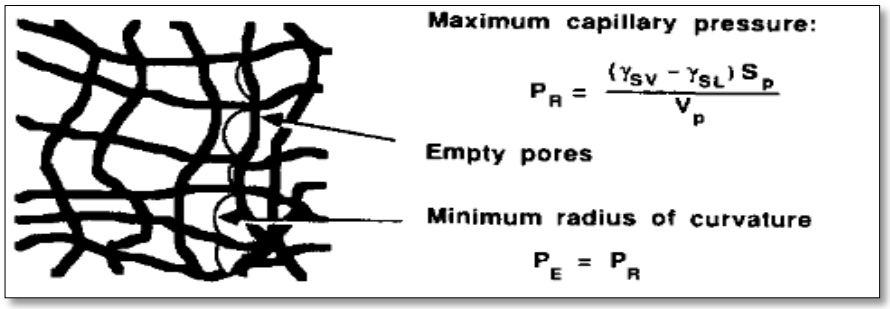

Figure 2.3.1.1 Schematic representation of drying process. S_p and V_p are surface area, respectively

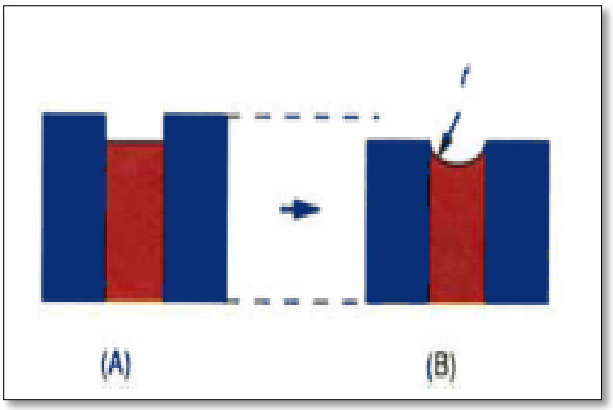

Figure 2.3.1.2 To prevent exposure of the solid phase **(A)** the liquid must adopt a curved liquid/vapor interface **(B)** Compressive forces on the solid phase cause shrinkage.

2.3.1.1 Drying Stress

Drying stress results from a pressure gradient in the pore liquid, therefore, this stress can be calculated with an analysis of the pressure, P in the liquid. For a small region of gel including a volume V_p of liquid filled pores and for a viscous solid network of the gel, then the rate of contraction of the pores (Θ) is calculated by Eq. 2.3.2.2 [35].

$$\Theta = V_p\,(3\dot{e}_s - P/K_G)\,/(1-y) \qquad \text{(Eq. 2.3.1.1)}$$

where $\dot{e}_s$ is the syneresis strain rate, K_G is the bulk viscosity of the gel network (if the liquid were absent), and y is the relative gel network density.

The change in quantity of the liquid (Θ) can be found from Darcy's law [36], given in Eq. 2.3.1.2.

$$\Theta = -\frac{D}{(1-y)\eta_L}\nabla^2 P \qquad \text{(Eq. 2.3.1.2)}$$

where D is permeability of the gel, η_L is liquid viscosity.

Because the volume of the pores must remain equal to the volume of the liquid, the differential equation describing pressure distribution in the pores is obtained.

$$\frac{D}{(1-y)\eta_L}\nabla^2 P - \frac{P}{K_G} = -3\dot{e}_s \qquad \text{(Eq. 2.3.1.3)}$$

Eq. 2.31.3 is solved for a plate of thickness 2L with pressure P_E at the surface neglecting syneresis,

$P(z)= P_E\Pi(\alpha,z)$ (Eq. 2.3.2.4)

$\alpha =(L^2\eta_L/DK_G)^{1/2}$ (Eq. 2.3.2.5)

$\Pi(\alpha,z)$ represents the permeability factor. The parameter α, is a rough evaluation of the pressure gradient in the gel. The pressure distribution is illustrated in Figure 2.3.2.2 for different values of α. As permeability decreases and α increases, pressure gradient becomes steeper [36-37].

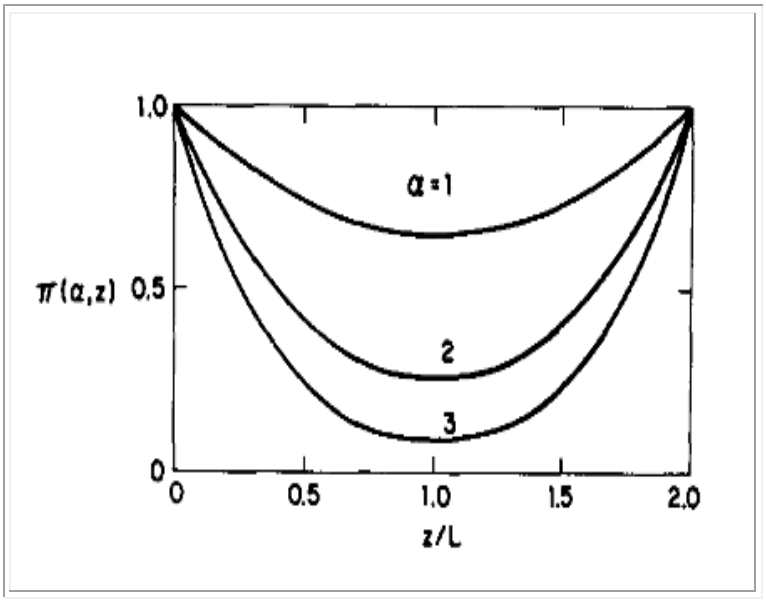

Figure 2.3.2.2: Permeability factor for a plate

During drying, pressure differences through the bulk leads to development of stress. The stress formed can be defined as in Eq. 2.3.2.6 [38].

$$\sigma_x = \frac{V_E L \eta_L}{3D} \quad \text{(Eq. 2.3.2.6.)}$$

where V_E is the drying rate. This equation indicates that the stress is directly proportional to the rate of drying since faster drying involves a greater liquid flux to the surface and therefore a steeper pressure gradient form. Moreover, from this equation, it can be said that the stress increases with the viscosity of the gel network, therefore, the cracking could be reduced by decreasing K_G. However, the structural changes that minimize K_G can also reduce the gel strength, resulting in more fracture in the gel. In addition to aging of the gel increasing the gel strength and therefore, reducing cracking of the gel, it is still required to be dried quite slowly to avoid cracking of any macroscopic piece.

G.W. Scherer et al. proposed that the uniform pressure distribution causes less stress. Figure 2.3.2.3 illustrates the observed behavior of warping of a plate dried by evaporation from one side. The plate initially warps upward due to the capillary pressure leading to more contraction at the upper surface than at the lower; after a dry region forms, the capillary pressure only proceeds on the wet region, resulting in faster shrinkage on the lower surface than the upper surface, and reversing the curvature [35, 38]

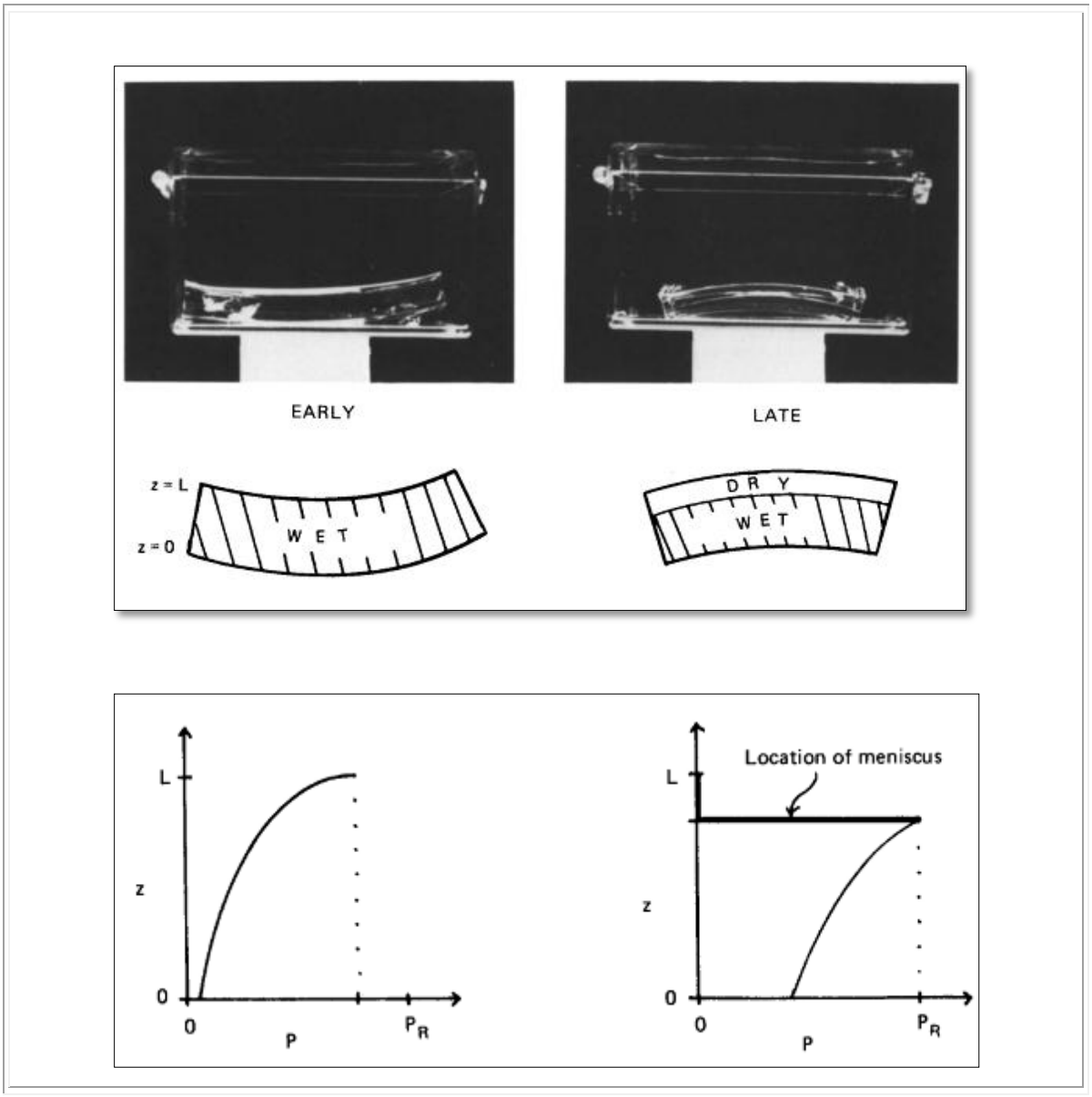

Figure 2.3.2.3 Warping of plate of silica gel dried by evaporation from upper surface

2.3.2 Supercritical Fluid Extraction

Supercritical fluid extraction is basically removal of materials from a medium using supercritical fluids. This process fundamentally consists of two steps: the extraction step and separation step. In the extractor, the supercritical fluid, which is solvent, flows through the feed material and dissolves the soluble components, which are solutes. In the separator, the loaded solution of solvent and solutes is expanded to low pressure and the extract is precipitated [39].

Extraction of the target solutes from solid materials, such as coffee beans is affected by the solubility, transportation through diffusion and the matrix of the solid materials. In extraction of the components from the solid materials, the materials are continuously contacted with a constant flow rate of supercritical fluid solvent [32, 39].

A typical extraction and separation stages necessary for a supercritical extraction is illustrated schematically in Figure 2.3.2.1 [40]. This typical extraction plant includes the following items: **1.** extraction vessel in the extraction stage; **2.** pressure reduction in a throttling section; **3.** separation vessel in separation stage; **4.** increase of pressure by a recycle pump or compressor.

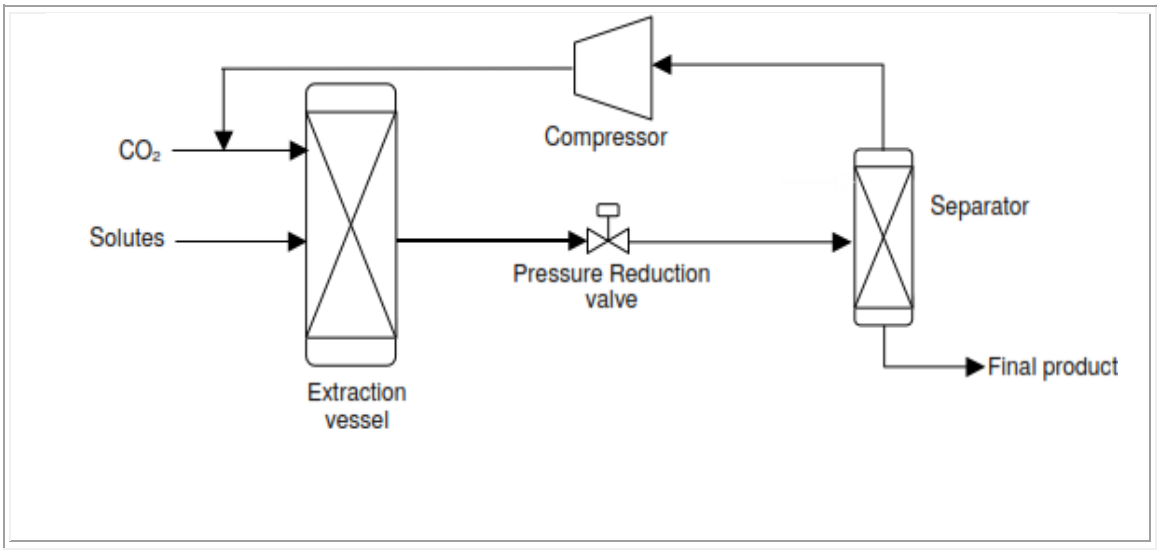

Figure 2.3.2.1: Typical Supercritical Extraction Process

The basic process consists of compressing and heating carbon dioxide to the operating vessel conditions. Raw material is placed into the extraction vessel. The extraction agent is compressed through the compressor and heated to supercritical conditions by a heat exchanger. The solutes dissolve in the supercritical fluid and the highly compressed supercritical fluid removes the extract from the raw material in the extraction vessel. The loaded supercritical fluid leaves the extractor and undergoes pressure reduction through throttling and enters a separation vessel in which the solutes and solvent separate. The gas is then recompressed to the supercritical operating pressure and passed into the extraction vessel [40].

2.3.3 Supercritical Fluid Drying of Wet Gels

Evacuation of the liquid solvent in such a way to avoid as much as possible its textural modifications preserving its original intact, nanoporous network is the most complicated step in aerogel production. Solvent elimination can be performed by different drying methods. One of these available drying techniques, ambient pressure drying at atmospheric pressure or vacuum and elevated temperature, leads to formation of a vapor-liquid interface causing crack formation by capillary tension and associated drying shrinkage in the pores of the gel. The product is called a xerogel [2, 39]. Freeze drying is another method in which the pore liquid is frozen and then sublimed in vacuum. The product of this process is called as cryogel. The solvent is required to be replaced by one with a low expansion coefficient and a high sublimation pressure. However, several obstacles are associated with this method, such as slow rate of sublimation and increase of the solvent volume upon crystallization. Then, stresses directed from the crust towards inside, leading to shrinkages and breakages of the crust layers. Therefore, freeze drying products are generally obtained as powder form [40, 41].

However, evacuation of the solvent from the porous structure of the wet gel without shrinkage and any physical damages on the gel structure can be achieved under supercritical conditions. Supercritical drying (SCD) of the wet gel is substitution of the primary solvent in the pores of the gel with supercritical fluids without any remnants of liquid solvent at a temperature and pressure above the critical temperature and pressure of the solvent. The ending product of this process is called as aerogel. Supercritical drying steps of the wet gel will be depicted in detail in the following sections.

Supercritical fluid extraction is an effective method in maintaining the integrity of a gel network during drying minimizing or completely eliminating the capillary pressure. The minimization of the capillary pressure can be achieved by using solvents having lower surface tension than that of water (72.8 $mN.m^{-1}$) or that of alcohol (22.3 $mN.m^{-1}$). A complete removal of capillary pressure can be obtained by using supercritical drying in which no phase boundary takes place between liquid and gas phases [40- 42].

2.3.3.1 Carbon Dioxide as Supercritical Fluid Extraction Solvent

In this process, supercritical carbon dioxide (sc-CO_2) is most commonly utilized extraction agent with its favorable properties. CO_2 has readily achievable critical conditions with critical temperature of 31.1 ^{o}C and critical pressure of 74 atm as well as nonflammable, chemically stable and nontoxic.

Because of its high density, CO_2 can also dissolve relatively large amount of material, which is desirable for extraction applications. Its critical temperature is low and therefore the extraction process can be performed almost at room temperature, thus the treated material will not be damaged. Thus, it is particularly an attractive medium for extraction of biological materials which are often thermally labile, lipophilic, nonvolatileand are required to be kept and processed around room temperature.

Furthermore, dispopsal of CO_2 is more enviromentally friendly than for most other organic solvents typically used in extraction processes. It is easily attainable in large quantities as a byproduct of several reactions, such as fermentation, combustion and ammonia synthesis. Moreover, once the extract returns to standard conditions of pressure and temperature, carbon dioxide returns to a gas phase and the extracted product precipitates because it is no longer soluble in the gas. Consequently, there is no need for an additional separation step, as in the case of other solvents used in the food industry. However, fluids listed in Table 2.2.2 other than CO_2 having critical temperatures in its vicinity cannot be easily handled and be obtained in a pure form. They may be toxic or cause explosive mixtures and highly reactive chemicals [23-25].

2.3.4 Supercritical Fluid Extraction of Wet Gels with Supercritical Carbon Dioxide

Supercritical fluid drying technique was firstly proposed by Kistler for aerogel production [42]. Shrinkage and crack formation by capillary forces occurring during conventional drying method can be avoided by removing the liquid from the pores above the critical temperature and critical pressure of the liquid. As indicated in Figure 2.3.3, there is no longer any distinction between liquid and vapor phases and there is no liquid-vapor interface; thus, there is no capillary pressure applied on the solid network.

In supercritical drying, a wet gel is loaded into an autoclave and heated along a path such as one indicated by arrow in Figure 2.3.4.1. Temperature and pressure are increased in such a way that the phase boundary is not crossed, once the critical point is passed. Supercritical carbon dioxide fluid drying has recently been able to be utilized in drying of temperature sensitive materials due to its low critical temperature. This drying process is used not only for inorganic materials but also for organic materials.

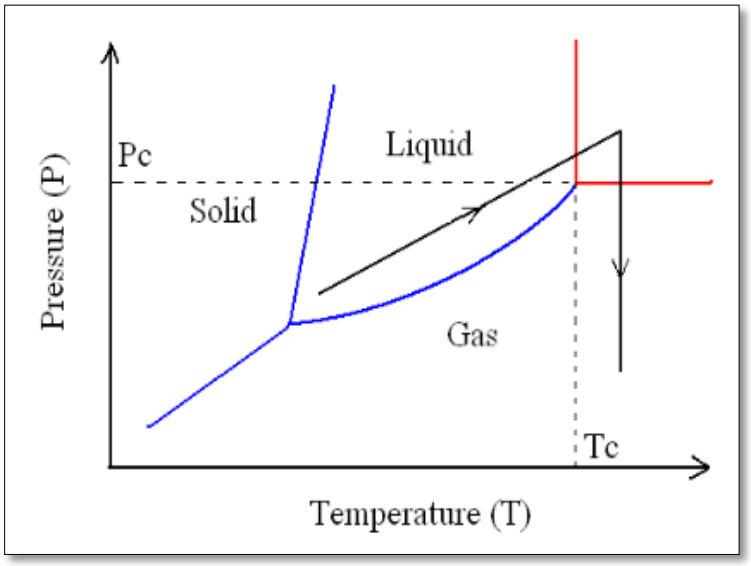

Figure 2.3.4.1: Schematic diagram of solid-liquid-vapor boundary

During supercritical drying, formation of two phases (a liquid and a vapor one) and surface tensions in the pores of the gels are prevented thereby collapse of the porous gel network is substantially avoided. As a consequence of supercritical drying of the wet gel, highly porous aerogel structure is obtained. Supercritical drying of the wet gel can be executed either in a continuous contact regime between the gel and the supercritical fluid with the presence of a continuous flow of sc-CO_2 during the process or in a batch vessel: sc-CO_2 is in contact with the wet gel in a discontinuous mode for a certain time. A characteristic flow diagram of the supercritical drying with sc-CO_2 in the continuous flow is illustrated in Figure 2.3.4.2. The wet gel is put in an extractor (E1 in Figure 2.3.4.2) and loaded with additional ethanol to prevent air drying of the sol-gel. The system is then pressurized to at least 5-6 MPa (P1 in Figure 2.3.4.2) with CO_2 and cooled to 5-10°C (H1 Figure 2.3.4.2). Liquid CO_2 is then flushed through the high pressure vessel to initialize the ethanol extraction. The vessel is gradually heated and pressurized over the critical temperature and pressure of the fluid. Subsequently, supercritical fluid is flushed through the extractor. The outlet flow of a mixture of sc-CO_2 and ethanol from the extractor is

partly expanded through an expansion valve (V5 in Figure 2.3.4.2). During this expansion pressure of the fluid decreases and supercritical phase of CO_2 converts to gas phase. Since lower solvation power of gaseous CO_2, the mixture is separated into two phases of a gaseous CO_2-rich flow and liquid stream in the separator (S1 in Figure 2.3.4.2). The system can be held in these conditions for several hours depending on the gel body dimension. CO_2 is then slowly released until the pressure reaches ambient pressure and the dried aerogel is taken from E1. Flow diagram of drying in the batch vessel is also shown in Figure 2.3.4.2. Liquid CO_2 is pumped into the extractor E1, loaded by wet gel, and brought to supercritical conditions.

Pure sc-CO_2 is continuously pumped through the vessel and replaced with the sc-CO_2 fluid enriched in ethanol. Then, the system is depressurized to the atmospheric pressure and the temperature is reduced to the room temperature and subsequently the aerogel is collected from the extractor [43, 44].

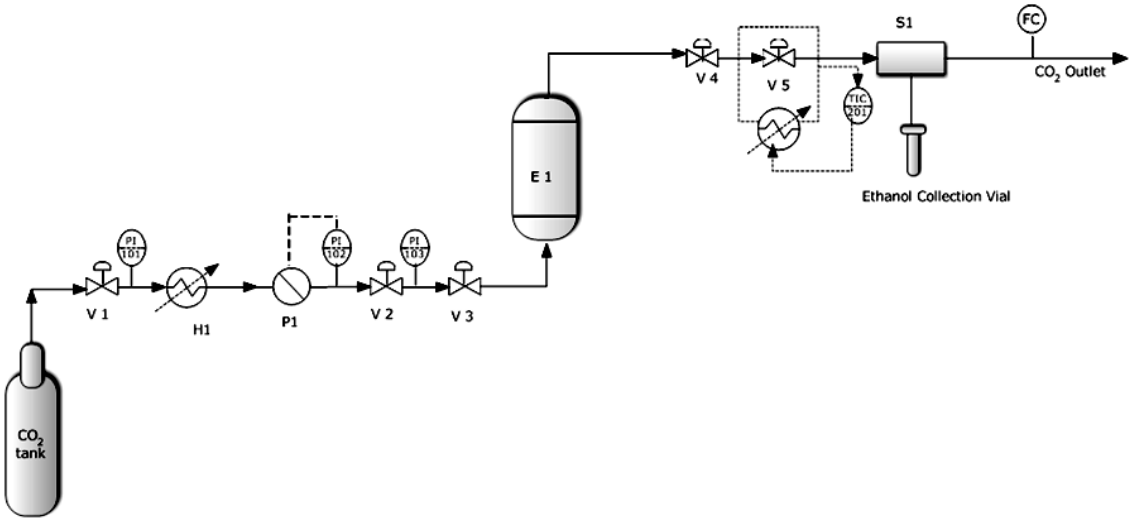

Figure 2.3.4.2: Schematic representation of process flow diagram of the supercritical drying with sc-CO_2 in continuous flow. V1-V5: valves; P1: Pump; E1: Autoclave; S1: Separator; PI-10x: Pressure gauges; TI-20x: Thermocouples; FC: Flow meter.)

2.3.5 Mass Transfer Principle

Mass transfer can be defined basically as the movement of any particular species from one spatial location to another. The mechanism of movement can be macroscopic as in the flow of a fluid in a pipe, which is called as convection. The transport of a species can be the result of random molecular motion in the presence of a composition gradient within a phase. This mass transfer due to molecular or microscopic processes is known as diffusion.

Diffusion is a transport phenomenon that describes the movement of matter of energy. It is typically stated that thermal or mass diffusion takes place when there is a temperature gradient or a concentration gradient. Heat or mass transfer via diffusion certainly occurs when those gradients exist; however, diffusion can occur even in the absence of heat or mass transfer. Diffusion is ultimately derived from inherent energy of the atoms and molecules. Diffusion can occur without heat or mass transfer since the diffusion in each direction.

In 1855, Adolph Fick proposed the concept of the diffusion by an anology with Fourier's law of heat conduction. The assumed linear relationship between diffusive flux and concentration gradient, known as Fick's first law of diffusion was born. In this equation, J_x represents the diffusion flux in the x-direction, D is the diffusion coefficient, C is the concentation and x is the position [45].

$$Jx = -D\frac{\delta C}{\delta x} \qquad \text{(Eq. 2.3.5)}$$

2.3.6 Mass Transfer Phenomena in Extraction

An extraction system involves a fluid phase, the supercritical solvent and dissolved extracts, and a solid phase in the extraction vessel. In the course of the extraction, mass transfer takes place between two phases, extractable materials in the solid phase dissolves in bulk fluid. The mechanism of dissolution can be rather simple if material is free on the surface. However, it may be more complicated when the extracted materials are located within the pores of the solid structure. In extraction, the mass transfer proceeds by diffusion through the pores, up to the bulk fluid where the components are swept along to the extractor outlet. Two models have been usually used to elucidate these mass transfer mechanisms during supercritical extraction of natural products [46]. These models can be classified as,

(1) Models based on differential mass balance (Sovavá, 1994; Perrut et al., 1997; Marrone et al., 1998; Reverchon and Marrone, 2001)
(2) Shrinking core model (Catcpole et al., 1996; Roy et al.,1996; Akgün et al.,2000; Döker et al., 2004).

Models based on differential mass balance include the resistances in both or one of the bulk phases. Mathematical models, based on mass balance, allow the calculation of yield in function of time and/or the determination of the remainder concentration in function of the extractor height in a certain extraction time [47]. Sovová model 1 could be chosen for describing of supercritical fluid extraction due to two reasons. Firstly, it can be widely used to describe yield and remainder concentration curves irrespective of the initial soluble material content of the raw material, and secondly, the dimensionless model parameters can be originated from physical parameters depending on extraction conditions or packed column characteristics. Sovová model assumes that the charge is homogenous and isotropic, and the soluble material is evenly dissolved in the raw material. Along the

column the particle size distribution, temperature, and pressure are constant, and pressure drop is negligible. The inlet solvent is solute free [46, 47].

According to the Sovová model during the grinding process the cells on the surface will be crushed, and q which is fraction of the soluble components becomes free on the surface and can be extracted by simple dissolution, which is characterized by the first stage of the yield curve. The other part of the soluble components, (1-q) fraction, remains inside the particles and can only reach the surface by diffusion, which is characterized by the second stage of the yield curve. The Sovová model divides the extraction process into steps shown in Figure 2.3.6 [47].

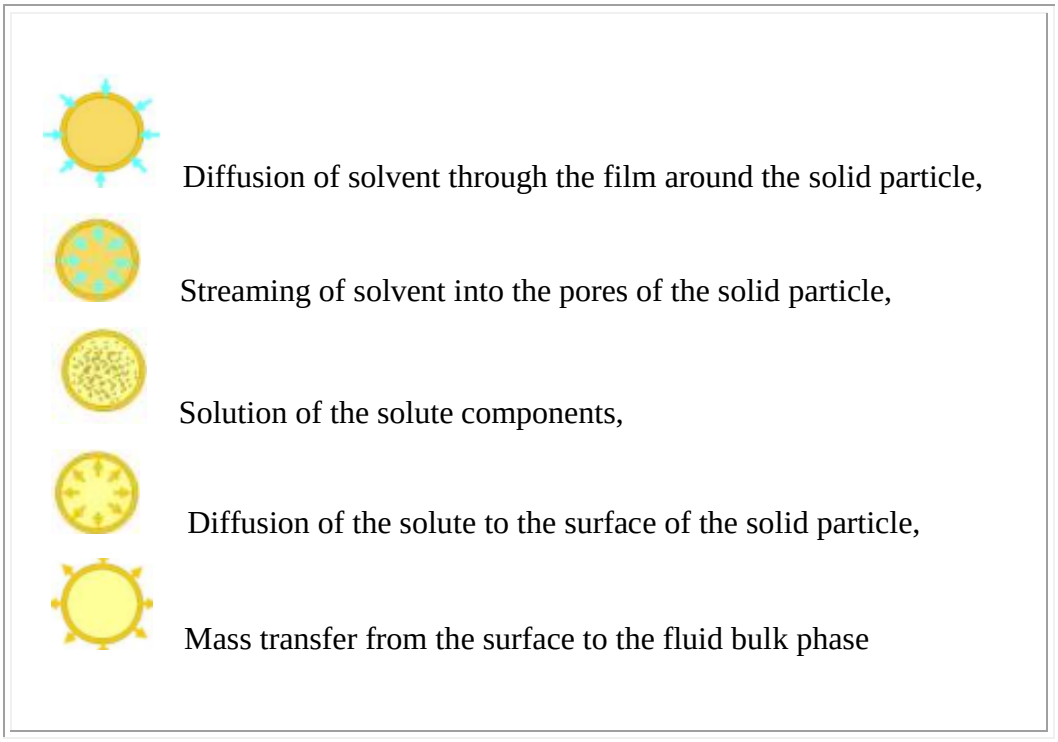

Figure 2.3.6: Steps of supercritical fluid extraction

2.3.7 Previous Supercritical Drying Research in the Literature

There has been quite little research into the mechanism of alcogel drying using sc-CO_2, despite the prevalence of this method as well as its attractiveness and the extensive study of it in several applications. The studies on mathematical modeling of this system are reviewed in the following sections.

M.J. Van Bommel and A.B. de Haan studied the drying of alcogel sheets with supercritical carbon dioxide. They proposed a method for predicting drying times of the alcogel sheets. They dried alcogel rods with 15 mm diameter with sc-CO_2. The drying times of the alcogels were estimated by running the experiment for a range of times at various operating conditions. The crack formation in the finished aerogels was examined and the extraction of the dried aerogels with cracks was assumed to be incomplete. However, they found that the crack-free aerogels could be obtained as a result of the drying with carbon dioxide under supercritical conditions. Among the operation conditions at which the experiments were conducted, the lowest temperature and pressure at which crack-free aerogels were obtained were at 35 °C and 85 bar, respectively. It was also found that operating temperature had a minor effect on the drying time and was also found that the diffusion of ethanol into the pores of the aerogel limits the drying time. This limitation was related to the thickness of the gel. Thus, gel thickness has a considerably large effect on the cost of the drying prcess of the wet gel.

Using the known drying time through the experimental study, a dimensionless mass transfer Fourier number was calculated to characterize drying process such that a properly finished gel should have the same Fourier number at constant conditions. Because F_o and D_{12} are constant, the ratio of required times for gel drying was correlated to be the ratio of

square of gel diameters. A correction factor of $\frac{1}{0.85}$ is applied in order to justify the difference in geometries between a rod and a plate.

$$\frac{tplate}{trod} = \frac{1}{0.85} \left(\frac{dplate}{drod}\right)^2 \quad \text{(Eq. 2.3.7.1)}$$

where d is the characteristic length of the sample: the radius in the case of the rod and the thickness in the case of the plate [49].

Alexander Orlovic et al. also developed a model and compared with the experimental drying data for alumina/silica gel with zinc chloride. The mathematical model of the supercritical extraction of the wet gel was represented as unsteady and one-dimensional diffusion of solvent through the aerogel pores filled with supercritical carbon dioxide.

They proposed four models to characterize the system, which are shrinking core model 1 in which Knudsen diffusivity is eliminated and average overall diffusivity is used and shrinking core model 2 in which Knudsen diffusivity is included and parallel- pore model and pore-in-series in which the pores which get gradually smaller as they grow deeper. In this study, the diffusivity was calculated using Fuller correlation assuming that the diffusivity was independent of composition.

In this study, the gel weight was also monitored with time. The wet gel was removed from the high pressure vessel each thirty minutes and weighed. The sample weight decreased as a function of time until there is no ethanol left and the pores are only filled with air. The model results were then compared to the curved obtained as a result of the experiment to determine whether the model predicted and accurate drying time and verify the intermediate behavior of the system. They resulted that the parallel pore and pore-in series models agreed well with the experimental data [50].

Another study in the modeling of supercritical drying process is developed by Mukhpadhyay and Rao [51]. A parallel pore model was used assuming that each pore is constant in radius, with one end closed, and the other end open to the flow of sc-CO_2. A tortuosity factor was applied to comprise pore connectivity and the fact that pores are not straight cylinders. In this study, it was assumed that two-way mass transfer of sc-CO_2 and ethanol in the pores takes place. Additionally, it was also proposed that this diffusive process of the components leads to spillage or volumetric swelling of the liquid. This phenomenon has been mentioned in several studies in the literature; however, it was the first time to be considered in the modeling of supercritical extraction. They acknowledged only volumetric swelling not volumetric shrinkage (suction). That was because they stated that the pore must be in single-phase, or a phase boundary would occur. The expansion of the fluid from the pores of the gel was determined by calculating the increase in volume over a time step and subtracting the amount of ethanol contained therein from the previous time step. This model developed in this study also accounted for the diffusivity varying with the composition and porous media effects.

Vignes equation was used to correlate diffusivity values as a function of the mass fraction of CO_2 and the diffusivities of solutions dilute in CO_2 and ethanol, based the Fuller and Tyn-Calus empirical correlations, respectively. Knudsen diffusion through the porous media was also taken into account and was calculated using the following equation.

$$D_k=\frac{2}{3}r_p\sqrt{\frac{8RT}{\pi M}} \quad \text{(Eq. 2.3.7.2.)}$$

This Knudsen term was then combined with the binary fluid diffusivity term D^l_{12} calculated by the Vignes correlation to determine the effective diffusivity of the wet gel:

$$\frac{1}{D_{12}} = \frac{1}{D^{l}_{12}} + \frac{1}{D_k} \quad \text{(Eq. 2.3.7.3.)}$$

C.A. Garcia-Gonzalez et al also investigated the drying profile with supercritical carbon dioxide of the wet gels [52]. The drying of the wet gels from different precursors (inorganic-silica-,organic-starch-), densities varying in the range of 0.08 and 0.15 g/cm^3 and morphologies which are cylindrical, monoliths and microspheres was studied. In their work, the effect of the use of different processing times during the dynamic supercritical drying of the wet gel on the drying profile and material textural properties. Moreover, they investigated the effect of the aerogel precursor type such as inorganic and organic precursor and aerogel structure with respect to density and morphology on the drying process. After preparing the silica gel monoliths, starch gel monoliths and silica gel microspheres, supercritical extraction of ethanol was carried out in which one of the outlet stream which is rich in ethanol was collected in vials filled with glass-wool and immersed in dry ice to mitigate the evaporation of ethanol. An alcoholmeter device was connected to the gaseous outlet of the setup in order to measure amount of ethanol in the gaseous stream which is rich in CO_2 at certain time intervals. As a result, they could obtain drying profile of the wet samples.

Additionally, they determined textural properties of the aerogels using low-temperature N_2 adsorption-desorption analysis. Specific surface area (a_s) was determined by BET (Brunauer-Emmett-Teller) method. Pore volume and mean pore diameter were also estimated using BJH (Barrett-Joyner-Halenda) method. They concluded that supercritical drying of the wet gels is governed by a mass transfer mechanisim based on a combination of convection and diffusion.

Chapter 3

EXPERIMENTAL METHOD and MATHEMATICAL MODELING OF ALCOGEL EXTRACTION

3.1 Chemicals for Silica Aerogel Synthesis

Tetraethylorthosilicate (TEOS) with a purity of 98% was supplied by AlfaAesar. Ethanol (EtOH) (99.9 %) was purchased from Merck Germany. Hydrochloric acid (HCl) (37 % purity) was supplied from AlfaAesar, Germany. Ammonium hydroxide (NH_4OH) (2.0 M in ethanol) was obtained from Aldrich, Germany. Carbon dioxide (99.9 %) was supplied from Messer Aligaz.

3.2 Preparation of Silica Wet Gel Monoliths

In this study, cylindrical silica alcogel rod with dimensions of 1.19 cm in diameter and 15.92cm in length synthesized using a conventional two step sol-gel process. Tetraethylorthosilicate (TEOS) was used as the silica precursor, HCl as the acid catalyst, and NH4OH as the condensation catalyst. As the first step, a solution of was prepared by mixing TEOS, ethanol and water with the mass ratio 1:1:0.34. Subsequently, the acid catalyst was added (0.048 M in ethanol) to obtain a pH of around 2.0 to initiate hydrolysis reactions and sol formation. The mixture was continuously stirred at room temperature for 40 minutes for hydrolysis. Then, the base catalyst (0.1 M in ethanol) until the pH of the

solution reaches 5.5 was added to the solution already obtained so as to increase the rate of condensation, which eventually lead to gelation of the solution. Before gelation initiated, the solution was poured into a plastic syringe-based mold with a diameter of 1.2 cm and with a length of 17 cm and sealed. The amount of the reactants used in the process is shown in Table 3.2.

Table 3.2 Amounts of reactants used in a typical gel synthesis procedure

Compound	**Amount added in the sol**	**Amount (moles)**
TEOS	6 g	Corresponds to 0.0048 moles
EtOH	6 g	Corresponds to 0.0217 moles to obtain a 50 wt. %solution of TEOS and EtOH
H_2O	2.04 g	Corresponds to 0.189 moles for a 4:1 molar ratio of H_2O/TEOS
HCl/EtOH Solution (0.048M)	1.1 ml	Corresponds to $9.6x10^{-6}$ moles of HCl and 0.0033 moles of EtOH
NH_4OH/EtOH Solution (0.1M)	3 ml	Corresponds to $5x10^{-5}$ moles of NH_4OH and 0.0085 moles of EtOH

The completion of the gelation was confirmed by tilting the mold to monitor its increasing viscosity until no more movement of the sol was observed. Since the wet gel were still fragile just after the gelation, it could be broken while trying to get it out of the

mold, at least 15 minutes were waited instead of following the next step of the process. After that, the resulting alcogel was soaked in an aging solution of equi-volume mixture of water and ethanol. The alcogel in the aging solution was kept in an oven at 323.15 K for 24 h. During this step, further condensation reactions take place that enhance mechanical strength of the wet gel via hydrolysis and condensation reactions of unreacted tetraethylortosilicate remaining on the wet gel. The replacement of water-ethanol solution with pure ethanol is called the solvent exchange step. The aging solution of 50%-50% (percentage by volume) water-ethanol was replaced with pure ethanol. The resulting alcogel was then soaked for 3 more days at room temperature; solvent exchange with fresh ethanol was repeated several times leading to remove any impurities from the pores along with minimization of water concentration within the pores. In order to extract ethanol from the pores of the wet gels, drying with supercritical CO_2 was used. This supercritical drying process was conducted as 313.15 K and 100 bar. The schematic representation of the whole process is illustrated in Figure 3.2.1. Prepared wet gel at the end of these steps is shown in Figure 3.2.2.

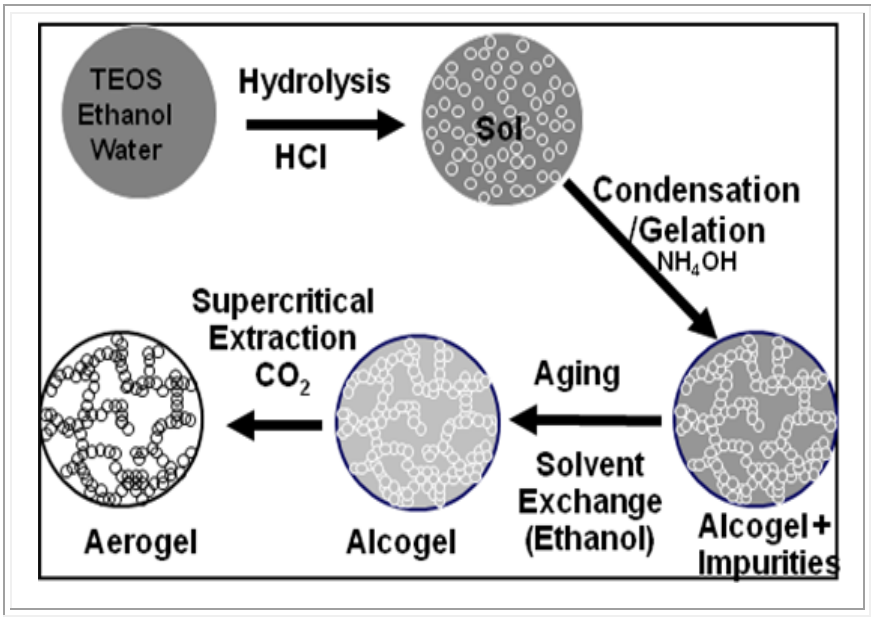

Figure 3.2.1: Schematic Representation of the Silica Aerogel Synthesis Procedure using two- step sol-gel method.

Figure 3.2.2: Cylindrical silica wet gel prepared in the laboratory (1.19 cm in diameter x 15.92cm in length)

3.3 Drying: Supercritical Extraction of Wet Gel

3.3.1 Experimental Setup for Continuous (or Dynamic) Supercritical Drying

A schematic diagram of the extraction unit used in this study is shown in Figure 3.3.1. It basically consists of an extractor with a volume of 26ml, a compressor, a separator, a carbon dioxide reservoir, a gas flow meter and a control unit that displays the temperature and pressure inside the extractor.

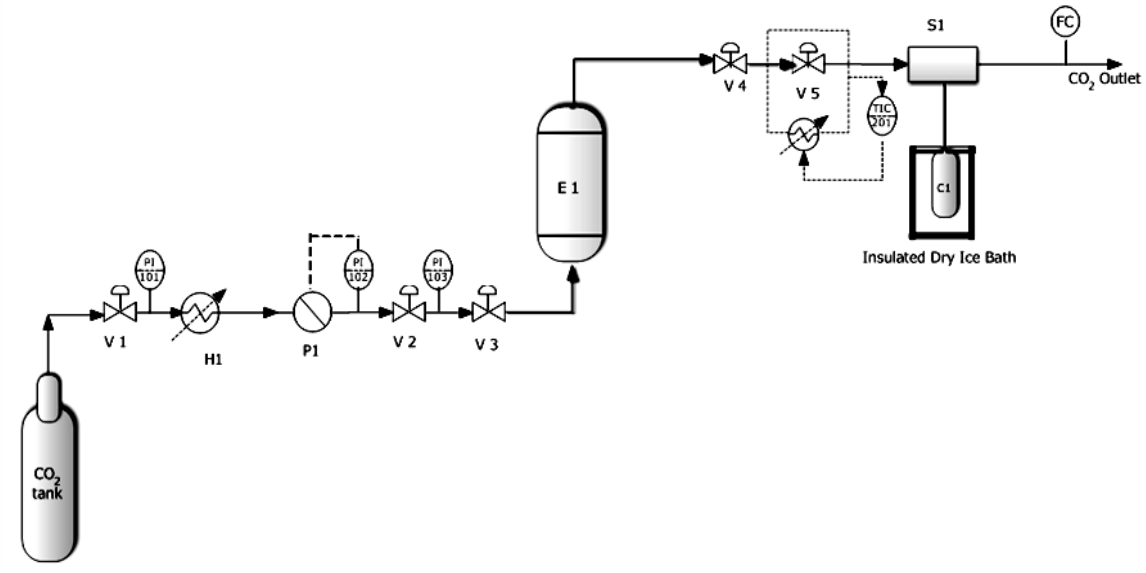

Figure 3.3.1: Schematic representation of process flow diagram of the supercritical drying with sc-CO_2 in Continuous Flow (V1-V5: valves; P1: Pump; E1: Autoclave; C1: Ethanol Collection Vial; PI-10x: Pressure gauges; TI-20x: Thermocouples; FC: Flow meter.)

Subsequent to the wet gel preparation, supercritical drying of the gel was carried out. At this point, the wet gel is still in the gel form that is a solid structure filtrated by liquid. Alcohol trapped inside the silica structure starts to evaporate; thus, liquid-vapor

phase boundaries develop with time in the pore. Therefore, this step is considerably crucial to remove trapped alcohol carefully achieving monolith aerogel production without any cracks and pore structure deformation. The supercritically carbon-dioxide-dried silica aerogel cylindrical rod was produced in the drying equipment of Applied Separations Speed SFE (tubular reactor, length=15.94 cm, diameter=1.43 cm, volume=26 ml), shown in Figure 3.3.2. At the beginning of the drying experiments, it is essential to reduce the evaporation of the ethanol from the gel rod. Initially, the extractor (E1 in Figure 3.3.1 and Figure 3.3.3) was then completely filled with ethanol to prevent contact of the sample air and evaporation of the solvent from the gel causing the shrinkage of the solid and the occurrence of cracks during pressure build-up. The wet gel rod was carefully taken out of the mold and immersed in pure ethanol. Then, the wet gel was taken from the ethanol and inserted quickly into the extractor.

Temperature of the extractor vessel and of the micro-metering valve (V5 in Figure 3.3.1) controlling the CO_2 flow rate, were set to 313.15 K. After a certain duration time for the temperature stabilization, the system was pressurized with carbon dioxide until the desired operating pressure of 10 MPa is reached by the pump (P1 in Figure 3.3.1) in this experiment.

The outlet micro-metering valve was adjusted to a CO_2 flow rate of 1.5 L/min. The outlet flow containing ethanol-rich phase fractions was collected in a way that evaporation of ethanol collected lessened. During the experiment, the sample collection vial was kept at 1 bar and -78 °C to separate almost all the ethanol from the carbon dioxide. It was collected in glass vials sealed and immersed in a dry ice bath, which is illustrated in Figure 3.3.5. The gaseous CO_2 stream was vented through a hood. Finally, the dried sample (in Figure 3.3.6) was collected from the vessel.

Figure 3.3.2: Drying Equipment of Applied Separations Speed SFE

Figure 3.3.3: Extraction vessel (tubular reactor, length=15.94 cm, diameter=1.43 cm, volume=26 ml)

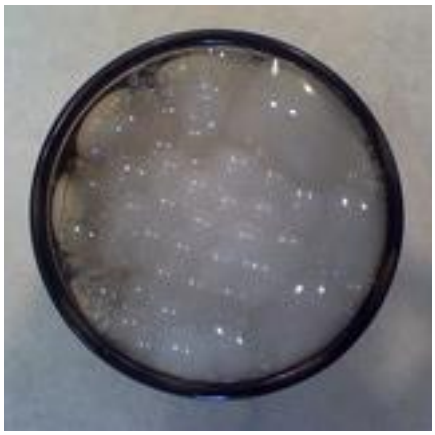

Figure 3.3.4: Dry ice bath prepared to maintain the outlet stream at low temperature

Figure 3.3.5: Sample collection vial immersed in dry ice bath

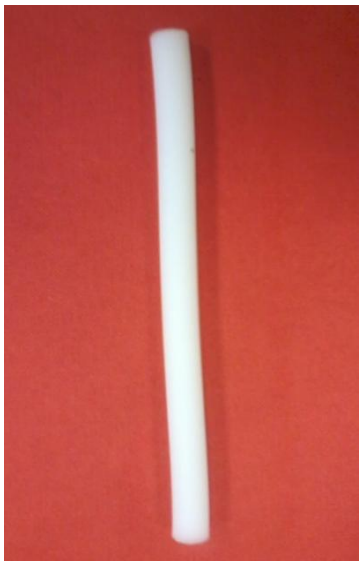

Figure 3.3.6: Dried Aerogel with sc-CO_2-assisted drying

3.3.2 Mathematical Modeling of Alcogel Extraction in Batch Vessel

In this study, mass transfer models were used to simulate supercritical drying of the wet gel both in a batch vessel and a continuous contact regime between the gel and continuous sc-CO_2 flow. In the first part of this section, mass transfer model equations derived for the wet gel drying in the batch vessel is given. Simulations were carried out at various operating conditions for aerogels of varying shapes and different thicknesses. Extraction from spheres with diameters of 1cm, 2 cm and 3 cm and from cylinders with diameters of 1 cm and a length of 6 cm in a 57 ml high pressure vessel was simulated. Vessel volume was similar to the volume of the extractor used to dry gels at Koç University. Extraction from a rectangular panel 1cm thick, 30 cm long and 30 cm wide in a 30 L vessel was simulated to mimic large-scale extraction runs carried out by Airglass.

In the second part, a mass transfer model for supercritical extraction of a cylindrical gel in continuous sc-CO_2 flow was developed. Coupled partial differential equations governing the mass transfer mechanism inside of the gel as well as in the bulk flow of sc-CO_2 in the vessel was obtained. In the model, the gel has the same body dimensions prepared in the laboratory (1.19 cm in diameterx15.92 cm in length). Additionally, the same operation conditions (1.5 L sc-CO_2/min volumetric flow rate and 313.15 K and 100 bar) of the extraction performed in the laboratory were used in the constitutive equations.

3.3.2.1 Proposed Mechanism

Proposed model for drying is a two-way mass transfer of sc-CO_2 and ethanol to and from the porous network of a silica aerogel. In the beginning of the process, the pores in the alcogel are totally filled with ethanol. The alcogel is surrounded by sc-CO_2 at the operating temperature and pressure. Sc-CO_2 diffuses into the ethanol phase in the pores and ethanol diffuses out of the pores into sc-CO_2 phase. As the drying process progresses, the amount of ethanol in the gel decreases, whereas amount of CO_2 in the liquid filling in the pores increases and the process continues until the wet gel is totally dried. In this study, mass transfer equations were based on Fick's second law in spherical, cylindrical and rectangular coordinates, respectively. One dimensional diffusion of ethanol from the gel into the bulk fluid and diffusion of CO_2 into the gel from the bulk fluid into the gel are illustrated in Figure1 for spherical, cylindrical and rectangular alcogels.

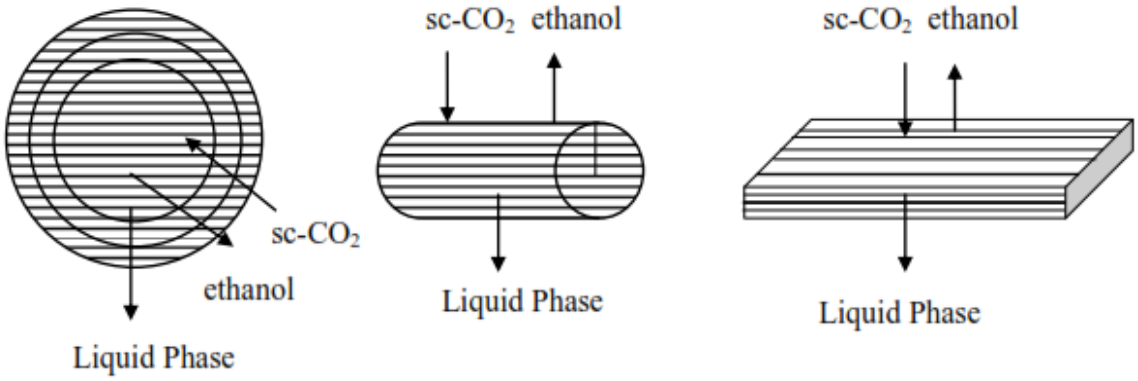

Figure 3.3.2.1 One Dimensional Model Schematics of Drying with sc-CO_2

3.3.2.2. Mass Transfer Model

Extraction of wet gels in a batch vessel is described in three cases, as follows. These are also depicted in Figure 3.3.2.2 (a), Figure 3.3.2.2 (b) and Figure 3.3.2.2 (c). In the first case, the gel is placed in a perfectly mixed vessel. Since the solution in the vessel is assumed to be perfectly mixed, convective mass transfer from the solid surface to the liquid is fast. Then, ethanol is instantly transferred from the surface of the gel into the sc-CO_2 and there is no concentration gradient throughout the fluid phase in the vessel around the gel. For this case, mass transfer coefficient can be considered to be infinitely large. In the second case, the vessel is filled with stationary sc-CO_2 and mass transfer coefficient can be considered as zero. Therefore, there is a concentration gradient of ethanol in the bulk sc-CO_2 phase in the vessel where the concentration of ethanol smoothly decreases as the distance from the surface of the gel increases. The third case is the case where the mass transfer coefficient is between those two extreme cases depending on the convective currents in the system. In this case, ethanol in the pores diffuses into sc-CO_2 in the vessel

and a flow around the gel occurs by natural convection due to temperature gradients which exist in the fluid in the vessel. A number of mass transfer coefficient values between the values in two extreme cases were used in the simulations to determine a reasonable range for the mass transfer coefficient in this case. In the range determined, effect of mass transfer coefficient on drying time was also investigated.

(a) Extraction in well-mixed batch vessel (Kx≈∞)

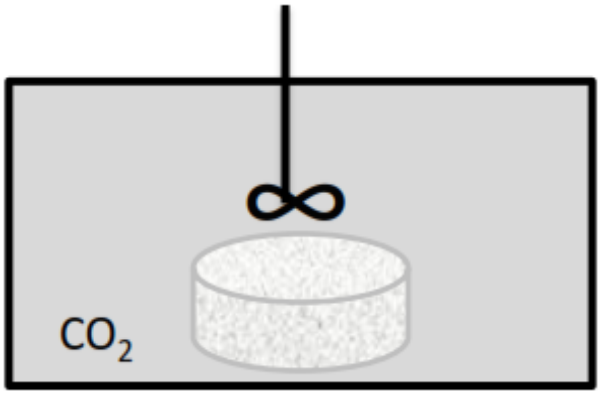

(b) Extraction in stationary sc-CO_2 in batch vessel (Kx≈0)

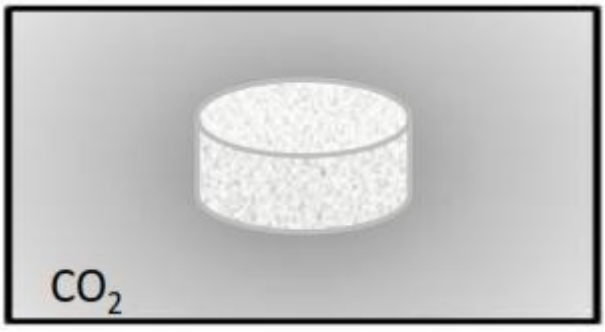

(c) Extraction of the gel via natural convection in batch vessel

Figure 3.3.2.2 (a) Extraction in well-mixed batch vessel (Kx≈∞) **(b)** Extraction in stationary sc-CO_2 in batch vessel (Kx≈0) **(c)** Extraction of the gel via natural convection in batch vessel

3.3.2.2.1 Assumptions

- Pores of the wet gel are assumed equally accessible,
- The pore size distribution of the wet gel and dried gel is assumed to be the same,
- The diffusion of ethanol in the pores can be described by Fick's second law of diffusion ,
- Ethanol concentration is initially uniform throughout the gel volume.

3.3.2.2.2 Derivations of Mass Transfer Model Equations

Partial differential equations governing mass transfer in the pores of the wet gels were derived performing mass balances for one component in the system over a differential volume and segment of each wet gels.

In spherical wet gels:

Differential shell of spherical wet gel is presented in Figure 3.3.2.2.2.1.

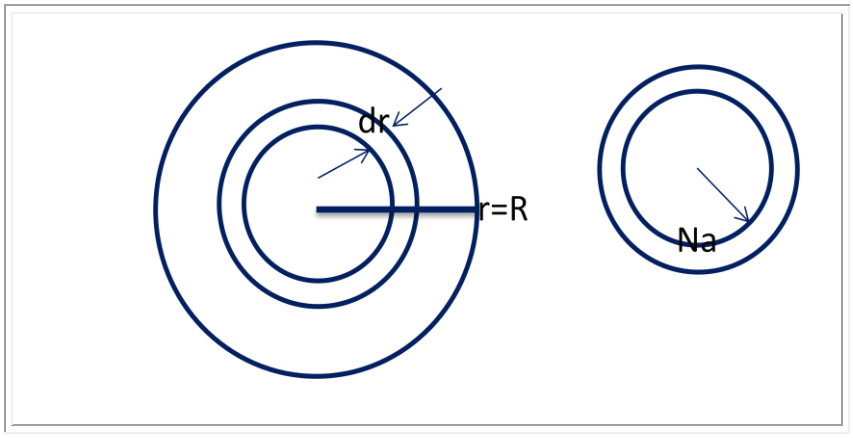

Figure 3.3.2.2.2.1: Schematic representation of differential shell of spherical wet gel

$$\varepsilon = \frac{V_{pore}}{V_{total}}\ , \qquad V_{pore}=4\pi r^2 \Delta r \text{Ɛ}, \qquad A_{pore}=4\pi r^2 \text{Ɛ}$$

where ε is porosity of the gel structure, V_{pore} is porous volume of the gel network, V_{total} is total volume of the gel structure, r is radius of the gel, A_{pore} represents surface area of the pore and Na is molar flux of ethanol (kmol/m^2s).

Molar mass balance of ethanol over differential segment of the spherical wet gel is done, as follows.

$$(m_{ethanol})_{in} - (m_{ethanol})_{out} + (m_{ethanol})_{generated} = (m_{ethanol})_{accumulated}$$

$$(N_a|_r - N_a|_{r+\Delta r}) * (A_{pore}) = \frac{\partial (C_a * V_{pore})}{\partial t}$$

$$\lim_{\Delta r \to 0} \frac{(N_a r^2|_r - N_a r^2|_{r+\Delta r})}{\Delta r} = \frac{\partial (C_a r^2)}{\partial t}$$

$$-\frac{\partial}{\partial r}(N_a r^2) = \frac{\partial (C_a)}{\partial t} r^2$$

$$N_a = -D_e \frac{\partial Ca}{\partial r}$$

$$\frac{\partial}{\partial r}(D_e \frac{\partial C_a}{\partial r} r^2) = \frac{\partial (C_a)}{\partial t} r^2$$

In Cylindrical Wet Gel:

Differential volume of cylindrical wet gel is presented in Figure 3.3.2.2.2.2.

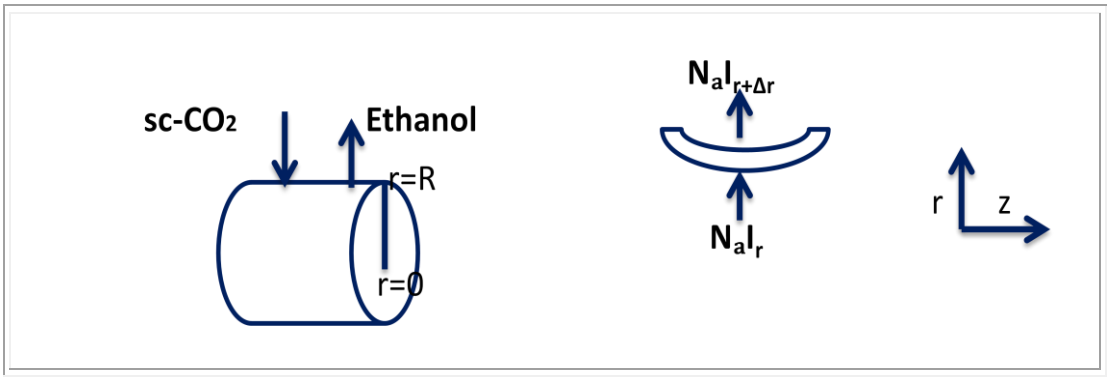

Figure 3.3.2.2.2.2: Schematic representation of a differential volume of cylindrical wet gel

$$\varepsilon = \frac{V_{pore}}{V_{total}}, \quad V_{pore}=2\pi r l \Delta r \mathcal{E}, \quad A_{pore}=2\pi r l \mathcal{E}$$

where, ε is porosity of the gel structure, V_{pore} is porous volume of the gel network, V_{total} is total volume of the gel structure, r is radius of the gel, l is length of the gel, A_{pore} represents surface area of the pore and Na is molar flux of ethanol (kmol/m^2s).

Molar mass balance of ethanol over the differential volume of the cylindrical wet gel is done, as follows.

$$(m_{ethanol})_{in} - (m_{ethanol})_{out} + (m_{ethanol})_{generated} = (m_{ethanol})_{accumulated}$$

$$(N_a|_r - N_a|_{r+\Delta r}) * (A_{pore}) = \frac{\partial (C_a * V_{pore})}{\partial t}$$

$$\lim_{\Delta r \to 0} \frac{(N_a|_r - N_a|_{r+\Delta r})}{\Delta r} = \frac{\partial (C_a r)}{\partial t}$$

$$N_a = -D_e \frac{\partial C_a}{\partial r}$$

$$\frac{\partial}{\partial r}\left(D_e \frac{\partial C_a}{\partial r} r\right) = \frac{\partial (C_a * r)}{\partial t}$$

$$\frac{\partial D_e}{\partial r}\frac{\partial C_a}{\partial r} + \frac{\partial}{\partial r}\left(\frac{\partial C_a}{\partial r}\right) D_e + \frac{1}{r}\frac{\partial C_a}{\partial r} D_e = \frac{\partial (C_a)}{\partial t}$$

In Rectangular Wet Gel:

Differential volume of rectangular wet gel is presented in Figure 3.3.2.2.2.3.

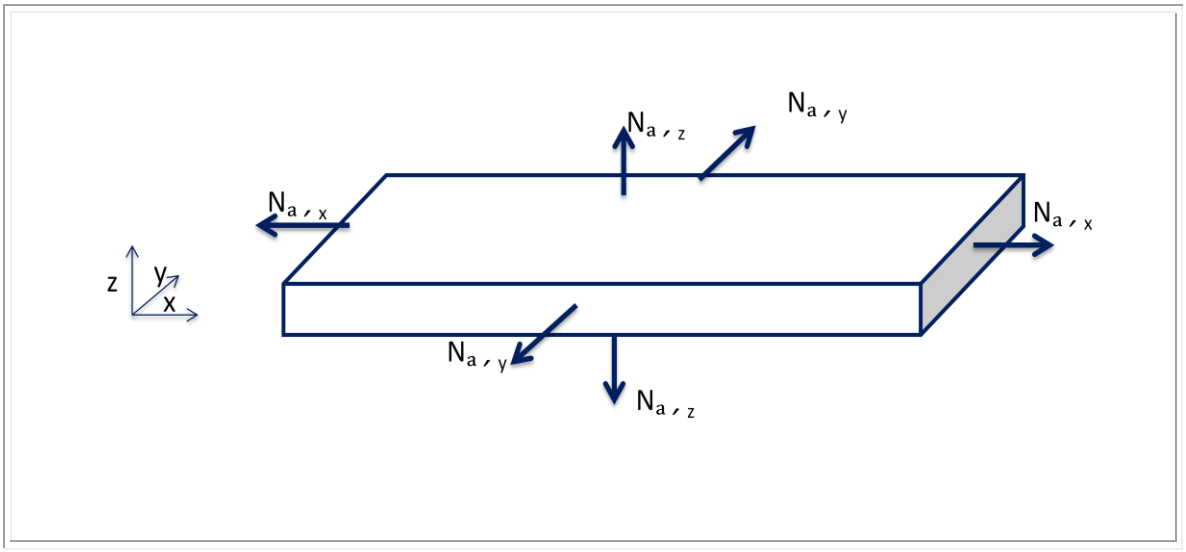

Figure 3.3.2.2.2.3: Schematic representation of a differential volume of rectangular wet gel

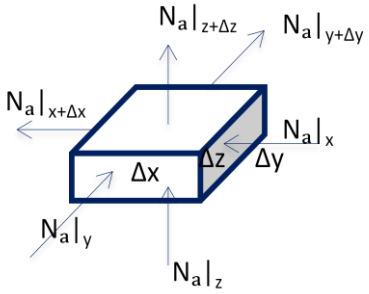

Molar mass balance of ethanol over the differential volume of the rectangular wet gel is done, as follows.

$$(m_{ethanol})_{in} - (m_{ethanol})_{out} + (m_{ethanol})_{generated} = (m_{ethanol})_{accumulated}$$

$$\varepsilon = \frac{V_{pore}}{V_{total}}, \quad V_{pore} = \Delta x \Delta y \Delta z \varepsilon, \quad A_{pore,x} = \Delta y \Delta z \varepsilon, \quad A_{pore,y} = \Delta x \Delta z \varepsilon, \quad A_{pore,z} = \Delta x \Delta y \varepsilon$$

$$N_{a,x} = -D_e \frac{\partial C_a}{\partial x}, \quad N_{a,y} = -D_e \frac{\partial C_a}{\partial y}, \quad N_{a,z} = -D_e \frac{\partial C_a}{\partial z}$$

$$(N_a|_x - N_a|_{x+\Delta x}) * (A_{pore,x}) + (N_a|_y - N_a|_{y+\Delta y}) * (A_{pore,y}) + (N_a|_z - N_a|_{z+\Delta z}) * (A_{pore,z}) = \frac{\partial (C_a V_{pore})}{\partial t}$$

$$\frac{(N_a|_x - N_a|_{x+\Delta x})}{\Delta x \Delta y \Delta z \mathcal{E}} \Delta y \Delta z \mathcal{E} + \frac{(N_a|_y - N_a|_{y+\Delta y})}{\Delta x \Delta y \Delta z \mathcal{E}} \Delta x \Delta z \mathcal{E} + \frac{(N_a|_z - N_a|_{z+\Delta z})}{\Delta x \Delta y \Delta z \mathcal{E}} \Delta x \Delta y \mathcal{E} = \frac{\partial (C_a \Delta x \Delta y \Delta z \mathcal{E})}{\partial t \, \Delta x \Delta y \Delta z \mathcal{E}}$$

$$\lim_{\Delta x \to 0} \frac{(N_a|_x - N_a|_{x+\Delta x})}{\Delta x} + \lim_{\Delta y \to 0} \frac{(N_a|_y - N_a|_{y+\Delta y})}{\Delta y} + \lim_{\Delta z \to 0} \frac{(N_a|_z - N_a|_{z+\Delta z})}{\Delta z} = \frac{\partial (C_a)}{\partial t}$$

$$-\frac{\partial (N_{a,x})}{\partial x} - \frac{\partial (N_{a,y})}{\partial y} - \frac{\partial (N_{a,z})}{\partial z} = \frac{\partial (C_a)}{\partial t}$$

$$-\frac{\partial}{\partial x}\left(-D_e \frac{\partial C_a}{\partial x}\right) - \frac{\partial}{\partial y}\left(-D_e \frac{\partial C_a}{\partial y}\right) - \frac{\partial}{\partial z}\left(-D_e \frac{\partial C_a}{\partial z}\right) = \frac{\partial (C_a)}{\partial t}$$

$$\frac{\partial D_e}{\partial x}\left(\frac{\partial C_a}{\partial x}\right) + \frac{\partial}{\partial x}\left(\frac{\partial C_a}{\partial x}\right) D_e + \frac{\partial D_e}{\partial y}\left(\frac{\partial C_a}{\partial y}\right) + \frac{\partial}{\partial y}\left(\frac{\partial C_a}{\partial y}\right) D_e + \frac{\partial D_e}{\partial z}\left(\frac{\partial C_a}{\partial z}\right) + \frac{\partial}{\partial z}\left(\frac{\partial C_a}{\partial z}\right) D_e = \frac{\partial (C_a)}{\partial t}$$

3.3.2.3 Model Equations

The differential equations for unsteady-state diffusion of ethanol and sc-CO_2 in the pores of the alcogels are given, as follows.

The differential equation for unsteady-state diffusion of ethanol through the cylindrical pores of the spherical alcogel is given by:

$$\left(\frac{\partial \mathrm{Ca}}{\partial \mathrm{r}}\frac{\partial \mathrm{De}}{\partial \mathrm{r}} + \mathrm{D_e}\frac{2}{\mathrm{r}}\frac{\partial \mathrm{Ca}}{\partial \mathrm{r}} + \frac{\partial}{\partial \mathrm{r}}\left(\frac{\partial \mathrm{Ca}}{\partial \mathrm{r}}\right)\mathrm{D_e}\right) = \frac{\partial \mathrm{Ca}}{\partial \mathrm{t}} \qquad \text{(Eq. 3.3.2.3.1)}$$

where C_a is concentration of ethanol in the gel, D_e is effective diffusion coefficient and t is time and r is the direction that diffusion occurs in aerogel.

The initial and boundary conditions are given by:

Initial Conditions : t=0, $Ca(r,0)=C_i$ (3.3.2.3.1a)

which shows that the pores in the gel are initially filled with ethanol with a concentration of C_i. This is fixed by the density of pure ethanol.

Boundary Conditions:t>0, $\frac{\partial C_a}{\partial r}=0$ at r=0 (3.3.2.3.1b)

$$\frac{\partial \mathrm{Cv}}{\partial \mathrm{t}} = \frac{(\mathrm{N_a}\ \mathrm{A})}{\mathrm{V}} \quad \text{at r=R} \qquad \text{(3.3.2.3.1c)}$$

$$\mathrm{N_a} = \mathrm{K_x}(\mathrm{Ca_s}-\mathrm{C_v})$$

Ca_s is the concentration of ethanol at the surface of the aerogel, C_v is concentration of ethanol in the bulk flow and Na is molar flux of ethanol from the pores, R is radius of spherical alcogel, A is external surface area of the gel, K_x is mass transfer coefficient.

The differential equations representing diffusion of CO_2 to the pores of the spherical alcogel obtained and initial and boundary conditions are also given in the following equation.

$$\left(\frac{\partial Ce}{\partial r}\frac{\partial De}{\partial r} + D_e\frac{2}{r}\frac{\partial Ce}{\partial r} + \frac{\partial}{\partial r}\left(\frac{\partial Ce}{\partial r}\right)D_e\right) = \frac{\partial Ce}{\partial t} \quad \text{(Eq. 3.3.2.3.2)}$$

where, Ce is concentration of sc-CO_2 in the gel, De is effective diffusion coefficient and t is time and r is the direction that diffusion occurs in the gel.

The initial and boundary conditions are given by:

Initial Conditions : t=0, $C_e(r,0)=0$ (Eq. 3.3.2.3.2a)

Boundary Conditions:t>0, $\frac{\partial Ce}{\partial r}=0$ at r=0 (Eq. 3.3.2.3.2b)

$$\frac{\partial C_f}{\partial t} = \frac{(N_e A)}{V} \quad \text{at } r = R \qquad \text{(Eq. 3.3.2.3.2c)}$$

$$N_e = K_x\left(C_{e,s} - C_f\right)$$

where C_e is initial concentration of sc-CO_2, Ne is molar flux of sc-CO_2, $C_{e,s}$ is concentration of sc-CO_2 on the surface of the aerogel, R is radius of spherical gel, A is external surface area of the gel, C_f is concentration of sc-CO_2 in the bulk and K_x is mass transfer coefficient.

Similarly, the ethanol diffusion through the pores of the cylindrical alcogel are described by ,

$$\left(r\frac{\partial Ca}{\partial r}\frac{\partial D_e}{\partial r}+D_e\frac{1}{r}\frac{\partial Ca}{\partial r}+\frac{\partial}{\partial r}\left(\frac{\partial Ca}{\partial r}\right)D_e\right)=\frac{\partial Ca}{\partial t} \qquad \text{(Eq. 3.3.2.3.3)}$$

The initial and boundary conditions are given by:

Initial Conditions : t=0, $Ca(r,0)=C_i$ (Eq. 3.3.2.3.3a)

Boundary Conditions : t>0, $\frac{\partial Ca}{\partial r}=0$ at r=0 (Eq. 3.3.2.3.3b)

$$\frac{\partial C_v}{\partial t}=\frac{(N_a*A)}{V} \quad \text{at } r=R \qquad \text{(Eq. 3.3.2.3.3c)}$$

$$N_a=K_X\left(C_{a,s}-C_v\right)$$

$C_{a,s}$ is the concentration of ethanol at the surface of the cylindrical alcogel, C_v is concentration of ethanol in the bulk flow and N_a is molar flux of ethanol from the pores, R is radius of the cylindrical alcogel, A is external surface area of the gel, K_x is mass transfer coefficient.

sc-CO_2 diffusion through the pores of the cylindrical alcogel are described by,

$$\left(r\frac{\partial Ce}{\partial r}\frac{\partial De}{\partial r}+D_e\frac{1}{r}\frac{\partial Ce}{\partial r}+\frac{\partial}{\partial r}\left(\frac{\partial Ce}{\partial r}\right)D_e\right)=\frac{\partial Ce}{\partial t} \qquad \text{(Eq. 3.3.2.3.4)}$$

The initial and boundary conditions are given by:

Initial Conditions : t=0, $C_e(r,0)=0$ (Eq. 3.3.2.3.4a)

Boundary Conditions: t>0, $\frac{\partial Ce}{\partial r}=0$ at r=0 (Eq. 3.3.2.3.4b)

$$\frac{\partial C_f}{\partial t} = \frac{(N_e A)}{V} \quad \text{at } r = R \qquad \text{(Eq. 3.3.2.3.4c)}$$

$$N_a = K_X\left(C_{e,s} - C_f\right)$$

where C_e is initial concentration of sc-CO_2, N_e is molar flux of sc-CO_2, $C_{e,s}$ is concentration of sc-CO_2 on the surface of the alcogel, R is radius of cylindrical alcogel, A is external surface area of the gel, C_f is concentration of sc-CO_2 in the bulk and K_x is mass transfer coefficient.

For the panel, the differential equation of ethanol diffusion as well as initial and boundary conditions are given below.

$$\left(\frac{\partial}{\partial x}\left(\frac{\partial Ca}{\partial x}D_e\right) + \frac{\partial}{\partial y}\left(\frac{\partial Ca}{\partial y}D_e\right) + \frac{\partial}{\partial z}\left(\frac{\partial Ca}{\partial z}D_e\right)\right) = \frac{\partial Ca}{\partial t} \qquad \text{(Eq. 3.3.2.3.5)}$$

Initial Conditions : t=0, $Ca(z,0)=C_i$ (Eq. 3.3.2.3.5a)

Boundary Conditions: t>0,

$$\frac{\partial C_v}{\partial t} = \frac{(N_a A)}{V} \quad \text{at } z=L \qquad \text{(Eq. 3.3.2.3.5b)}$$

$$N_a = K_x(C_{a,s}-C_v)$$

where $C_{a,s}$ is the concentration of ethanol at the surface of the rectangular alcogel, C_v is concentration of ethanol in the bulk flow and N_a is molar flux of ethanol from the pores, R is radius of the rectangular alcogel, A is external surface area of the gel, K_x is mass transfer coefficient.

The differential equation of CO_2 diffusion through the panel as well as initial and boundary conditions are given below.

$$\left(\frac{\partial}{\partial x}\left(\frac{\partial Ce}{\partial x} * D_e\right) + \frac{\partial}{\partial y}\left(\frac{\partial Ce}{\partial y} * D_e\right) + \frac{\partial}{\partial z}\left(\frac{\partial Ce}{\partial z} * D_e\right)\right) = \frac{\partial Ce}{\partial t} \quad \text{(Eq. 3.3.2.3.6)}$$

The initial and boundary conditions are given by:

Initial Conditions : t=0, $C_e(z, 0) = 0$ (Eq. 3.3.2.3.6a)

BoundaryConditions: t>0, $\frac{\partial C_f}{\partial t} = \frac{(N_e A)}{V}$ at z=L (Eq. 3.3.2.3.6b)

$$N_e = K_x\left(C_{e,s} - C_f\right)$$

where $C_e(z,0)$ is initial concentration of sc-CO_2, Ne is molar flux of sc-CO_2, $C_{e,s}$ is concentration of sc-CO_2 on the surface of the alcogel, L is thickness of the rectangular alcogel, A is external surface area of the gel, C_f is concentration of sc-CO_2 in the bulk and K_x is mass transfer coefficient.

3.3.3 Mathematical Modeling of Alcogel Extraction in Continuous Supercritical Drying

3.3.3.1 Proposed Mechanism

Proposed model for the extraction of the solvent from the pores of the wet gel in the continuous flow is the same as the batch supercritical drying. Gel extraction in the continuous flow also involves a two-way mass transfer of sc-CO_2 and ethanol to and from the porous network of the silica wet gel. In the beginning of the process, the fluid in the pore is assumed to be at rest, and entirely ethanol, thus, the concentration of the solvent within the gel is rather high. The alcogel is surrounded by sc-CO_2 flow at the operating temperature and pressure. Due to the large concentration gradient between the pores of the wet gel and the surrounding flow, ethanol can readily diffuse out of from the pores of the gel and is swept away from the surface of the gel by continuous flow via convective mass transfer. Thus, it is expected that only convective mass transfer resistances control the drying process at this point. As the drying process progresses, the amount of ethanol in the gel decreases, while CO_2 content in the liquid filling in the pores increases. Then, as drying time progresses and less solvent remains in the gel network, diffusion contribution to the removal of ethanol from the pores of the gel becomes more governing; however, ethanol in the vicinity of the gel surface is still transferred to the vessel by convective mass transfer mechanism.

In this study, diffusion contribution to the ethanol removal from wet silica gel was based on Fick's second law in cylindrical coordinates. Unsteady state two dimensional diffusion of ethanol through both the axial length and radius of the silica gel into the bulk fluid and diffusion of CO_2 into the gel from the bulk fluid into the gel was derived. Additionally, mass transfer equation for the ethanol transport in the flow surrounding the gel was derived and coupled to the diffusion equation and then, the coupled equations were solved simultaneously.

3.3.3.2. Mass Transfer Model

Supercritical extraction of the cylindrical wet gel in continuous sc-CO_2 flow is illustrated in Figure 3.3.3.2.

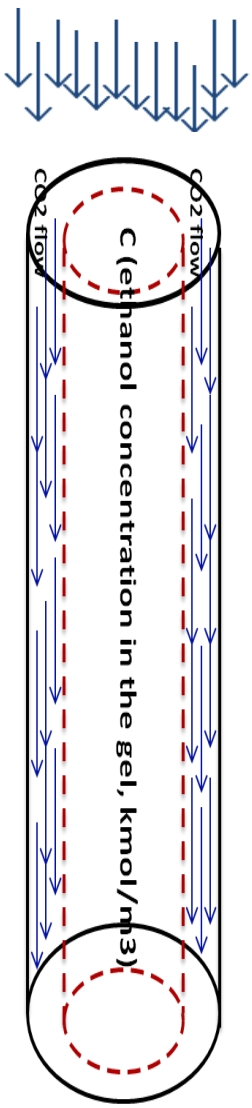

Figure 3.3.3.2: Schematic of drying of the wet gel with continuous sc-CO_2 flow in a high pressure vessel (26 ml)

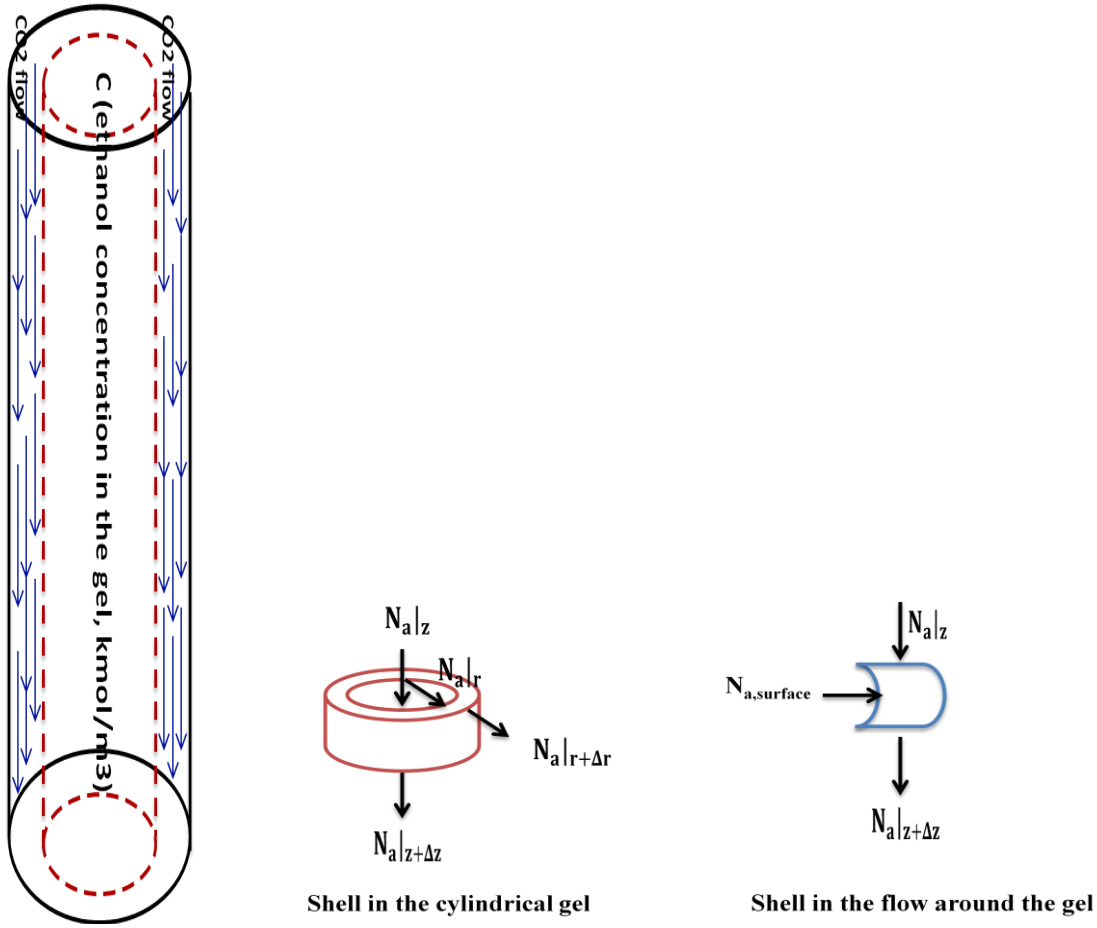

Figure 3.3.3.2.1: Schematic representation of shell mass balance in the continuous system

Molar mass balance of ethanol over the differential segments inside of the porous gel network and in the bulk flow in the vessel is individually done, as follows.

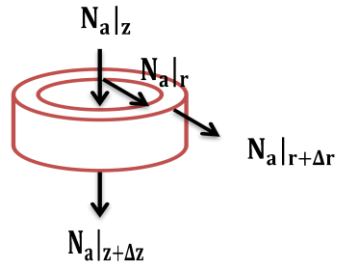

Shell in the cylindrical gel

$$(m_{ethanol})_{in} - (m_{ethanol})_{out} + (m_{ethanol})_{generated} = (m_{ethanol})_{accumulated}$$

$$\varepsilon = \frac{Vpore}{Vtotal}, \quad V_{pore} = 2\pi r \Delta r \Delta z \mathcal{E}, \quad A_{pore,r} = 2\pi r \Delta z \mathcal{E}, \quad A_{pore,z} = 2\pi r \Delta r \mathcal{E}$$

$$(N_a|_r - N_a|_{r+\Delta r})(A_{pore,r}) + (N_a|_z - N_a|_{z+\Delta z})(A_{pore,z}) = \frac{\partial (C_a V_{pore})}{\partial t}$$

$$\frac{(N_a|_r - N_a|_{r+\Delta r})(2\pi r \Delta z \mathcal{E})}{2\pi \Delta r \Delta z \mathcal{E}} + \frac{(N_a|_z - N_a|_{z+\Delta z})(2\pi r \Delta r \mathcal{E})}{2\pi \Delta r \Delta z \mathcal{E}} = \frac{\partial (C_a r)}{\partial t}$$

$$\lim_{\Delta r \to 0} \frac{(N_a|_r - N_a|_{r+\Delta r})}{\Delta r} + \lim_{\Delta z \to 0} \frac{(N_a|_z - N_a|_{z+\Delta z})}{\Delta z} = \frac{\partial (C_a r)}{\partial t}$$

$$N_{a,r} = -D_e\frac{\partial C_a}{\partial r}\ , \quad N_{a,z} = -D_e\frac{\partial C_a}{\partial z}$$

$$\frac{\partial}{\partial r}\left(D_e\frac{\partial C_a}{\partial r}r\right)+\frac{\partial}{\partial z}\left(D_e\frac{\partial C_a}{\partial z}r\right)=\frac{\partial(C_a r)}{\partial t}$$

$$\frac{1}{r}\frac{\partial}{\partial r}\left(r\,D_e\frac{\partial C_a}{\partial r}\right)+\frac{1}{r}\left(D_e\frac{\partial C_a}{\partial r}\right)+\frac{\partial}{\partial z}\left(D_e\frac{\partial C_a}{\partial z}\right)=\frac{\partial C_a}{\partial t}$$

Molar mass balance of ethanol over the differential segment in the bulk flow around the gel is done, as follows.

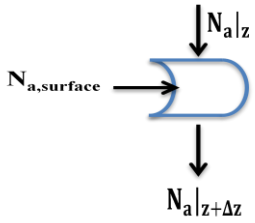

Shell in the flow around the gel

$$(m_{ethanol})_{in} - (m_{ethanol})_{out} + (m_{ethanol})_{generated} = (m_{ethanol})_{accumulated}$$

$$(N_{a,surface}A_{lateral,area}) + (N_a|_z - N_a|_{z+\Delta z})\,A_{cross\ sectional\ area} = \frac{\partial C_v V_{segment}}{\partial t}$$

$$V_{segment} = \pi\,(R^2-r^2)\,\Delta z, \quad A_{lateral,area} = 2\pi r\Delta z, \quad A_{cross\ sectional\ area} = \pi(R^2-r^2)$$

$$N_{a,surface} = K_x(C_{surface}-C_v), \qquad N_{a,z} = C_v v_z$$

where N_a is molar flux of ethanol (kmol/m^2s), C_a represents the ethanol concentration in the pores of the gel, C_v is ethanol concentration in the bulk flow, $C_{surface}$ is ethanol concentration on the gel surface, v_z is velocity of sc-CO_2 flow through the length of the vessel and K_x is mass transfer coefficient.

$$\left(\frac{K_x(C_{surface}-C_v)}{\pi(R^2\text{-}r^2)\Delta z}2\pi r\Delta z\right)+\left(\frac{C_v v_z|_z - C_v v_z|_{z+\Delta z}}{\pi(R^2\text{-}r^2)\Delta z}\,\pi(R^2\text{-}r^2)\right)=\frac{\partial C_v}{\partial t}$$

$$\left(\frac{2\,K_x r(C_{surface}-C_v)}{(R^2\text{-}r^2)}\right)+\lim_{\Delta z\to 0}\frac{(C_v v_z|_z - C_v v_z|_{z+\Delta z})}{\Delta z}=\frac{\partial(C_v)}{\partial t}$$

$$\left(\frac{2\,r\,K_x(C_{surface}-C_v)}{(R^2\text{-}r^2)}\right)-\frac{\partial}{\partial z}(v_z C_v)=\frac{\partial(C_v)}{\partial t}$$

$$\left(\frac{2\,r\,K_x(C_{surface}-C_v)}{(R^2\text{-}r^2)}\right)-v_z\frac{\partial C_v}{\partial z}=\frac{\partial(C_v)}{\partial t}$$

3.3.3.2.1 Model Equations

The contribution of mass transfer through diffusion phenomenon to the ethanol removal from the cylindrical wet gel was evaluated by using Fick's second law in cylindrical coordinates.

$$\frac{1}{r}\frac{\partial}{\partial r}\left(rD_e\frac{\partial C_a}{\partial r}\right)+\frac{1}{r}\left(D_e\frac{\partial C_a}{\partial r}\right)+\frac{\partial}{\partial z}\left(D_e\frac{\partial C_a}{\partial z}\right)=\frac{\partial C_a}{\partial t} \quad \text{(Eq 3.3.3.2.1)}$$

where C_a is concentration of ethanol in the wet gel, (kmol/m^3), D_e is effective diffusion coefficient, (m^2/s) and t is time (s), z and r is the direction that diffusion occurs in aerogel.

Additionally, variation of ethanol concentration in the bulk flow as a function of time and position is also depicted in the following equation developed.

$$\left(\frac{2\ r\ Kx\ (C_{surface}-C_v)}{(R^2\text{-}r^2)}\right)-v_z\frac{\partial C_v}{\partial z}=\frac{\partial (C_v)}{\partial t} \quad \text{(Eq 3.3.3.2.2)}$$

C_v represents ethanol concentration in the bulk flow, (kmol/m^3), R is the radius of the vessel (m), r is radius of the alcogel, K_x is mass transfer coefficient (m/s).

In Eq. 3.3.3.2.2, v_z is assumed to be constant as depicted as follows;

$$v_z=\frac{Q}{A_{\text{cross sectional area}}}$$

$$Q=\frac{\dot{m}}{\rho}$$

where Q is volumetric flow rate of sc-CO_2, ṁ is mass flow rate of the sc-CO_2, ρ is density of sc-CO_2.

ṁ is constant in the system and change in ρ is negligible; therefore, Q is assumed to be constant in the system. Since $A_{\text{cross sectional area}}$ and Q is constant in the system, v_z is assumed to be constant.

The initial and boundary conditions are given by:

Initial Conditions : t=0, $Ca(r,z,0) = C_i$ (3.3.3.2.1a)

t=0 $Cv(z,0) = 0$ (3.3.3.2.2a)

Boundary Conditions: t>0, $\frac{\partial Ca}{\partial r}=0$ at r=0 (3.3.3.2.1b)

t>0, $\frac{\partial Ca}{\partial r}=0$ at z=0 (3.3.3.2.1c)

t>0, $\frac{\partial Ca}{\partial r}=0$ at z=L (3.3.3.2.1d)

t>0, $N_a = K_x (C_{surface} - C_v)$ at r=r (3.3.3.2.2b)

3.3.4. Constitutive Equations for Model Parameters

In order to predict drying times accurately, fluid properties and effective diffusion coefficient are required. For the models in this study, effective diffusion coefficient was treated as composition dependent as CO_2 is miscible in ethanol; diffusivity of the liquid mixture is not constant and is a function of the mole fraction of CO_2. Effective diffusivity in this porous material was calculated using the binary diffusivity coefficient, material overall porosity and tortuousity, as shown in Eq. (Eq. 3.3.4.1). The binary diffusivity of ethanol and sc-CO_2 at supercritical drying temperature and pressure was calculated using

Eq. 3.3.4.3 given below, the porosity was taken as the overall porosity and tortuosity values of 1.5 and 3 were used (commonly used values for porous materials [54]).

$$D_e = \frac{D_{12}\,\varepsilon}{\tau} \qquad \text{(Eq. 3.3.4.1)}$$

To calculate the diffusivity at a particular composition, Vignes Correlation was used as given below:

$$D_{12}^{l} = (D^{og})^{x1}(D^{ol})^{1-x1} \qquad \text{(Eq. 3.3.4.2)}$$

,where (D^{og}) is binary diffusion coefficient of ethanol in sc-CO_2 in the ideally diluted state and (D^{ol}) is binary diffusion coefficient of sc-CO_2 in ethanol in the ideally diluted state.

For the prediction of the diffusivity of sc-CO_2 in ethanol (D^{ol}) at supercritical drying conditions and diffusivity of ethanol in sc-CO_2, the method of Wilke and Chang [48] shown by Eq. 3.3.2.4.3 was used.

$$D_{12} = 1.1728 * 10^{-16} \frac{T(\dot{x}_2 M_2)^{1/2}}{\mu_2 V_1^{0.6}} \qquad \text{(Eq. 3.3.4.3)}$$

Component 1 represents the solute which is ethanol, while component 2 is the solvent which is sc-CO_2. μ_2 in Pa.sec is the solvent viscosity, V_1 in m^3/kmol is the solute molar volume at the normal boiling point and $\dot{x}_2$ is the solvent association parameter and M_2 is the solvent molecular weight. $\dot{x}_2$ is 1.5 for ethanol and 1 for CO_2 [54]. Physical properties of the components are tabulated in Table 3.3.2.4.

Table 3.3.2.4: Physical properties of CO_2 (1) and ethanol (2) at 40 °C, 100 bar [52]

	at 40°C, 100 bar
ρ_1 (kg/m^3)	630
ρ_2 (kg/m^3)	760
D_{12}^{l} (m^2/s)	$1.117*10^{-8}$
D_{21}^{g} (m^2/s)	$1.585*10^{-8}$
μ_1 (Pa.s)	$4.52*10^{-5}$
μ_2 (Pa.s)	$2.502*10^{-5}$

Partial differential equations for diffusion of ethanol and sc-CO_2 in the pores were solved by Finite Difference Method (FDM), which is depicted in detail in the following section. The gel was divided into uniformly spaced grids. At each node, each derivative was approximated by an algebraic expression which references the adjacent nodes. These were simultaneously solved in the same algorithm and final concentration values of ethanol and CO_2 in the gel could be obtained. Subsequently, initial moles of ethanol occupying the pores of the gel were calculated using volume and density of pure ethanol at operating conditions. Similarly, the final mole of ethanol in the gel was calculated multiplying final concentration of ethanol by the volume occupied in the gel. Finally, percent ethanol extracted from the pores was calculated by difference in mole number of ethanol between initial and final case.

3.3.5 Finite Difference Method for Solution of Partial Differential Mass Transfer Equations

In the finite difference method, the governing equations are approximated by a point-wise discretization scheme where derivatives are replaced by difference equations that involve the values of the solution at the nodal points. In this method, the discretization process involves first dividing the solution region into a network of grid or mesh of intersecting lines, which are drawn parallel to the coordinate axes. The discrete intersecting points of these gridlines are called the grid or nodal points. Once the grid is generated, the governing equations and boundary conditions are then transformed into discretization equations at each nodal point to obtain a set of algebraic equations that involve the unknown values at the grid points. Finally, this set of algebraic equations is solved for the unknown nodal values.

The fundamental steps in obtaining a numerical statement of the problem using finite difference categorized, as follows [57].

1. State the mathematical statement of the problem in terms of governing equations, boundary conditions and initial conditions.

2. Discretize the solution domain into a network of discrete nodal points. The unknown values are sought only at those discrete points rather than obtaining a continuous solution in the domain.

3. Obtain discretization equations for all nodal points by approximating the governing differential equations and boundary conditions. This discretization procedure leads to a set of algebraic equations involving the unknown values at the nodal points.

4. Use an appropriate solution algorithm to solve the set of algebraic equations involving the unknown values at the nodal points.

5. Post-processing of the data to evaluate secondary quantities.

3.3.5.1 Discretization of The Domain

In this method, two dimensional calculation domain is divided into equal or unequal small regions with increments of Δx and Δy in the x and y directions, respectively, as shown in Figure 3.3.5.1.

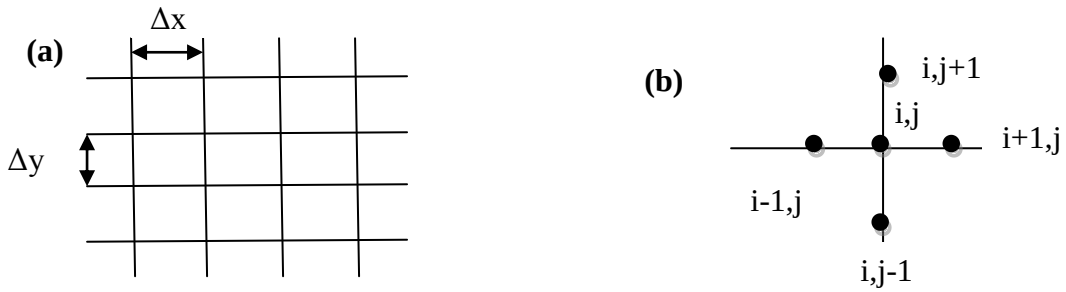

Figure 3.3.5.1: Finite discretization scheme

The finite difference discretization scheme is one of the simplest forms of discretization and does not easily include the topological nature of equations. A classical finite difference approach approximates the differential operators constituting the field equation locally. Therefore, a structured grid is required to store local field quantities. For each of the points of the structured grid the differential operators appearing in the main problem specification are rendered in a discrete expression. The order of the differential operator of the original problem formulation directly dictates the number of nodes which are involved [57].

3.3.5.2 Discretization of the Mathematical Model

The discretization equation or finite difference equations can be derived using Taylor series method. In the Taylor series method, each derivative is approximated with the help of a difference formula that is derives from truncated Taylor series expansion, while in control volume method, the governing equation is discretized by integrating it over an appropriately chosen control volume.

3.3.5.2.1 The Taylor Series Method

In the Taylor series method, each space and time derivatives are approximated by appropriate finite difference approximation formulas, which are derived by using the Taylor series expansions. Therefore, this method involves two steps. First, appropriate numerical finite difference formulas are selected and then discretization equation is obtained by substituting these formulas in the governing equation.

3.3.5.2.1.2 Numerical Differentiation-Finite Difference Formulas

Numerical differentiation of a governing differential equation is carried out by approximating the derivatives with the finite difference formulas, which are derived using the truncated Taylor series expansions. A function f(x,y) at the point (i+1,j) can be expressed in terms of the function value and its derivatives at a neighboring point (I,j) using forward Taylor series expansion [57];

$$f_{i+1,j} = f_{i,j} + f'_{i,j}h + \frac{1}{2!}f''_{i,j}h^2 + \frac{1}{3!}f'''_{i,j}h^3 + \cdots + \frac{1}{n!}f_{i,j}{}^{n}h^n + R_n \quad \text{(Eq. 3.3.5.2.1.2)}$$

where $h=\Delta x=x_{i+1}-x_i$, n! represents the factorial of n, and $R_n(x)$ is a remainder term, representing the difference between the Taylor polynomial of degree n and the original

function. The remainder term is basically a representation of the truncation error, and it is expressed as

$$Rn = \frac{1}{(n+1)!} fi^{n+1} h^{n+1}$$

Similarly, a function f(i,j) at the point (i-1,j) can be expressed in terms of the function value and its derivatives at a neighboring point (i,j) using the backward Taylor series expansion

$$f_{i-1,j} = f_{i,j} - f'_{i,j}h + \frac{1}{2!}f''_{i,j}h^2 - \frac{1}{3!}f'''_{i,j}h^3 + \cdots + \frac{1}{n!}f_{i,j}{}^{n}h^n + R_n) \quad \text{(Eq. 3.3.5.2.1.3)}$$

3.3.5.2.1.3 Forward Difference Approximation: This approximation estimates the derivative at the point (i,j) using the values at the point (i,j) and a forward point (i+1,j). This formula is derived neglecting all the terms h^2 and higher in the forward Taylor series expansion given by Equation, and solving for the first derivative term [57].

$$f'_{i,j} = \frac{f'_{i+1,j} - f'_{i,j}}{h} + \frac{R1(x)}{h}$$

$$\frac{R1}{h} = \frac{fi,j''}{2!}h$$

$$fi,j' \approx \frac{f'_{i+1,j} - f'_{i,j}}{h}$$

3.3.5.2.1.4 Backward Difference Approximation: Similar to the forward difference approximation, the backward difference approximation formula is derived by neglecting all the terms of h^2 and higher in the backward Taylor series expansion given by Eq. and solving for the first derivative term as ;

Using the first derivative of the function *f* as an example, by Taylor's theorem [57],

$$\mathrm{fi,j'} \approx \frac{\mathrm{f'_{i,j} - f'_{i-1,j}}}{\mathrm{h}} + \frac{\mathrm{R1(x)}}{\mathrm{h}}$$

$$\frac{\mathrm{R1}}{\mathrm{h}} = \frac{\mathrm{f''}}{2!}\mathrm{h}$$

$$\mathrm{f'_{i,j}} \approx \frac{\mathrm{f'_{i,j} - f'_{i-1,j}}}{\mathrm{h}}$$

3.3.5.2.1.5 Central Difference Approximation: The equation obtained using forward Taylor expansion presented by Eq. 3.3.5.2.1.2 is subtracted from the equation obtained by backward Taylor series expansion shown in Eq. 3.3.5.2.1.3 to obtain;

$$\mathrm{f'_{i+1,j} - f'_{i-1,j}} = 2\mathrm{fi,j'h} + \frac{2\mathrm{fi,j'''}}{3!}(\Delta \mathrm{x})^3 + \cdots + \mathrm{R_n}$$

$\mathrm{R_n}$ is so small that it can be neglected,

$$\mathrm{f'_{i+1,j} - f'_{i-1,j}} = 2\mathrm{fi,j'h} + \mathrm{R_2}$$

Solving for the first derivative, the approximation is obtained as follows,

$$f'_i \approx \frac{f'_{i+1,j} - f'_{i-1,j}}{2h}$$

Similarly, second derivatives of the forward difference, backward difference and central difference approximations are obtained as follows,

Forward difference second derivative :

$$f''_i \approx \frac{f'_{i+2} - 2f'_{i,+1} + f'_i}{2h}$$

Backward difference second derivative:

$$f''_i \approx \frac{f'_i - 2f'_{i,-1} + f'_{i-2}}{2h}$$

Central difference second derivative:

$$f''_i \approx \frac{f'_{i+1} - 2f'_i + f'_{i-1}}{h^2}$$

Chapter 4

RESULTS & DISCUSSION

Results obtained in this study are going to be introduced in two main sections. In the first section, simulation results carried out to investigate the effects of various process parameters on drying time of the wet gel and the results of simulations investigating effect of several operation variables including mass transfer coefficient, temperature, gel porosity and tortuosity as well as thickness of the gels in the batch supercritical drying are depicted. In the second section,

4.1. Results of Mathematical Modeling of Alcogel Supercritical Drying in Batch System

4.1.1. Effect of Mass Transfer Coefficient on Extraction Time

The effect of mass transfer coefficient on drying time was investigated using a broad range of mass transfer coefficient. Figure 4.1.1 (a) demonstrates that as mass transfer coefficient increases; the time for the drying reduces approaching a limiting value and extraction time stays almost constant at values of the mass transfer coefficient higher than 0.0015 m/s. There is no impact of increasing the value on extraction time. It can be said that mass transfer is predominantly controlled by diffusion after this limiting value and ethanol molecules which reach the surface of the gel are instantly swept away from the surface. However, drying performed with the lowest mass transfer coefficient is primarily controlled by diffusion. From this figure, mass transfer coefficient in the case depicted in

Figure 4.1.2 (c) could also be assumed to be in between $1.8*10^{-5}$ m/s and $2.8*10^{-6}$ m/s considering the drying times obtained in our laboratory.

Figure 4.1.1 (b) illustrates how concentration of ethanol changes from the center of the aerogel to the surface of the aerogel at two different temperature values (T=308 K and T=313 K, respectively). For these temperature values, mass transfer coefficient values are estimated to be $1.05*10^{-5}$ m/s and $1.3*10^{-5}$ m/s, respectively. At the center, concentration of the ethanol is quite high initially and since the gel is initially entirely filled with ethanol. Ethanol is surrounded by sc-CO_2 diffusing into the liquid phase and the concentration of CO_2 in the pore increases with time as ethanol is removed from the gel and is replaced by CO_2. Furthermore, this figure shows that concentration of ethanol throughout the gel decreases faster at higher mass transfer coefficient.

(a)

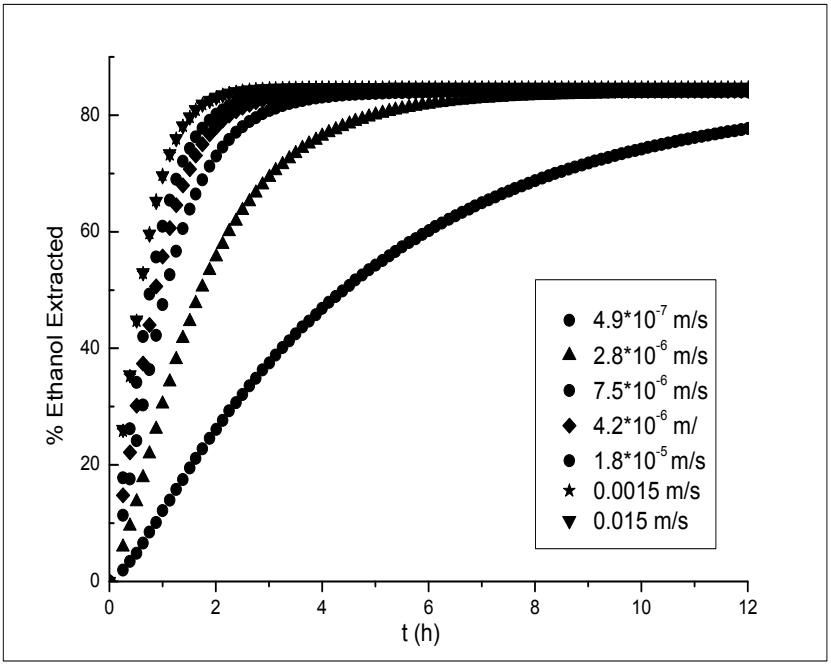

(b)

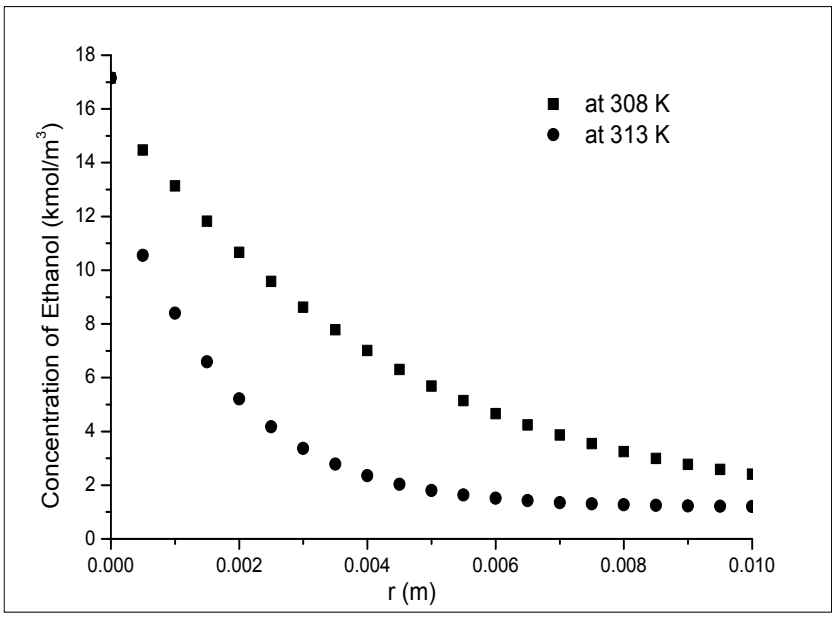

Figure 4.1.1: (a) Effect of mass transfer coefficient on ethanol removal from spherical aerogel (T= 323 K, P=100 bar, gel thickness =1 cm) (b) Concentration variation of ethanol through the radius of spherical gel (at T=308, P=100 bar, Kx=1.05*10^{-5} m/s, Kx=1.3*10^{-5} m/s and T= 313 K, gel thickness =1 cm, for 5 h drying time)

4.1.2. Effect of Temperature on Extraction Time

Figure 4.1.2 (a), Figure 4.1.2 (b) and Figure 4.1.2 (c) show effect of temperature on percent ethanol removal in spherical, cylindrical and rectangular shaped gels as a function of time at different operating temperatures of 308 K, 313 K and 323 K, respectively. It is found that temperature does not significantly affect extraction time. It is slightly higher at elevated temperatures since diffusivity of CO_2 also increases with temperature. Additionally, increase in temperature could also accelerate mass transfer and improve the extraction yield.

(a)

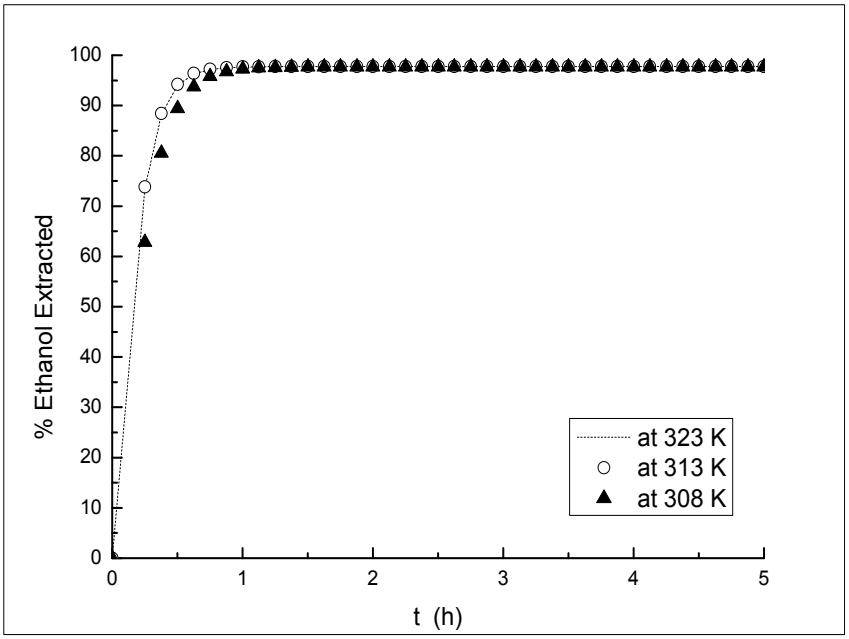

(b)

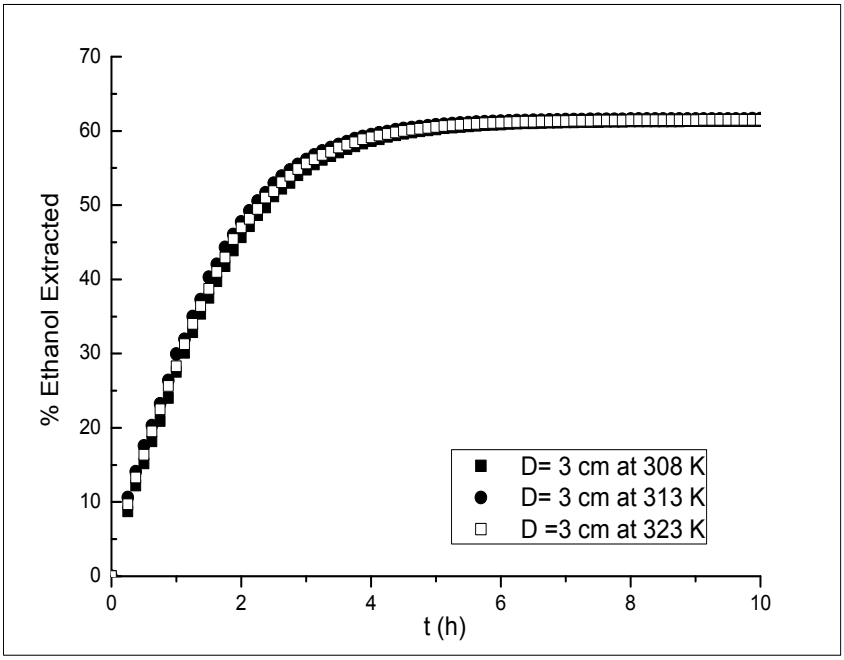
% Ethanol Extracted
t (h)
D= 3 cm at 308 K
D= 3 cm at 313 K
D =3 cm at 323 K
0
10
20
30
40
50
60
70
0
2
4
6
8
10

(c)

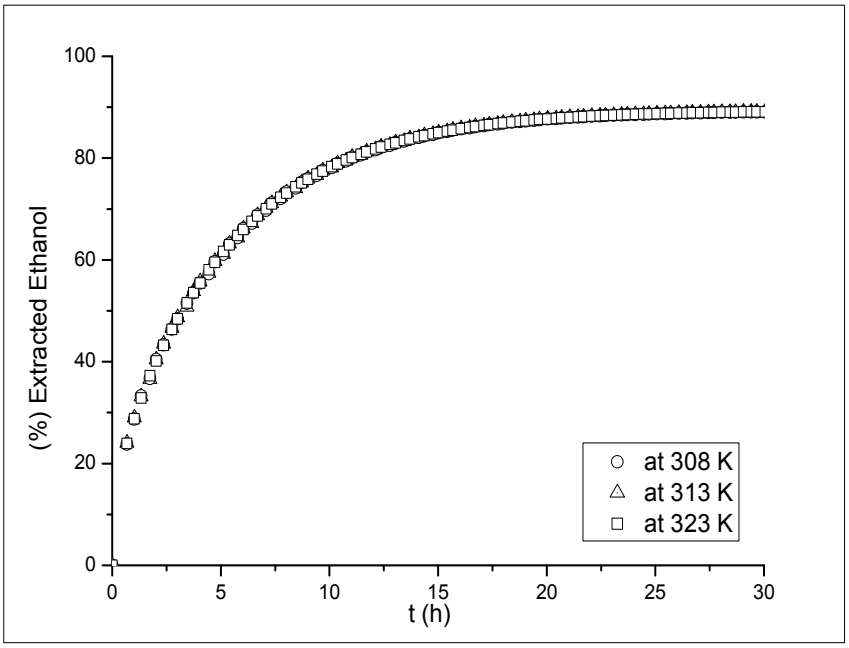

Figure 4.1.2 : (a) Effect of temperature on removal over time in spherical alcogel (at T=308 K, T= 313 K and T= 323 K, gel diameter= 2cm) (b) (b) Effect of temperature on removal over time in cylindrical alcogel (at T=308 K, T= 313 K and T= 323 K, gel diameter= 2cm) (c) Effect of temperature on removal over time in rectangular alcogel (at T=308 K, T= 313 K and T= 323K, gel thickness= 1cm)

4.1.3. Effect of Gel Thickness on Extraction

The dimension of the gel body is one of parameters greatly influencing drying times of the wet gel. Figure 4.1.3.1 shows the effect of gel thickness for alcogels with different geometry of alcogel. As expected, the gels with larger dimensions need longer drying times due to the presence of larger amount of ethanol in the pores. Extraction occurs in a shorter time in thinner gels, whereas it takes a longer time in thicker gels. Figure 4.1.3.1 (a) and Figure 4.1.3.1 (b) also illustrate that almost 60 % of ethanol could be extracted from the spherical and cylindrical gels with 1.5 cm thickness, whereas approximately 95 % of ethanol in the gels with 0.5 cm thickness is extracted. That is because as the amount of ethanol in the pores increases, the amount of ethanol diffused into the vessel increases, as well. As a result, the concentration of ethanol in the fluid surrounding the gel in the vessel becomes higher. Hence, concentration gradient between ethanol in the gel and vessel decreases with time and becomes zero at some point in time. After this time, the remaining amount of the ethanol in the gel cannot be extracted. The difference between drying times for aerogel with different thickness (0.5 cm, 1 cm and 1.5 cm) is around 3 hr. Additionally, variation of drying time with thickness of three samples of rectangular and spherical silica gels is also illustrated in Figure 4.1.3.2 (a) and 4.1.3.2 (b), respectively. As a consequence, it can be said that drying time strongly depends on the gel thickness.

(a)

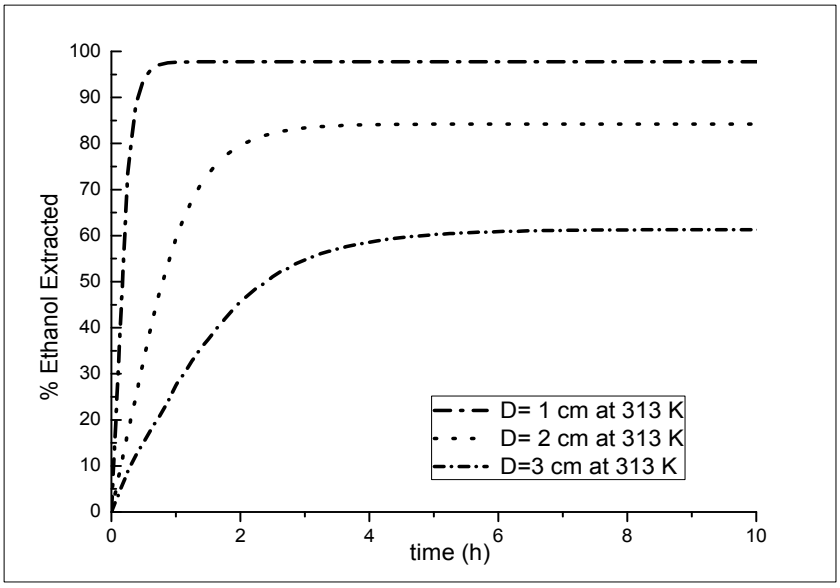
% Ethanol Extracted
time (h)
D= 1 cm at 313 K
D= 2 cm at 313 K
D=3 cm at 313 K

(b)

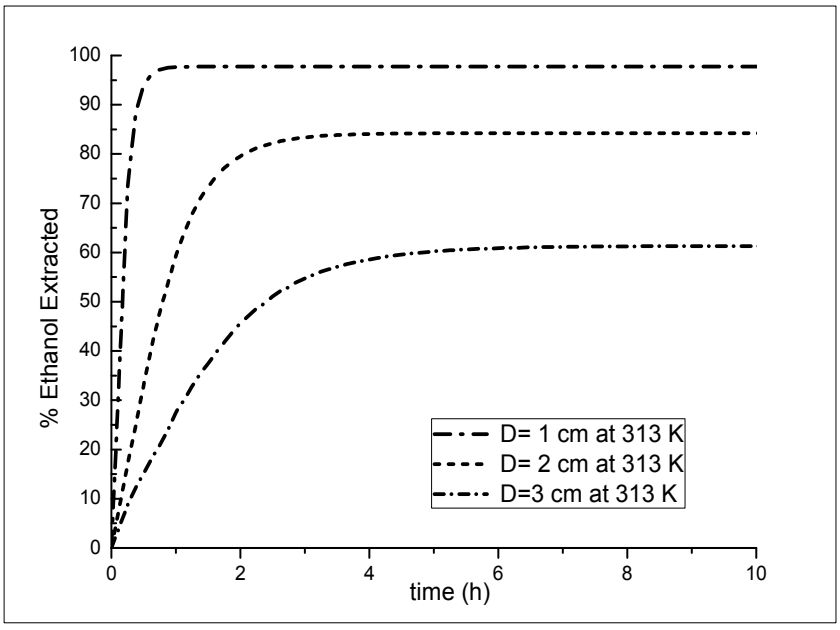
% Ethanol Extracted
time (h)
D= 1 cm at 313 K
D= 2 cm at 313 K
D=3 cm at 313 K

(c)

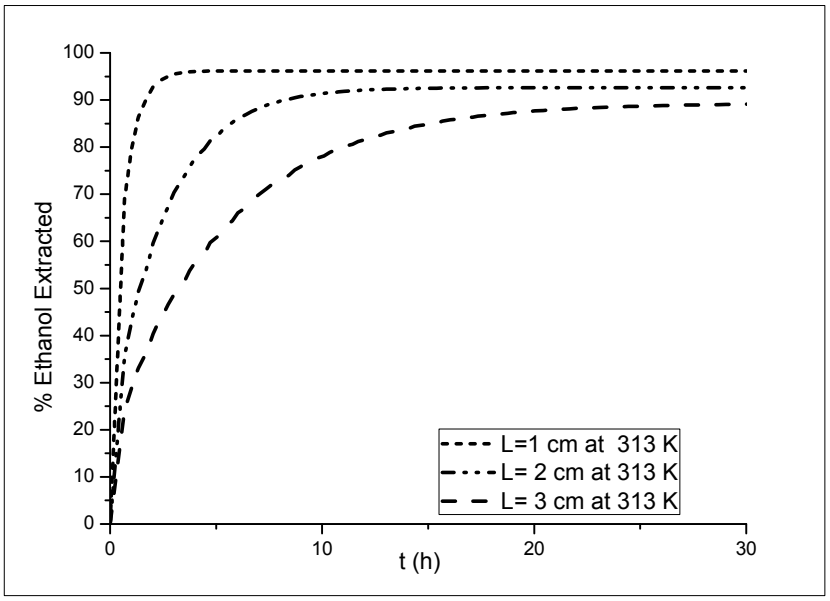

Figure 4.1.3.1: (a) Effect of gel thickness on removal over time in spherical alcogel (at P=100 bar, T= 313 K gel diameter= 1cm, gel diameter= 2cm and gel diameter=3 cm) (b) Effect of gel thickness on removal over time in cylindrical alcogel (at P=100 bar, T= 313 K gel diameter= 1cm, gel diameter= 2cm and gel diameter=3 cm) (c) Effect of gel thickness on removal over time in rectangular alcogel (at P=100 bar, T=308 K, T= 313 K and T= 323 K, gel thickness= 1cm)

(a)

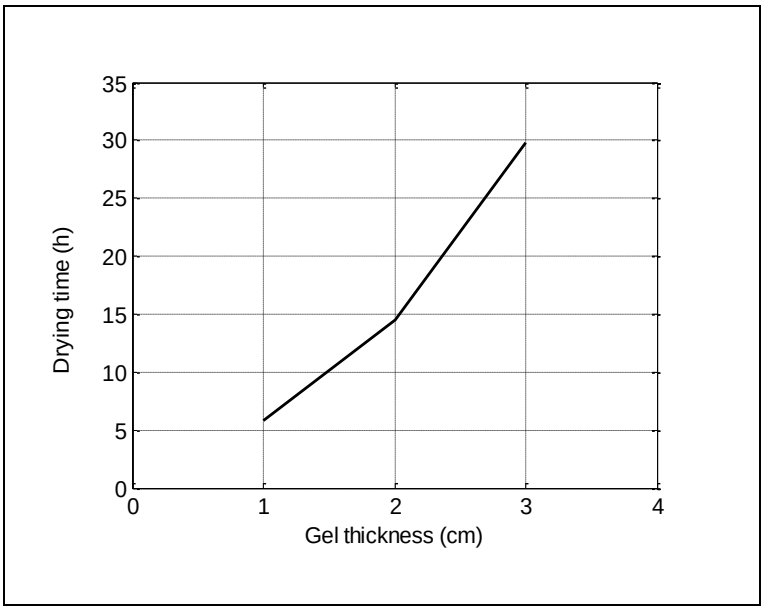

(b)

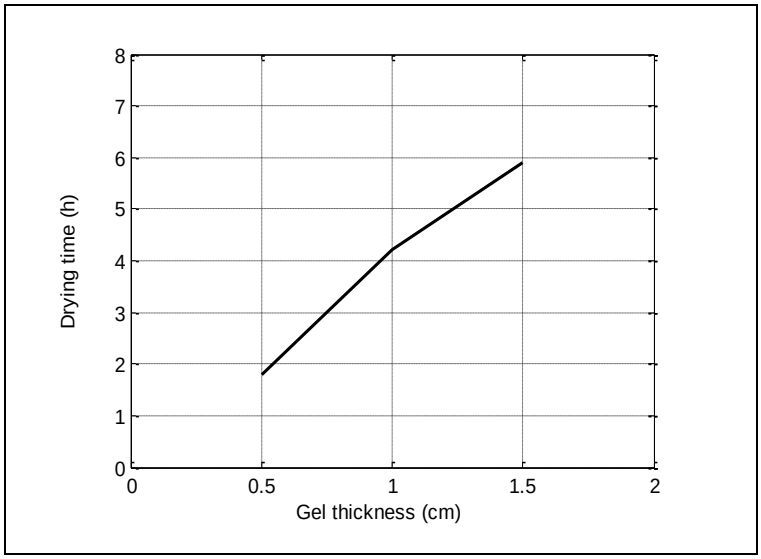

Figure 4.1.3.2: (a) Variation of drying time with gel thickness in rectangular wet gel (b) Variation of drying time with gel thickness in spherical wet gel

4.1.4 Effect of Effective Diffusion Coefficient on Extraction

Effective diffusivity in the porous materials such as aerogel is directly related to binary diffusion coefficient and material overall porosity, while it is inversely related to tortuousity. Effect of these parameters on the extraction time of the spherical wet gel was investigated, individually.

4.1.4.1 Effect of Gel Tortuosity on Extraction

Effect of gel tortuosity on extraction time of spherical gels with the tortuosity values of 2, 2.5 and 3 was studied. Figure 4.1.4.1 (a) demonstrates that tortuous gels are extracted in a longer period of time. The tortuous path in the gel hinders ethanol extraction from the pores and time increases. The gel with the highest tortuosity is extracted in 4 h, while the gel with the lowest tortuosity is extracted in almost 2 h.

(a)

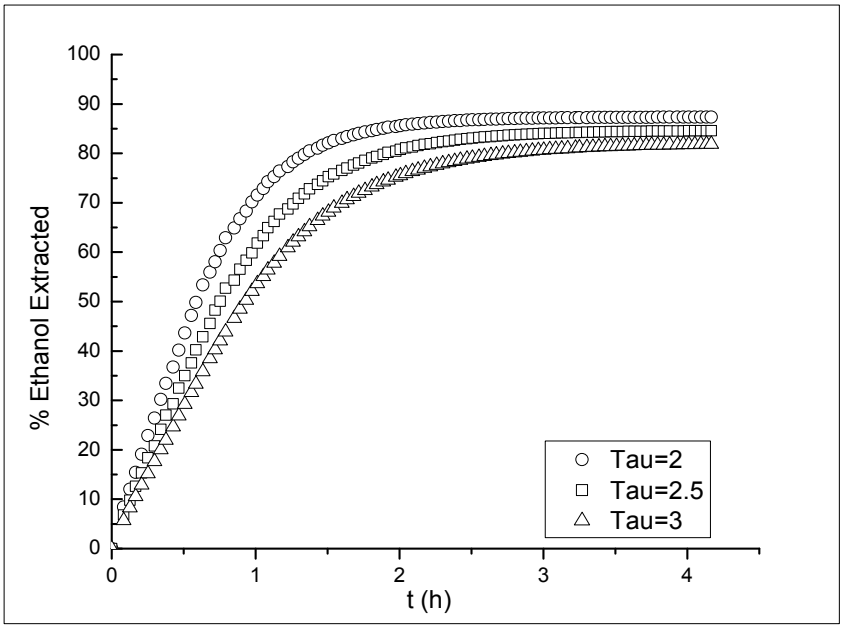

Figure 4.1.4.1: (a) Effect of tortuosity on ethanol removal over time in spherical aerogel (T= 313 K, P=100 bar, gel thickness =2 cm, Kx=1.3*10^{-5} m/s)

4.1.4.2 Effect of Gel Porosity on Extraction

Extraction time of ethanol from the spherical gels with the porosity of 98 %, 95% and 92 %, respectively was examined. Figure 4.1.4.2 (a) shows that extraction time barely decreases with increasing porosity. Ethanol is extracted slightly faster in the gel with the highest gel porosity. That is because effective diffusivity shows a small increase with increasing porosity. This result is also important to estimate drying time of polymer-silica aerogel composites such as PDMS-Silica aerogel and PVP- Silica aerogel composites. The composite aerogels are less porous than the silica aerogels. Thus, the time for extraction of

ethanol from the pores of the gel is expected to be longer than the time for extraction of silica aerogels.

(a)

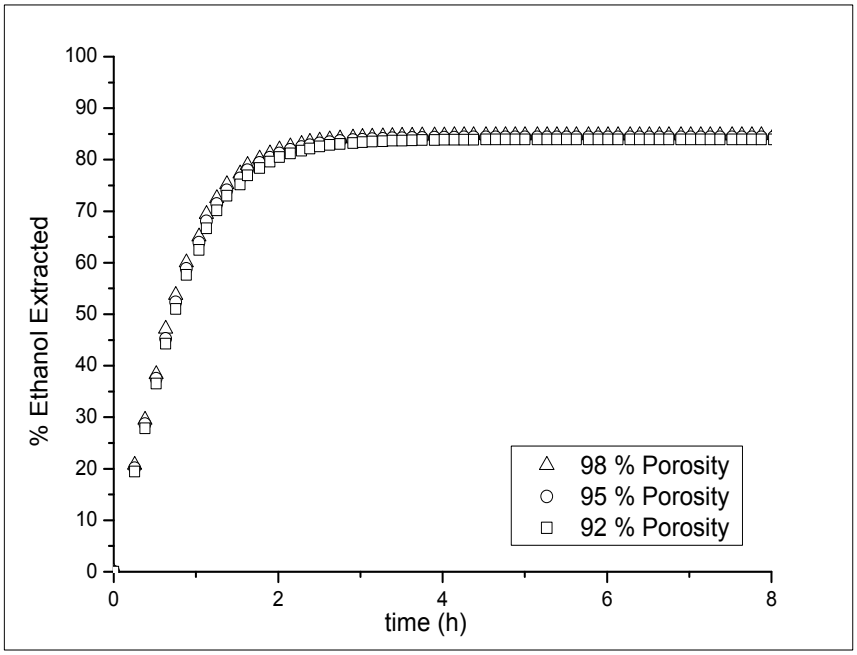

Figure 4.1.4.2: (a) Effect of porosity on ethanol removal over time in spherical aerogel (T= 313 K, P=100 bar, gel thickness =2 cm, Kx=1.3*10^{-5} m/s)

4.1.5. Comparison of Analytical and Numerical Solution of Extraction in a Well-mixed, Infinitely Large Volume of Solution (Kx≈∞)

An analytical solution for leaching of salt from a cylindrical solid waste is proposed by P. Colombo et al. [54]. The salt is placed in a liquid which is assumed to be well mixed; thus, fast convective mass transfer from the solid surface to the liquid takes place. Eq. 4.1.5 represents the analytical solution proposed in the study. The mass transfer mechanism in this process is analogous with the first case of the extraction in the batch vessel, which is described in the section 3.3.2.2. In this case**,** the gel is put in a perfectly mixed, very large batch vessel and ethanol is removed from the pores of the gel to well mixed sc-CO_2. In order to evaluate how well the simulation results predict, partial differential model equations were solved in MATLAB and then, the results were compared with the analytical solution result. In Figure 4.1.5.1, concentration profiles which was calculated from the analytical solution (Eq. 4.1.5.) for various values of the dimensionless time; Dt/L^2 are shown. Figure 4.1.5.2 illustrates the concentration profiles at various dimensionless time obtained from the simulation. As can be seen, the profiles obtained from the simulation fit sufficiently well with the profiles calculated from the analytical solution.

$$c(t,x) = \frac{4c_0}{\pi}\sum_{n=0}^{\infty}\frac{(-1)^n}{2n+1}\exp\left[-\frac{(2n+1)\pi^2 Dt}{4L^2}\right]\left[\cos\frac{(2n+1)\pi x}{2L}\right] \quad \text{(Eq. 4.1.5)}$$

where c is concentration of ethanol in the gel, co is initial concentration of ethanol in the gel, x represents the direction through the thickness of the gel, L is half thickness of the gel from the center, D is diffusivity (m^2/s).

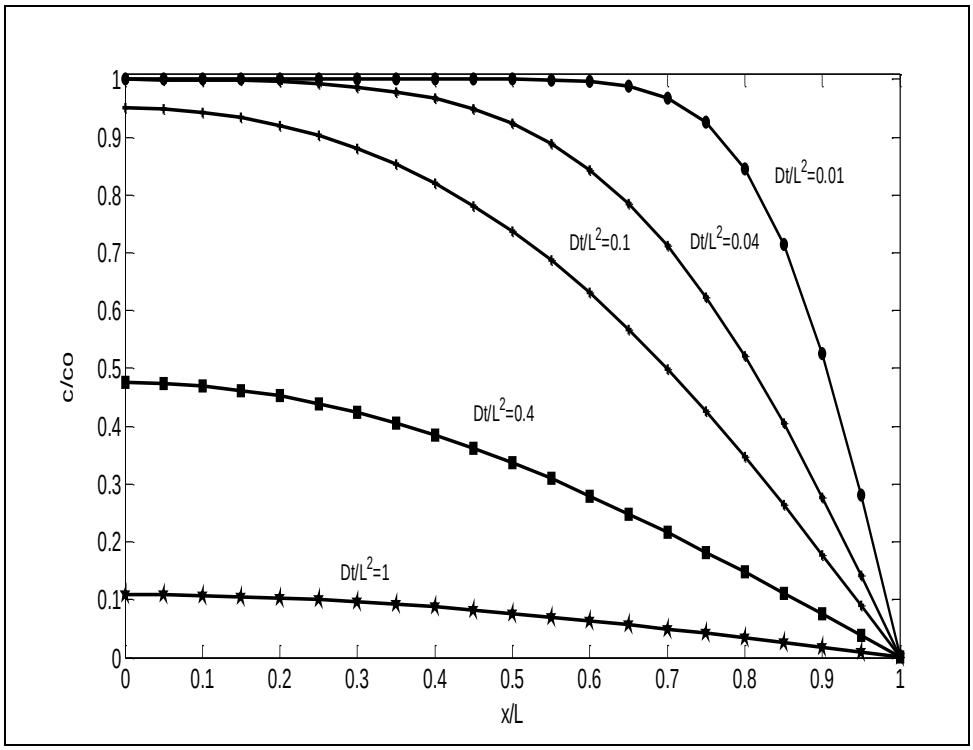

Figure 4.1.5.1: Dimensionless concentration profiles for salt diffusion in the solid waste at various dimensionless numbers (Dt/L^2) as obtained from Eq. 4.1.5.

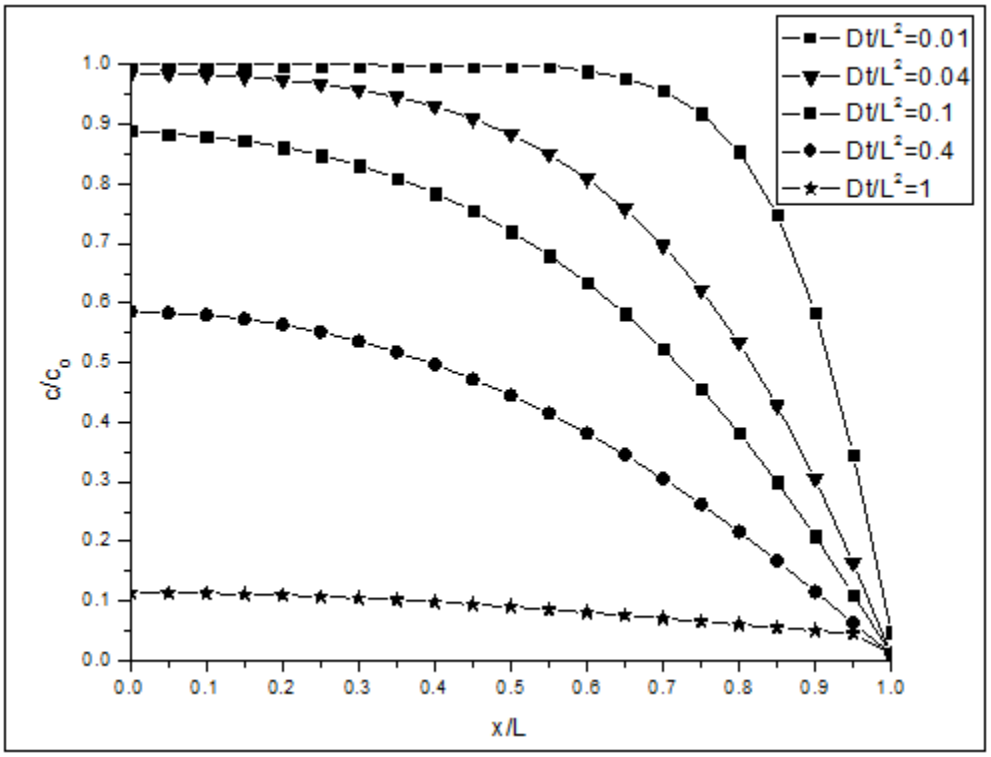

Figure 4.1.5.2: Dimensionless concentration profiles of ethanol with various dimensionless times (Dt/L^2) as obtained from simulation

4.2 Results of Modeling of Alcogel Supercritical Drying with Continuous CO_2 Flow

4.2.1. Wet Gel Drying Profile Study

Similar to the batch supercritical CO_2-assisted drying of the silica wet gel, the extraction curve obtained as a result of the continuous supercritical drying showed a time-dependent profile. The extraction curve of ethanol is shown in Figure 4.2.1. At the beginning of the extraction period, extraction rate, which represents extracted amount of ethanol per unit time increased with time and then, it declined continuously over the whole time course. Approximately 70 % of the ethanol in the porous structure of the wet gel was removed during the initial period of time of 30 minutes, and then the extraction rate dropped over the whole extraction period, particularly for the removal of the last about 5 % of ethanol remaining in the pores of the gel. From this ethanol extraction profile, it can be said that diffusion controlled mass transfer mechanism became predominant as drying time progressed and less ethanol remained in the gel.

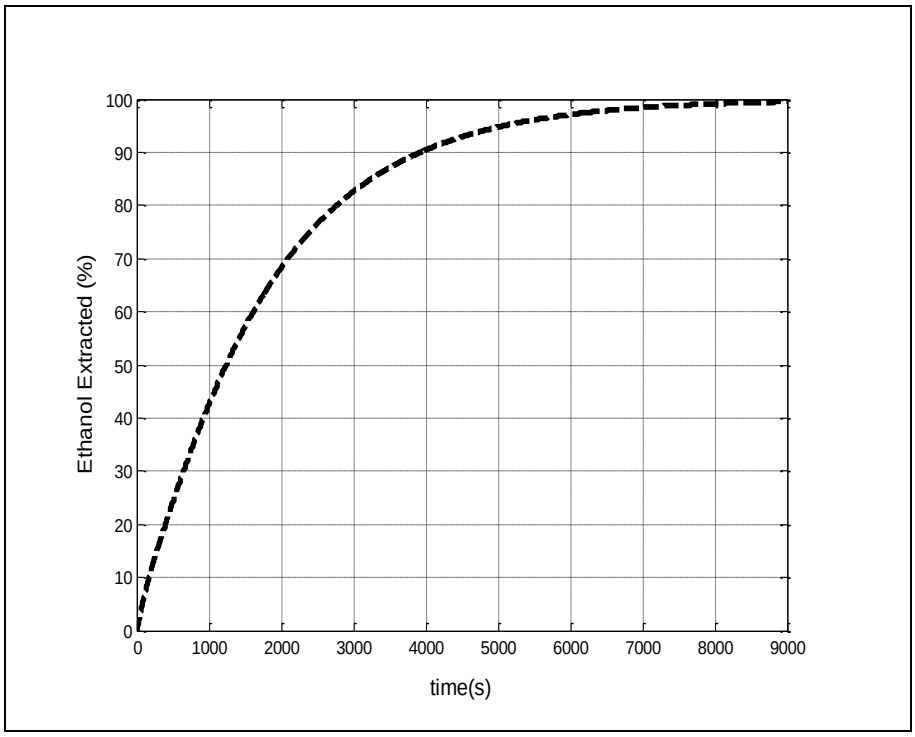

Figure 4.2.1: Ethanol extraction profile of the wet gel rod at 10 MPa and 313.15K

4.2.2 Comparison of Model Results with Experimental Data

Ethanol extracted from the porous structure of the cylindrical wet gel prepared in the laboratory was collected in the collection vials, immersed in the dry ice bath, in certain time intervals during the whole process of supercritical extraction. The mass of ethanol collected is shown in Figure 4.2.2.1. As can be seen, at the initial period of 10 min, large amount of ethanol is extracted. This is because initially, concentration gradient of ethanol between the liquid phase in the pores of the gel and the bulk flow of sc-CO_2 in the vessel is somewhat large. Therefore, ethanol is readily able to diffuse out of the pores into sc-CO_2 phase. The ethanol diffused in the vicinity of the gel surface is removed by convective mass

transfer due to the presence of the continuous flow of sc-CO_2 in the vessel. Consequently, at this point, it is expected that only convective mass transfer resistances influence extraction process. In the first period of time of 40 min, more than 73 % of ethanol was collected. Then, drying rate (amount of ethanol extracted per unit time) slowed down. It is supposed that diffusion controlled mass transfer became more predominant during the process after this point. Especially, the last 1.5 % of ethanol remaining in the gel was removed in a quite long time.

Figure 4.2.2 illustrates supercritical extraction of cylindrical wet gel prepared and the data obtained from the model. It can be seen that the present model proposed for supercritical drying of the wet gels with sc-CO_2 for replacement of ethanol from the porous structure of the gel fits satisfactorily well with the experimental data.

(a)

(b)

Figure 4.4.2.1: Ethanol extracted from the pores of the wet gel in the certain time intervals during the supercritical drying experiment in the laboratory.

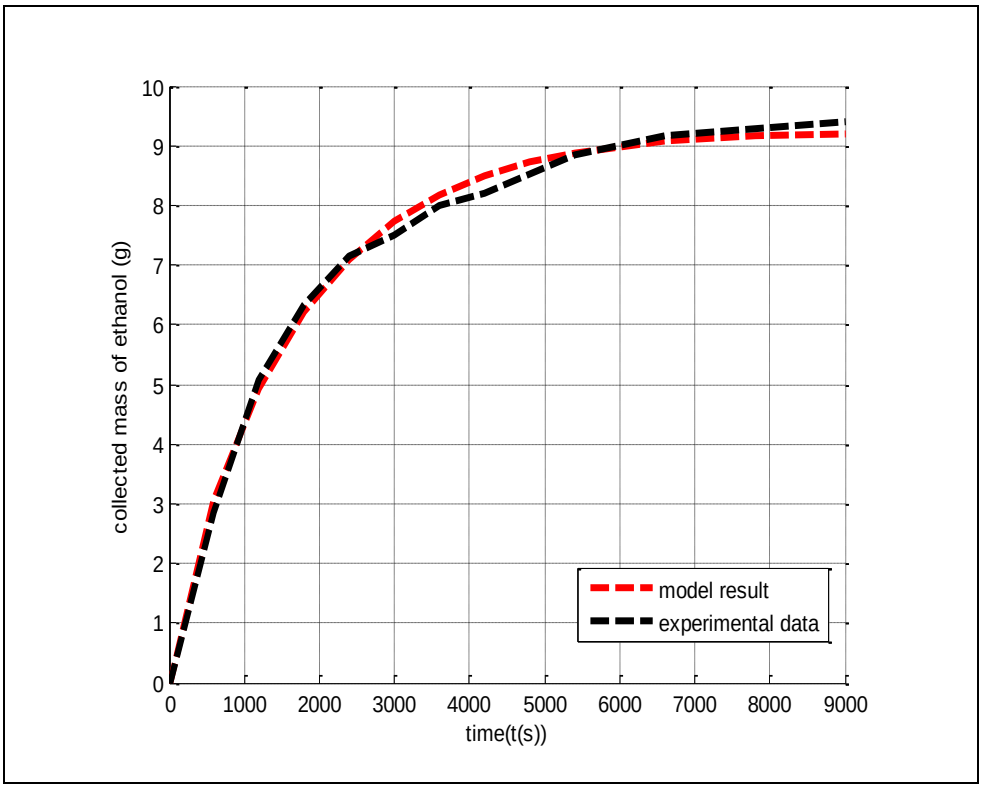

Figure 4.2.1.2: Comparison of experimental data profile and supercritical extraction model profile

Using this profile of extraction data of the model, a mass transfer coefficient was reggressed and then, was compared with the calculated mass transfer values using correlations in the literature. However, a mass transfer coefficient value, which is exactly fit with such a system of liquid- supercritical CO_2 extraction in the continuous flow, has not already been included in the literature. Therefore, a few Sherwood number correlations for the system which is analogous with our system were used. The calculated values and estimated value of the mass transfer coefficient are tabulated in Table 4.2.2. As can be seen, the predicted and calculated values are not too much different from each other.

Table 4.2.2: Calculated Mass Transfer Values

Sherwood Number Correlations	**Kx(m/s)**
$\mathrm{Sh} = 0.3 + \frac{0.62R_e}{\mathrm{Re}^{1/2}\mathrm{Sc}^{1/3}(1+(0.4/\mathrm{Sc})^{2/3})^{1/4}}\left(1+\left(\frac{R_e}{282000}\right)^{5/8}\right)^{4/5}$ [52]	$1.227*10^{-4}$
$\mathrm{Sh}=2+1.1*\mathrm{Re}^{0.6}\,\mathrm{Sc}^{1/3}$ [55]	$1.089*10^{-4}$
$\mathrm{Sh}=0.206*(\mathrm{Re})^{0.8}(\mathrm{Sc})^{1/3}$ [56]	$1.251*10^{-4}$
Regressed Value :	$2.56*10^{-4}$

4.2.3. Concentration Variation of Ethanol in the System as a Function of Time and Position

4.2.3.1. Variation of Ethanol Concentration in the Bulk Flow

Figure 4.2.3.1 illustrates variation of ethanol concentration in the bulk flow as a function of time at varying distances from the inlet of the vessel to the outlet of the vessel. In the beginning of the extraction, the continuous bulk flow of CO_2 is free from ethanol. Thus, concentration gradient of ethanol is initially so large that ethanol could naturally diffuse out of the pores of the gel to the bulk flow. Then, ethanol concentration in the vessel at that point instantly increased, as can be seen in the figure. Then, it declined over the whole course of the process. This is because ethanol at these certain points in the vessel is continuously swept through the vessel by a continuous flow of sc-CO_2 via convective mass transfer mechanism. However, as can be seen from this figure, all concentration profiles (at these distances) except the profile at the distance around the vessel outlet show the same behavior. That means ethanol concentration almost never change in the z direction. This is due to the presence of the same amount of mass flux to the bulk flow from the gel in the r direction in each point in the z direction in the gel since concentration of ethanol in the gel merely change in the r direction not in the z direction and thus, ethanol concentration at every point of the gel surface is the same. The reason is that the gel thickness is far smaller than the length of the gel ($L/D \approx 26.75$); therefore, the path for the diffusion of the ethanol in the r direction is rather short and then, ethanol is tend to readily diffuse through the gel thickness rather than diffusing through the z direction. As a result, mass transfer of ethanol in the gel most primarily occurs in the r direction.

Moreover, the gel is expected to be placed at the bottom of the vessel in the upright position barely moving and therefore; it is assumed that no ethanol diffuses through the

bottom of the container and convectional mass transfer flux of flowing sc-CO_2 contributes to removal of the ethanol at this point of the vessel and thus faster drop of the ethanol concentration at the vessel outlet occurs.

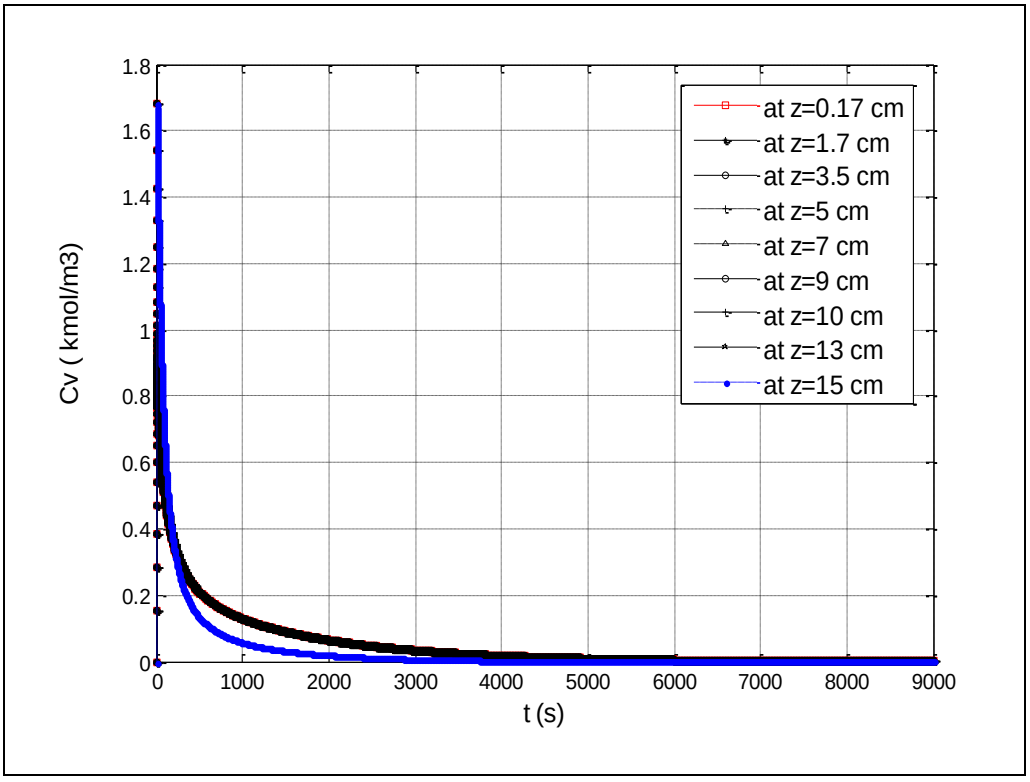

Figure 4.2.3.1: Variation of ethanol concentration in the bulk flow as a function of time

4.2.3.2. Variation of Ethanol Concentration in the Gel

Concentration of ethanol in the gel is a function of time and position. The change of ethanol concentration at the surface and at the center of the gel as a function of time is shown in Figure 4.2.3.2.1 and Figure 4.2.3.2.2, respectively. In Figure 4.2.3.2.1, ethanol concentration gradually decreased as time progressed. Initially, the gel is full of pure ethanol at rest and then, sc-CO_2 also diffused into the pore liquid and ethanol content decreased in the pore mixture with time. Similarly, variation of ethanol at the surface of the gel, which is given in Figure 4.2.3.2.2 also decreased with time. However, at the surface, it rapidly dropped off since at the center diffusion controlled mass transfer occurred, while at the surface ethanol was primarily removed through convective mass transfer owing to the continuous flow of sc-CO_2 around the gel. That is because diffusion is a more sluggish mechanism of the mass transfer than convective mass transfer.

Additionally, variation of ethanol concentration at the beginning of the process and at the end of the extraction is plotted as a three dimensional (3D) profile, given in Figure 4.2.3.3 and Figure 4.2.3.4 (a). Initially, the pores of the gel network are entirely occupied with pure ethanol; therefore, ethanol concentration is constant and is uniform in both directions, which is shown in Figure 4.2.3.3. In other 3D profile, which is given in Figure 4.2.3.4 (a) ethanol concentration variation in both directions of r and z at the end of the process is demonstrated. It is obvious that ethanol concentration mainly changed in the r direction instead of the z direction since the ratio of length of the gel to the thickness of the gel is quite large; thus, the path for the diffusion of ethanol is shorter in the r direction and readily achievable. As a consequence, the diffusion process could be considered one-dimensional in the r direction. This means that the mass transfer of ethanol in the z direction could be neglected.

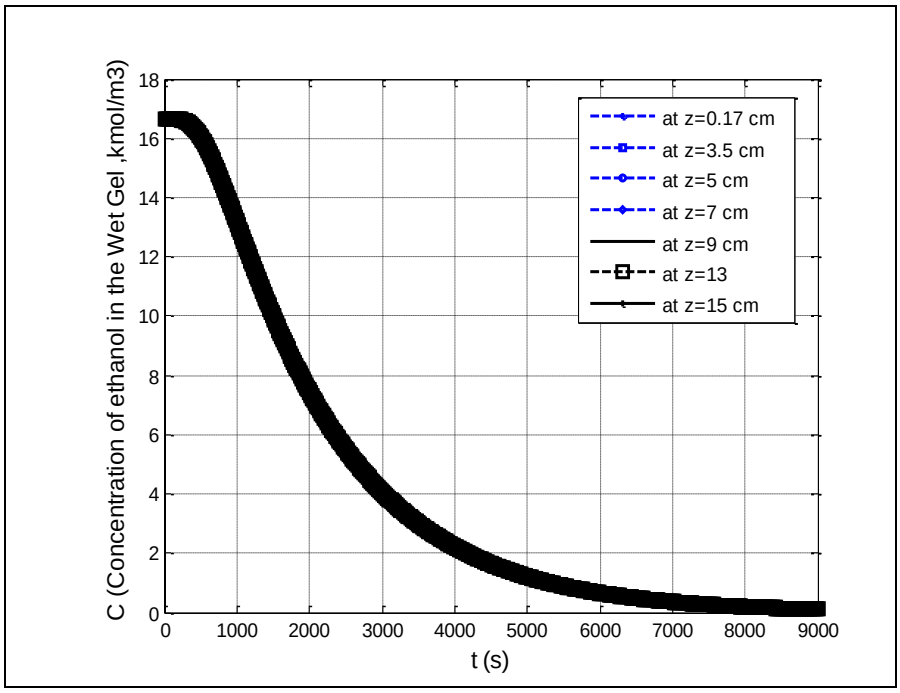

Figure 4.2.3.1: Variation of ethanol concentration with time at the center of the gel

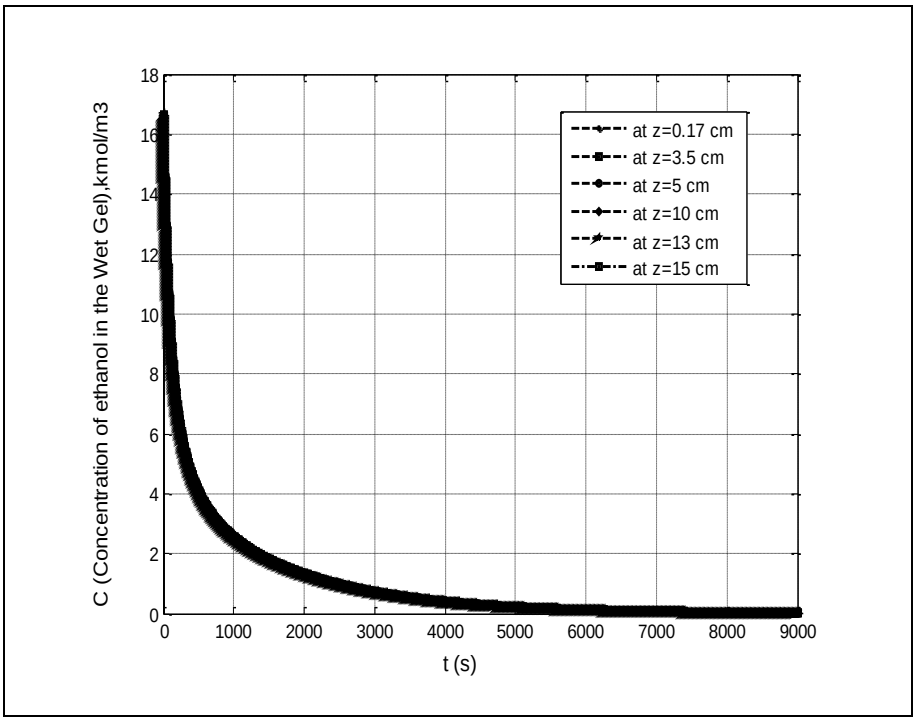

Figure 4.2.3.2: Variation of ethanol concentration as a function of time at the surface of the gel

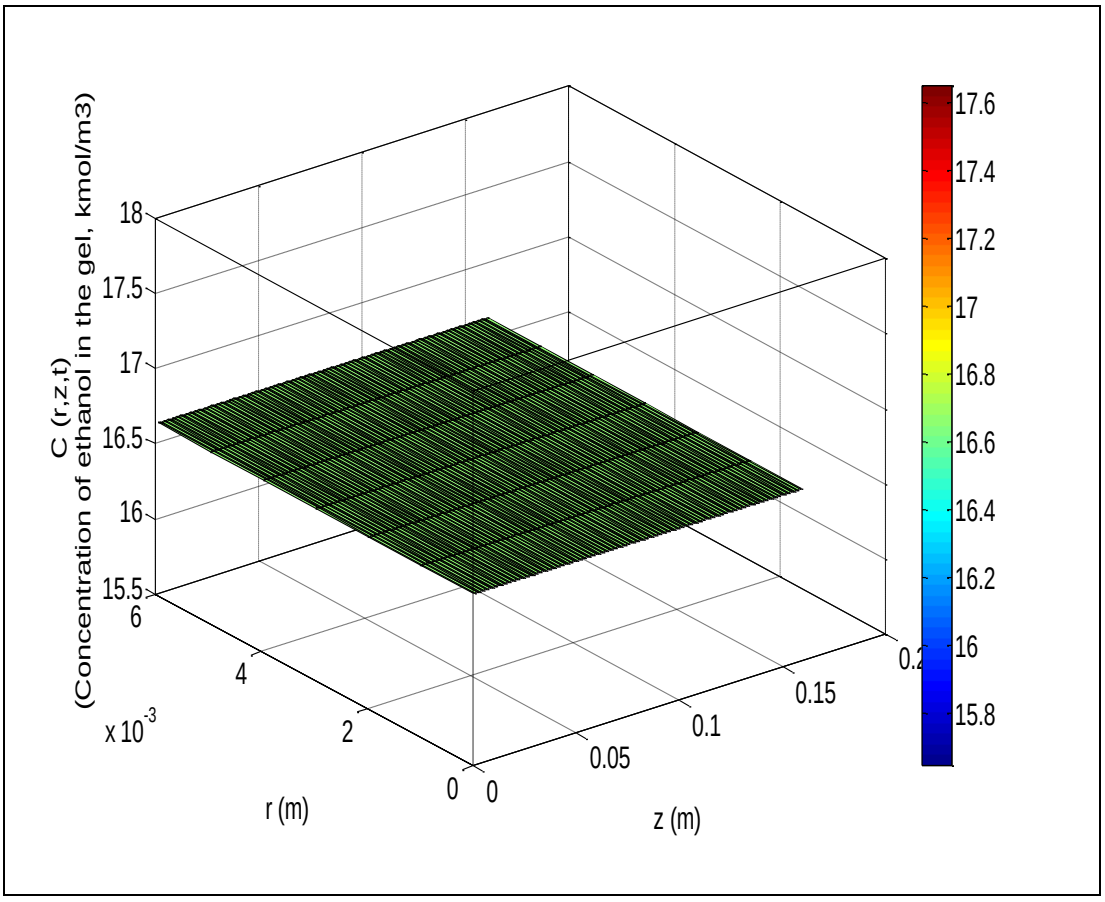

Figure 4.2.3.3: 3D ethanol concentration profile for r=0.059 cm and L=15.9 cm (at the beginning of the extraction)

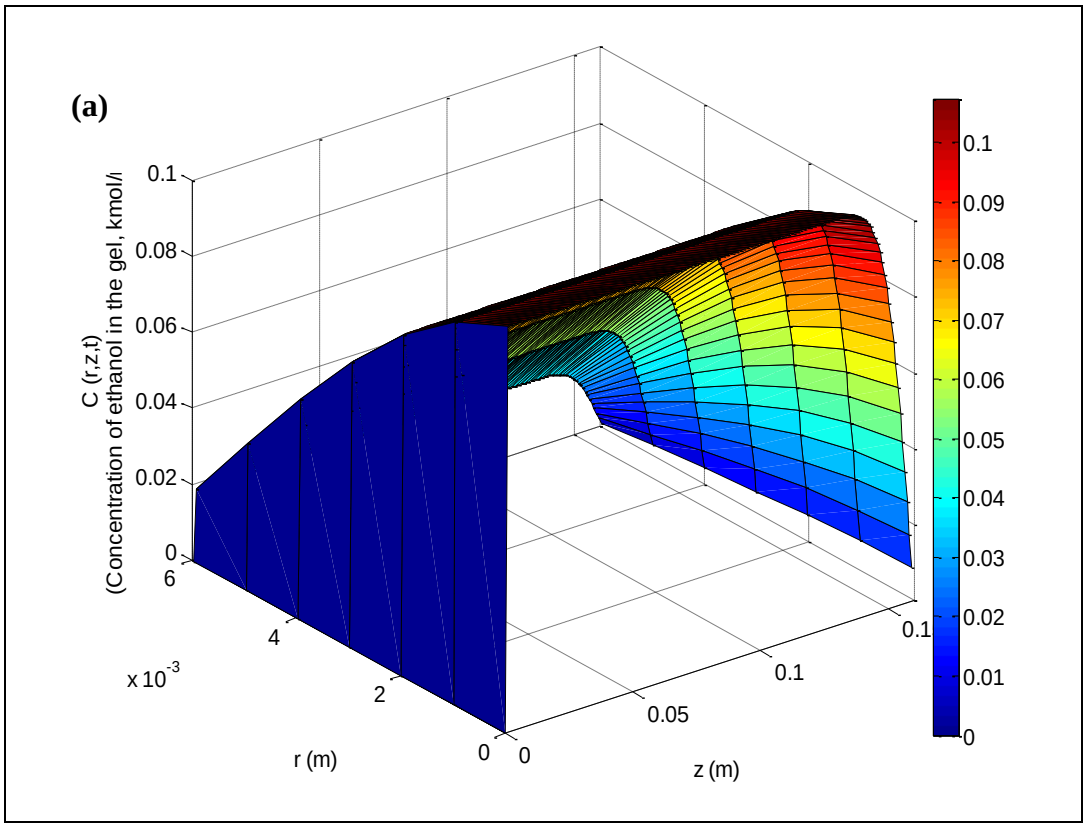
(a)
C (r,z,t)
(Concentration of ethanol in the gel, kmol/l
0.1
0.08
0.06
0.04
0.02
0
6
4
2
0
x 10-3
r (m)
0
0.05
0.1
z (m)
0.1
0.09
0.08
0.07
0.06
0.05
0.04
0.03
0.02
0.01
0

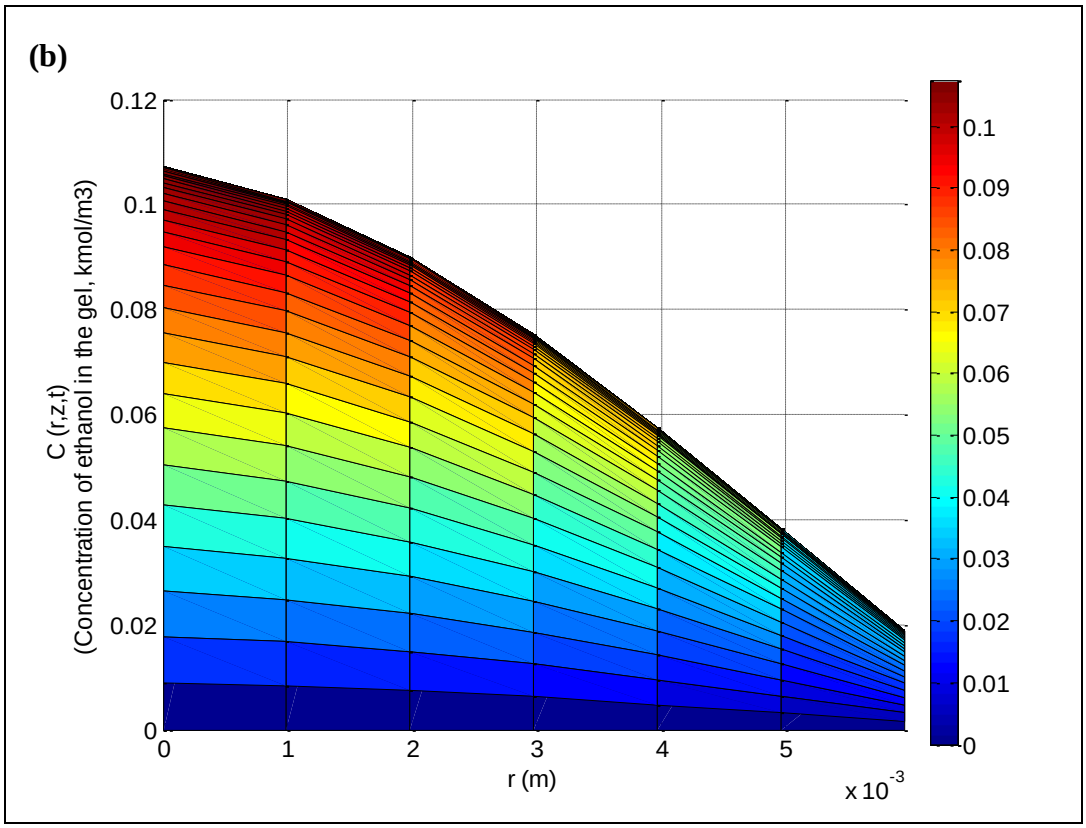
(b)
C (r,z,t)
(Concentration of ethanol in the gel, kmol/m3)
0.12
0.1
0.08
0.06
0.04
0.02
0
0
1
2
3
4
5
r (m)
x 10-3
0.1
0.09
0.08
0.07
0.06
0.05
0.04
0.03
0.02
0.01
0

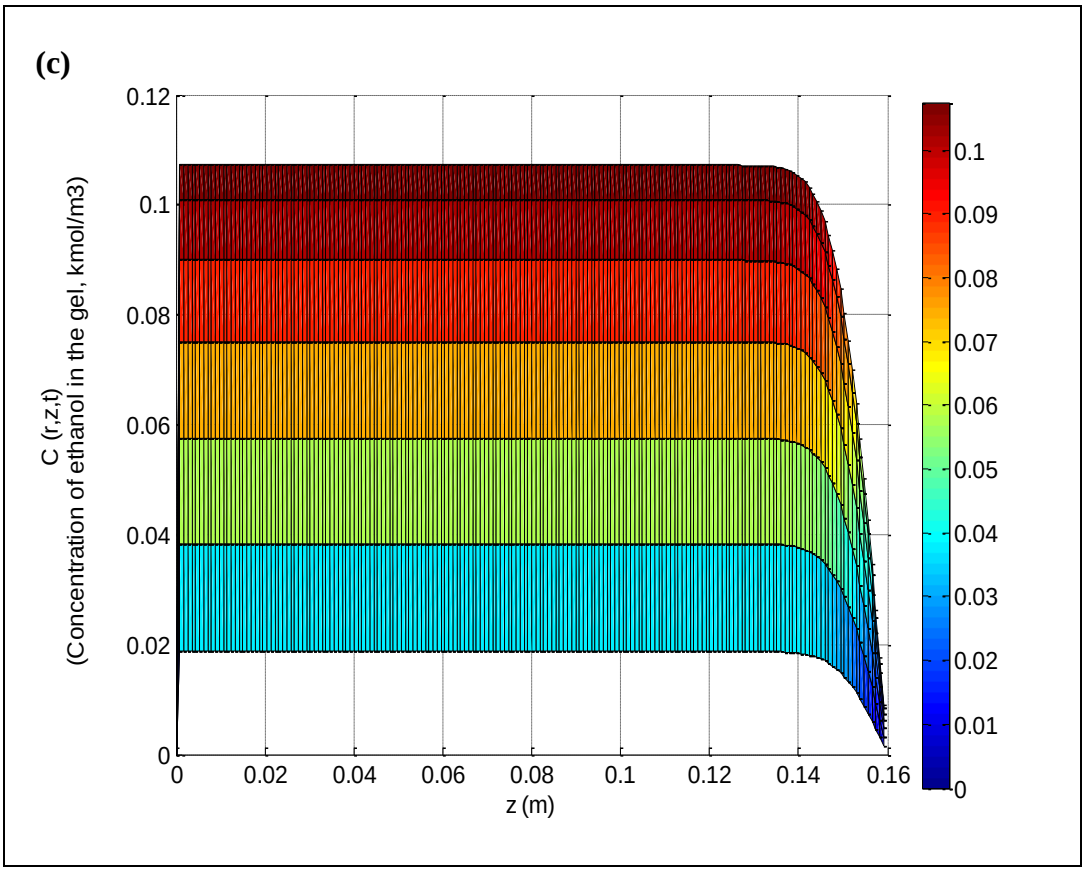

Figure 4.2.3.4: (a) 3D ethanol concentration profile for r=0.059 cm and L=15.9 cm (at the end of the extraction) (b) Concentration profile of ethanol in the gel in the r direction (at the end of the extraction) (c) Concentration profile of ethanol in the gel in the z direction (at the end of the extraction)

CHAPTER 5

CONCLUSION

In this study, mathematical models for supercritical drying have been developed to predict drying times of wet gels. If drying time can be accurately estimated, production cost and time could be efficiently optimized. In this study, mathematical models were developed to predict extraction time of silica alcogels. The models were used to simulate two types of supercritical drying: batch supercritical drying and continuous supercritical drying, respectively. This study has included convectional mass transfer mechanism contribution to the solvent removal in the model equations, which has not been present in research into the modeling of supercritical drying of wet gels in the literature. Moreover, comparison of experimental study of continuous supercritical drying of the wet gels with model results could be executed in our study, unlike studies in the literature.

In the first part, extraction of solvent fully occupying the pores of spherical, cylindrical and rectangular alcogels of varying dimensions into supercritical CO_2 in the batch system was studied. The effect of operation variables, including temperature, mass transfer coefficient, gel body properties, such as porosity and tortuosity, as well as thickness of the gels on drying time in the batch supercritical drying was investigated. It was found that mass transfer coefficient and gel dimensions have a large effect on the extraction time. Time for the diffusion of sc-CO_2 notably decreased with increasing mass transfer coefficient and increased with increasing thickness. Furthermore, it was found that

operating temperature slightly affects extraction time. Moreover, that extraction time for a gel with higher tortuosity was found lower.

Another conclusion in the batch supercritical drying is that supercritical drying of the wet gels in the batch system is governed by a mass transfer mechanism based on a combination of convection and diffusion. However, supercritical extraction of wet gels was expected to be predominantly governed by diffusion as drying time progressed and less solvent remained in the gels.

In the second part in which supercritical extraction of the gel (1.19 cm in diameter x15.92cm in length) with continuous sc-CO_2 was performed in the laboratory, it was found that the present model proposed for the continuous supercritical dying of the wet gels with sc-CO_2 for replacement of ethanol from the porous structure of the gel fitted sufficiently well with the experimental data. Furthermore, the mass transfer coefficient regressed from experimental data was compared with the correlations proposed in the literature for supercritical extraction for the operation conditions (1.5 L sc-CO_2/min volumetric flow rate and 313.15 K and 100 bar) at which supercritical extraction was executed. The predicted and calculated values were found to be close each other. Moreover, the experimental study also indicated that the process is a function of time.

Similar to the batch supercritical drying model result, as a consequence of both experimental and model study it was concluded that continuous supercritical drying of the wet gel is conducted by both convective and diffusion mass transfer mechanism in the course of the extraction. Diffusion contribution to the process increased towards the end of the process; however, convective mass transfer was still present.

Finally, as future work of this study, effects of operation conditions on continuous supercritical drying of alcogel could be investigated. Additionally, drying time of polymer-composite alcogels could be estimated by accounting for gel porosity and tortuosity by incorporation of polymer.

BIBLIOGRAPHY

[1] Gerona, M.M.i., *Silica Aerogels: Synthesis and Characterization*. 2002, University of Barcelona. p. 273.

[2] Soleimani Dorcheh, A. and M.H. Abbasi, *Silica aerogel; synthesis, properties and characterization.* Journal of Materials Processing Technology, 2008. **199**(1-3): p. 10-26.

[3] Gurav, J. L., et al. (2010). Silica aerogel: Synthesis and applications. Journal of Nanomaterials, 2010.

[4] Pajonk, G.M., *ChemInform Abstract: Aerogel Catalysts.* ChemInform, 1991. **22**(33): p. no-no.

[5] Cantin, M., et al., *Silica aerogels used as Cherenkov radiators.* Journal Name: Nucl. Instrum. Methods, v. 118, no. 1, pp. 177-182; Other Information: Orig. Receipt Date: 31-DEC-74; Bib. Info. Source: NL (Netherlands (sent to DOE from)), 1974: p. Medium: X.

[6] Buzykaev, A., et al., *Aerogels with high optical parameters for Cherenkov counters.* Nuclear Instruments and Methods in Physics Research Section A: Accelerators, Spectrometers, Detectors and Associated Equipment, 1996. **379**(3): p. 465-467.

[7] Rubin, M. and C.M. Lampert, *Transparent silica aerogels for window insulation.* Solar Energy Materials. **7**(4): p. 393-400.

[8] Hrubesh, L.W., *Aerogel applications.* Journal of Non-Crystalline Solids, 1998. **225**: p. 335-342.

[9] Rideal, E. K. (2007). An Introduction to Surface Chemistry: Nash Press.

[10] Weissmüller, J., et al. (2010). *Deformation of solids with nanoscale pores by the action of capillary forces*. Acta Materialia**, 58**(1), 1-13.

[11] Hench, L.L. and J.K. West, *The sol-gel process.* Chemical Reviews, 1990. **90**(1): p. 33-72.

[12] Rakesh P. Patel., N.S.P., Ajay M Suthar, *An Overview of Silica Aerogels.* International Journal, 2009. **1**(4): p. 1052-1057.

[13] Bergna, H. E., & Roberts, W. O. (2006). *Colloidal silica: Fundamentals and applications* (Vol. 131). Boca Raton, Fla.: Taylor & Francis.

[14] Brinker, C. J., & Scherer, G. W. (1990). *Sol-gel science: The physics and chemistry of sol-gel processing*. Boston: Academic Press.

[15] Chandradass, J., et al. (2008). Synthesis of silica aerogel blanket by ambient drying method using water glass based precursor and glass wool modified by alumina sol. Journal of Non-Crystalline Solids, **354**(34), 4115-4119.

[16] Turova, N. Y. (2002). *The chemistry of metal alkoxides*. Boston, Mass.: Kluwer Academic Publishers.

[17] Tillotson, T. M., Hrubesh, L.W. (1992). Transparent ultralow-density silica aerogels prepared by a two-step sol-gel process. Journal of Non-Crystalline Solids, **145**(C), 6.

[18] Tan, H., et al. (2010). Mullite fibers prepared from an inorganic sol-gel precursor. Journal of Sol-Gel Science and Technology, **53** (2), 378-383.

[19] Ward, D.A. and E.I. Ko, *Preparing Catalytic Materials by the Sol-Gel Method.* Industrial & Engineering Chemistry Research, 1995. **34** (2): p. 421-433.

[20] J. Tlusty and M. Polacek, The Stability of Machine Tools Against Self Excited Vibrations in Machining, International Research in Production Engineering, ASME, (1963) 465-474. Hench, L.L. and J.K. West, *The sol-gel process.* Chemical Reviews, 1990. **90**(1): p. 33-72.

[21] Loy, D. A., et al. (1997). Direct Formation of Aerogels by Sol - Gel Polymerizations of Alkoxysilanes in Supercritical Carbon Dioxide. Chemistry of Materials, **9**(11), 2264-2268.

[22] I. Minis and T. Yanushevsky, A New Theoretical Approach for the Prediction of Machine Tool Chatter in Milling, Trans. ASME Journal of Engineering for Industry, **115** (1993), 1-8.

[23] Loy, D. A., et al. (2005). *Evolution of porosity and morphology in alkylene-bridged polysilsesquioxane xerogels as a function of gel aging time*, Boston, MA.

[24] Brunner, G. (2004). *Supercritical fluids as solvents and reaction media* (1. Ed.). Amsterdam: Elsevier.

[25] McHugh, M.A. and V.J.Krukonnis, *Supercritical fluid extraction: Principles and practice*, ed. Butterworth, Boston, 1986.

[26]. Brenneck, J.F. and Eckert, C. A, *Phase equilibria for supercritical fluid process design*. AlCheE J., **35**, 1409-1427 (1989).

[27] R.J. Maxwell, *Supercritical Fluid Tecvhnology in Oil and Lipid Chemistry,* ed. J. W. King and G. R. List, AOCS Press, Champaign,p .20 (1996).

[28] G. Brunner, J. Supercritical Fluids, **13**, 283 (1998).

[29] E. Reverchon, J. Supercritical Fluids, **10**, 1 (1997).

[30] Zabaloy, M. S.; Vasquez, V. R.; Macedo, E. A. Viscosity of pure supercritical fluids. *J.of Supercrit. Fluids.* 2005**, 36**, 106–117.

[31] Subra, P.; Jestin; P. Powders elaboration in supercritical media: comparison with conventional routes. *Powder Technol.* 1999**, 103**, 2-9.

[32] Y. Arai, T. Sako, Y. Takebayashi (Eds.), *Supercritical Fluids, Molecular Interactions, Physical Properties, and New Applications.*

[33] Clifford, T.(ed.), *Fundamentals of supercritical*. Oxford Science Publications. Chapter 2, (1999)

[34] Gabriela Illiann Burgos Solórzano, Supercritical Fluid Technology: Computational and Experimental Equilibrium Studies and Design Of Supercritical Extraction Processes, PhD, Of The University Of Notre Dame, Indiana

[35] George W. Scherer, *Aging and Drying of Gels,* Journal of Non-Crystalline Solids **100** (1988) 77-92.

[36] G.W. Scherer, J. Non-Cryst. Solids **91** (1987) 101.

[37] C.J. Brinker and G.W. Scherer, J. Non-Cryst. Solids **70** (1985) 301.

[38] T .W. Zerda, I. Artaki and J.J. Jonas, J. Non-Crst. Solids **81** (1986) 365.

[39] M. Mukhopadhyay, B.S. Rao, Modeling of supercritical drying of ethanolsoaked silica aerogels with carbon dioxide, Journal of Chemical Technology and Biotechnology **83** (2008) 1101–1109

[40] Vági, E., Simandi B., Vásárhelyné Perédi K., Daood H., Kery Á., Doleschall F., Nagy B., *Supercritical carbon dioxide extraction of carotenoids, tocopherols and sitosterols from industrial tomato by-products*, Journal of Supercritical Fluids **40** (2007), 218-226.

[41] Rey, L. R., & May, J. C. (2004). *Freeze-drying/lyophilization of pharmaceutical and* biological products (2. ed., rev. and exp. ed. Vol. 137). New York: Dekker.

[42] Povh, N.P., Marques, M.O.M. and Meireles, M.A.A., 2001. Supercritical CO2 extraction of essential oil and oleoresin from chamomile (Chamomilla recutita [L.] Rauschert). J. Supercritical Fluids, 21(3): 245-256.

[43] Brunner, G. (2004). Supercritical fluids as solvents and reaction media (1. ed. ed.). Amsterdam: Elsevier.

[44] Namatsu, H. Supercritical drying method and supercritical drying apparatus, US6576066 (2003)

[45]] G. Rogacki, P. Wawrzyniak, *Diffusion of ethanol–liquid CO_2 in silica aerogel*, Journal
of Non-Crystalline Solids **186** (1995) 73–77.

[46] P. Wawrzyniak, G. Rogacki, J. Pruba, Z. Bartczak, Diffusion of ethanol–carbon dioxide in silica gel, Journal of Non-Crystalline Solids 225 (1998) 86–90.

[47] Sovavá H., Rate of the vegetable oil extraction with supercritical CO2-I. Modeling of extraction curves, Chemical Engineering Science **49** (1994), 409-414.

[48]Willson, R.C. and C.L. Cooney, *Supercriitcal fluid extraction for recovery of fermentation products*, Abstr.Pap. Am. Chem. Soc., **190** (1985) 158.

[49] Van Bommel MJ and Haan AB, *Drying of aerogel with supercritical carbon dioxide*. J. Non-cryst Solids **186**: 78 (1995).

[50] Aleksander Orloic, Stojan Petrovic and Dejan Skala, *Mathematical Modeling and Simulation of gel drring with supercritical caron dioxide*, J. Serb. Chem. Soc. **70** (1) (2005) 125-136.

[51] Mamata Mukhopadhyay and Bhatta Sankara Rao, *Modeling of supercritical drying of ethanol-soaked silica aerogels with carbon dioxide",* Journal of Chemical Technology and Biotechnology, **83** (2008) 1101-1109.

[52] C. A. Garcia-Gonzalez, M.C. Camino-Rey, M. Alnaief, C. Zetzl, I. Smirnova, Supercritical drying of aerogels using CO_2: *Effect of extraction time on the end material textural properties*, *Journal of Supercritical Fluids*, **66** (2012) 297-306.

[53] Robert H. Perry. Don W. Green (1999*): Perry's Chemical Engineers' Handbook*. New York, McGraw-Hill.

[54] P. Colombo, R. Doty, O. Dougherty, M. Fuhrmann, Y. Sanborn, Leaching Mechanisms of Solidified Low-Level Waste The Literature Survey, 1985